

DEVELOPMENT OF EFFECTIVE BAFFLE CONFIGURATION FOR SLOSH RESPONSE CONTROL IN LIQUID STORAGE TANKS

Thesis

Submitted in partial fulfilment of the requirements for the degree of

DOCTOR OF PHILOSOPHY

by

NIMISHA P



DEPARTMENT OF CIVIL ENGINEERING

NATIONAL INSTITUTE OF TECHNOLOGY KARNATAKA

SURATHKAL, MANGALORE-575025

FEBRUARY 2023

DEVELOPMENT OF EFFECTIVE BAFFLE CONFIGURATION FOR SLOSH RESPONSE CONTROL IN LIQUID STORAGE TANKS

Thesis

Submitted in partial fulfilment of the requirements for the degree of

DOCTOR OF PHILOSOPHY

by

NIMISHA P

(187507CV017)

Under the guidance of

Dr. B.R. JAYALEKSHMI and Dr. KATTA VENKATARAMANA



DEPARTMENT OF CIVIL ENGINEERING

NATIONAL INSTITUTE OF TECHNOLOGY KARNATAKA

SURATHKAL, MANGALORE-575025

FEBRUARY 2023

DECLARATION

By the Ph.D Scholar

I hereby declare that the Research Thesis entitled "**Development of effective baffle configuration for slosh response control in liquid storage tanks**" which is being submitted to the National Institute of Technology Karnataka, Surathkal in partial fulfilment of the requirements for the award of the degree of **Doctor of Philosophy in Civil Engineering**, *is a bona fide report of the research work carried out by me*. The material contained in this Research Thesis has not been submitted to any University or Institution for the award of any degree.



NIMISHA P

Register No. 187507CV017

Department of Civil Engineering

National Institute of Technology Karnataka, Surathkal

Place: NITK Surathkal

Date: 20-02-2023

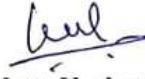
CERTIFICATE

This is to certify that the Research Thesis entitled "**Development of effective baffle configuration for slosh response control in liquid storage tanks**", submitted by **NIMISHA P** (Register Number: **187507CV017**) as the record of the research work carried out by her, *is accepted as the Research Thesis submission* in partial fulfilment of the requirements for the award of degree of **Doctor of Philosophy**.


07/03/23

Prof. B.R. Jayalekshmi

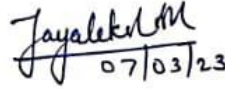
Research Guide
Professor
Department of Civil Engineering
NITK, Surathkal



Prof. Katta Venkataramana

Research Guide
Professor
Department of Civil Engineering
NITK, Surathkal




07/03/23

Prof. B.R. Jayalekshmi

Chairman-DRPC
Head of the Department
Department of Civil Engineering
NITK, Surathkal

Chairman (DRPC)
Department of Civil Engineering
National Institute of Technology Karnataka, Surathkal
Mangalore - 575 025, Karnataka, INDIA

ACKNOWLEDGEMENT

First and above all, I would like to thank the almighty for showering the perseverance and patience for the successful completion of my doctoral work. Since its inception, NITK Surathkal has always been a harbinger of educational excellence and research throughout the country. I am extremely fortunate to be associated with this great institution. I acknowledge my thanks to the ministry of HRD for providing the PhD fellowship and financial support for the completion of my doctoral work.

I would like to express my deep sense of gratitude to my guide and research supervisor, Dr. B.R. Jayalekshmi, Professor and Head, Department of Civil Engineering, NITK Surathkal, for giving me an opportunity to pursue my research work under her valuable guidance. Without her constant supervision and persistence, this thesis would not have been possible. With great pleasure, I acknowledge my sincere gratitude to my research supervisor, Dr. Katta Venkataramana, Professor and former Dean Academic, Civil Engineering Department, NITK Surathkal, for all his inspiration, relentless guidance, encouragement and help in successful completion of the research program.

I am greatly indebted to RPAC members Prof. Palanisamy T of the Civil Engineering Department (Secretary DRPC) and Prof. Subba Rao from the Department of Water Resources and Ocean Engineering for their timely evaluation and valuable suggestions during the progress of the research work. I genuinely thank Prof. Sreevalsa Kolathayar, for all the support for the purchase of experimental equipment. I take this opportunity to thank former department heads, namely Prof. Varghese George and Prof. K. Swaminathan, for providing the necessary infrastructure and resources for my research work.

I gratefully acknowledge the support and help rendered by Ms. Amalu P A, Ms. Praneetha Jogi (Junior research scholars), Ms. Anagha B V (Former M.Tech. Student), Ms. Amrita, Ms. Sreya M V, Mr. Vinoda Krishna (Co-research scholars) for the successful completion of my research work. I am truly thankful to all of my friends at NITK for making my stay at NITK a truly fun-filled and cherishable one. I sincerely thank my seniors, Dr. Radhika M Patel and Dr. Archana Satheesh, for the support they extended for the successful completion of my research work. I wish to thank Dr.

Jisha S.V, Associate Professor, Mar Baselios College of Engineering and Technology, Kerala (Former research scholar, NITK), for the software guidance.

I also like to extend my gratitude to all the teaching faculty and supporting staff of the Civil Engineering Department for their encouragement, help and support provided during the research work. I sincerely thank Mr. Subhash, the Computer Lab staff, for the software-related support. I would like to express my sincere gratitude to the authorities of NITK Surathkal for providing me with excellent facilities and a comfortable stay on campus.

I am forever indebted to my parents, Mr. Ashokan P and Mrs. Gouri P, who made me what I am today and for their unconditional faith and love. I am genuinely thankful to my brother Mr. Maneesh P for the great support he has extended for the successful completion of my research work. I would like to thank my husband, Dr. Arun B S, for being my backbone and constant encouragement. Without his valuable support and suggestions, this research work would not have been a success. I also thank my in-laws for their full-hearted support during my studies. Last but not least, I thank all my family members, friends and all those who have contributed directly and indirectly towards the completion of my work.

Nimisha P

ABSTRACT

The quantification and damping of slosh responses have become important due to the increasing demand for the safety of the liquid tanks under severe external excitations. There is uncertainties in the selection of an effective configuration of the baffle plate as an anti-slosh mechanism. Therefore, the present study focuses on the development of an effective configuration of perforated baffle plate by analysing the slosh responses of the liquid tanks under seismic ground motions and pitch excitations. Initially, modal analysis was carried out to investigate the dynamic characteristics of cylindrical as well as rectangular liquid tanks. Subsequently, nonlinear dynamic analysis under seismic ground motions of different PGA/PGV ratios has been carried out, considering the models of rectangular tanks with and without baffle plates. A detailed parametric study is carried out by considering the effects of the percentage of perforation, inter perforation distance, size of perforations, offset distance of the perforated plate, the distance between the perforated baffle plates, alignment of perforations, and the vertical position of perforated baffle plate on the slosh damping efficiency of liquid tanks. The slosh responses are observed in terms of free surface elevation and hydrodynamic pressure as major response parameters. The parametric study is extended for the response of a small-scale model under pitch excitation as well. Finally, the experimental validation of the developed configuration of the baffle plate is done on the same small-scale model using a shake table test.

Modification coefficients for the standard modal expressions are suggested for the accurate estimation of the fundamental impulsive frequency of cylindrical tanks. The frequency values decrease with the installation of baffle plates in the rectangular tanks. The optimum perforation of the baffle plate is in the range of 5% to 17%, considering the responses under convective as well as impulsive conditions that should be selected based on the frequency characteristics of the sloshing liquid and the input motion along with the requirements for weight reduction. The study identified different zones and damping ranges to pilot the positioning of the perforated baffle plate in the liquid tanks. Additionally, a novel 'zig-zag blocking alignment' of perforations for the perforated baffle plates to damp the slosh response under both convective and impulsive modes of response, which can be applied even under severe sloshing conditions, has been developed.

Keywords: Liquid sloshing; perforated baffle plate; slosh damping; Computational Fluid Dynamics; seismic ground motion; pitch excitation

TABLE OF CONTENTS

LIST OF FIGURES.....	vii
LIST OF TABLES.....	xiii
LIST OF SYMBOLS.....	xv
LIST OF ABBREVIATIONS.....	xvii
CHAPTER 1: INTRODUCTION	1
1.1 General.....	1
1.2 Sloshing of liquid.....	1
1.2.1 Liquid-tank models.....	2
1.2.2 Fluid-structure interaction.....	4
1.2.3 Control of liquid sloshing.....	4
1.3 Problem identification.....	5
1.4 Organization of the thesis.....	6
1.5 Summary.....	7
CHAPTER 2: LITERATURE REVIEW.....	9
2.1 Overview.....	9
2.2 Modelling approach.....	10
2.3 Approaches for modelling fluid–structure interaction.....	11
2.4 Modal characteristics.....	12
2.5 Liquid sloshing.....	13
2.6 Analytical approach.....	15
2.7 Numerical approach.....	16

2.8 Experimental studies.....	21
2.9 Effect of baffle on the performance of tank-liquid system.....	24
2.10 Response under horizontal and vertical excitations.....	26
2.11 Response under rocking and harmonic excitations.....	27
2.12 Response under seismic excitation.....	28
2.13 Impulsive and convective components of response.....	29
2.14 Effect of roof.....	30
2.15 Seismic codes for liquid tanks.....	31
2.16 Summary and research gaps.....	31
CHAPTER 3: OBJECTIVES AND SCOPE OF THE STUDY.....	33
3.1 General.....	33
3.2 Objectives	33
3.3 Scope of the study	33
CHAPTER 4: METHODOLOGY.....	35
4.1 General.....	35
4.2 Numerical analysis of liquid tanks.....	35
4.2.1 Governing equations.....	35
4.2.2 Boundary conditions.....	37
4.2.3 Finite element formulation.....	38
4.3 Modal analysis of liquid storage tanks.....	42
4.3.1 Dynamic characteristics of cylindrical tanks.....	42
4.3.2 Dynamic characteristics of rectangular tanks.....	46

4.4 Development of an effective configuration of perforated baffle plate.....	46
4.4.1 Analysis of geometric configuration of perforated baffle plates under seismic ground motion.....	47
4.4.1.1 Mesh convergence study.....	51
4.4.2 Analysis of geometric configuration of perforated baffle plates under pitch excitation.....	53
4.4.2.1 Mesh convergence study.....	56
4.4.2.2 Validation of numerical procedure.....	57
4.4.3 Experimental evaluation of developed configuration of perforated baffle plate.....	60
4.5 Summary.....	62
CHAPTER 5: MODAL ANALYSIS OF LIQUID STORAGE TANKS.....	63
5.1 General.....	63
5.2 Dynamic characteristics of cylindrical tanks.....	63
5.2.1 Effect of aspect ratio of the tank.....	63
5.2.2 Effect of thickness of tank wall.....	66
5.2.3 Effect of density of filled liquid.....	68
5.2.4 Effect of material property.....	70
5.2.5 Formulation of modification coefficients.....	70
5.3 Dynamic characteristics of rectangular tanks.....	76
5.4 Summary.....	79

CHAPTER 6: IDENTIFICATION OF AN EFFECTIVE CONFIGURATION OF PERFORATED BAFFLE PLATE.....	81
6.1 General.....	81
6.2 Analysis of geometric configuration of perforated baffle plates under seismic ground motion.....	81
6.2.1 Analysis of slosh response of the tank fitted with single baffle plate...	85
6.2.1.1 Effect of percentage of perforation of baffle plate.....	85
6.2.1.2 Effect of clear spacing of perforations.....	91
6.2.1.3 Effect of offset of perforated baffle plate from the tank wall.	93
6.2.2 Analysis of slosh response of the tank fitted with multiple baffle plates.....	97
6.2.2.1 Effect of percentage of perforations.....	97
6.2.2.2 Effect of alignment of perforations.....	100
6.2.3 Effective configuration of perforated baffle plates.....	101
6.3 Analysis of geometric configuration of perforated baffle plates under pitch excitation.....	107
6.3.1 Effect of area of perforations.....	108
6.3.2 Effect of inter perforation distance.....	109
6.3.3 Effect of size of perforations.....	111
6.3.4 Effect of distance between perforated baffle plates.....	112
6.3.5 Effect of alignment of perforations.....	113
6.3.6 Effect of vertical position of perforated baffle plate.....	117

6.3.7 Effect of fill depth of liquid	118
6.3.8 Effect of frequency and amplitude of input motion.....	119
6.4 Experimental evaluation of developed configuration of perforated baffle plate.	121
6.4.1 Effect on pressure.....	121
6.4.2 Effect on free surface elevation.....	124
6.4.3 Liquid deformation.....	124
6.5 Summary.....	126
CHAPTER 7: CONCLUSIONS.....	127
7.1 General.....	127
7.2 Conclusions of the study.....	127
7.3 Summary.....	132
7.4 Major contributions.....	132
7.5 Scope of future work.....	133
APPENDIX I.....	135
REFERENCES.....	151
LIST OF PUBLICATIONS.....	165
CURRICULUM VITAE.....	167

LIST OF FIGURES

Fig. 1.1	(a) Sloshing Damage to Oil Storage Tanks during 2011 Tohoku, Japan Earthquake (Hatayama 2013) (b) Damage on the roof of a tank due to excessive sloshing (Manser et al. 2017).....	2
Fig. 1.2	Single lumped mass model.....	3
Fig. 1.3	Two mass model.....	3
Fig. 1.4	Spring-mass model for ground supported tank as per IS1893 (part2):2014.....	3
Fig. 4.1	Schematic diagram of liquid tank with baffle plates.....	36
Fig. 4.2	Geometry of circular tank.....	43
Fig. 4.3	Geometric configuration of (a) tank (b) 15% perforated baffle plate.....	50
Fig. 4.4	Time history records of ground motions.....	50
Fig. 4.5	Different alignment of perforations analysed under seismic ground motions.....	52
Fig. 4.6	Mesh convergence in terms of free surface elevation under seismic ground motion.....	52
Fig. 4.7	Model details (a) Geometry of liquid tank with baffle plate (b) Alignment of perforations (i) Case 1 (ii) Case 2 (iii) Case 3 (iv) case 4	54
Fig. 4.8	Mesh convergence in terms of free surface elevation under pitch excitation.....	57
Fig. 4.9	Configuration of liquid tank model based on Xue and Lin 2011.....	58
Fig. 4.10	Comparison of numerical results with experimental data from Xue and Lin (2011) (at $x=-0.275$ m)	58
Fig. 4.11	Geometric details of validation model (based on Xue et al. 2012).....	59

Fig. 4.12	Validation of numerical simulation based on experimental data from Xue et al. 2012 (a) Hydrodynamic pressure (b) Free surface elevation...	60
Fig. 4.13	Test setup.....	61
Fig. 5.1	(a) Variation of frequency with aspect ratio; Comparison of frequency for different aspect ratio (b) FEA and IS (c) FEA and ACI (d) FEA and EN8.....	64
Fig. 5.2	Comparison of frequency values for different wall thickness (a),(b) FEA and IS (c),(d) FEA and ACI (e),(f) FEA and EN8.....	67
Fig. 5.3	Comparison of frequency values for different liquids (a) FEA and IS (b) FEA and ACI (c) FEA and EN8.....	69
Fig. 5.4	Comparison of frequency for different grades of concrete (a) FEA and IS (b) FEA and ACI (c) FEA and EN8.....	71
Fig. 5.5	ANN models Considering IS code of practice: (a) case 1 (b) case 2.....	73
Fig. 5.6	Scatter plots based on ANN analysis (a) f_{P_IS} and f_{FEA} (b) f_{P_ACI} and f_{FEA} (c) f_{P_EN8} and f_{FEA}	73
Fig. 5.7	Scatter plots based on regression analysis (a) f_{P_IS} and f_{FEA} (b) f_{P_ACI} and f_{FEA} (c) f_{P_EN8} and f_{FEA}	76
Fig. 5.8	Scatter plots based on applicability check (a) f_{P_IS} and f_{FEA} (b) f_{P_ACI} and f_{FEA} (c) f_{P_EN8} and f_{FEA}	76
Fig. 6.1	Free surface elevation at a point (-10,0,0) on left wall of the unbaffled tank.....	82
Fig. 6.2	Variation of hydrodynamic pressure for tank model 'T' (a) along height of the tank wall (b) in time domain.....	83
Fig. 6.3	Variation of turbulence kinetic energy along the length of the tank.....	85

Fig. 6.4	Temporal variation of free surface elevation at a point (-10,0,0) on left wall of the tank under (a) Imperial Valley (b) El Centro (c) Kobe.....	87
Fig. 6.5	Variation of peak surface elevation at a point (-10,0,0) with respect to the percentage of perforation.....	88
Fig. 6.6	Power spectral density corresponding to the free surface elevation under (a) Imperial Valley (b) El Centro (c) Kobe.....	90
Fig. 6.7	Variation of peak surface elevation with clear spacing 'b'.....	92
Fig. 6.8	Effect of offset distance of perforated baffle plate on free surface elevation.....	93
Fig. 6.9	Streamlines of flow corresponding to (i) $x_w=2$ m (ii) $x_w=4$ m (iii) $x_w=6$ m (iv) $x_w=8$ m under (a) Imperial Valley (b) El Centro (c) Kobe.....	95
Fig. 6.10	Fluctuations of liquid medium under (a) Imperial Valley (b) El Centro (c) Kobe.....	96
Fig. 6.11	Effect of percentage of perforation with reference to (a) free surface elevation (b) peak convective pressure (c) peak impulsive pressure.....	99
Fig. 6.12	Effect of alignment of perforation with reference to (a) peak impulsive pressure (b) peak convective pressure.....	101
Fig. 6.13	Peak value of hydrodynamic pressure for various baffle configurations (a) Impulsive pressure (b) convective pressure.....	103
Fig. 6.14	Effectiveness of case 5 configuration with reference to (a) sloshing surface elevation (b) turbulence eddy dissipation.....	104
Fig. 6.15	Slosh damping action by case 5 baffle configuration (a) details of case 5 configuration (b) streamlines of flow in case 5 configuration.....	105
Fig. 6.16	Applicability of case 5 configuration in terms of (a) Hydrodynamic pressure (b) Free surface elevation at (-0.275,0,0).....	107

Fig. 6.17	Variation of response with percentage of perforation in terms of (a) Free surface elevation (b) hydrodynamic pressure.....	109
Fig. 6.18	Variation of response with percentage area of solid in terms of (a) Free surface elevation (b) Contours of pressure gradient corresponding to peak surface elevation for the ratio a_s/a_p of (i) 60% (ii) 80% (iii) 100%.....	110
Fig. 6.19	Variation of response with number of perforations in terms of (a) Free surface elevation (b) Turbulence kinetic energy.....	112
Fig. 6.20	Variation of response with distance between perforated baffle plates (a) Free surface elevation (b) Velocity streamlines of flow for the tank models with x_b/x_w equal to (i) 0.25 (ii) 0.5 (iii) 1 (iv) 1.25.....	114
Fig. 6.21	Variation of response with alignment of perforation in terms of (a) dynamic pressure (b) Impulsive pressure (c) sloshing surface elevation (d) power spectral density	116
Fig. 6.22	Variation of response with vertical position of baffle plate in terms of (a) Free surface elevation (b) Free surface deformation of tank models with (i) $z_b=0$ (ii) $z_b=5$ (iii) $z_b=10$	118
Fig. 6.23	Variations in the peak surface elevations with fill depth of liquid.....	119
Fig. 6.24	Variation in free surface elevation with (a) Frequency of input motion (b) Amplitude of input motion.....	120
Fig. 6.25	Variation in pressure at probe 1 for (a) unbaffled tank (b) tank fitted with solid baffles.....	122
Fig. 6.26	Variation in pressure at probe 1 for tank fitted with perforated baffles of percentage of perforations (a) 5% (b) 10% (c) 15%.....	123
Fig. 6.27	Variation in peak value of pressure for different models with and without baffle plates.....	124

Fig. 6.28	Variation in free surface elevation under amplitude of excitation of (a) 10mm (b) 5mm.....	125
Fig. 6.29	Maximum deformation of liquid in (a), (b) unbaffled tank (c) tank fitted with perforated baffle plates of zig-zag blocking alignment of perforations.....	125

LIST OF TABLES

Table 4.1	Material properties.....	43
Table 4.2	Formulae for natural period of liquid tanks.....	44
Table 4.3	Models generated for analysis under seismic ground motions.....	49
Table 4.4	Details of ground motion records used.....	50
Table 4.5	Models generated for analysis under pitch excitation.....	55
Table 4.6	Models fabricated for experimental study.....	61
Table 5.1	Modification coefficients.....	75
Table 5.2	Comparison of natural frequency of vibration.....	77
Table 5.3	Frequency of tank models with and without single baffle plate.....	77
Table 5.4	Frequency of tank models with and without multiple baffle plate....	78
Table 6.1	Maximum energy dissipation ratio corresponding to various clear spacing.....	93

LIST OF SYMBOLS

a_p	Total area of perforations	n	Number of perforations
		p	
a_s	Total area of solid in the perforated region	p	Pressure
b	Clear spacing between the perforations	r	Pearson correlation coefficient
		x	
		y	
D	Diameter of tank	T	Tank without baffle
E	Young's modulus of material	t	Time
H	Height of tank	t	Thickness of tank wall
		w	
h	Liquid fill depth	X	Horizontal distance measured from centre of the tank along x-direction
L	Length of the tank	x	Distance between the perforated baffle plates
		b	
l	Half the length of the tank	x	Offset distance of the first perforated baffle plate from the left tank wall
		w	
n	Mode number	z	Vertical distance of the base of the baffle plate from the base of the tank
		h	

GREEK SYMBOLS

α	Modification coefficient for case 1 ($H/D \leq 1$)	ρ	Liquid density
β	Modification coefficient for case 2 ($H/D > 1$)	ω	Excitation frequency
η	Free surface elevation	ω_n	Natural frequency of the liquid
θ_0	Amplitude of excitation		

SUPERSCRIPTS

b_n Number of baffle plates
 represented as tally marks

SUBSCRIPTS

% Percentage of perforation of
 the baffle plate

LIST OF ABBREVIATIONS

ACI	ACI 350.03	IS	IS1893(Part2):2014
ANN	Artificial Neural Network	FSI	Fluid-Structure Interaction
CFD	Computational Fluid Dynamics	PGA	Peak Ground Acceleration
EN8	Eurocode-8	PGV	Peak Ground Velocity
FEA	Finite Element Analysis	VOF	Volume of Fluid

CHAPTER 1

INTRODUCTION

1.1 GENERAL

Liquid storage tanks are an essential part of our infrastructure. Depending upon the location, the tanks are of three types; elevated tanks, ground-supported tanks and underground tanks. These can be of different shapes such as rectangular, circular and intze type. These can be made of RCC or steel. The liquid storage tanks should remain intact even after any natural calamity. However, a large number of damages have been reported caused due to improper geometry of the structure, incorrect assessment of dynamic effect and insufficient design of staging. The proper design of storage tanks is important. The stored liquid can be of any kind, namely water, oil, gas and fuel. This may include explosive liquids also. Therefore, there should be appropriate design standards to deal with the storage tanks.

The major concern in the design of storage tanks is the interaction effects between two types of materials. The interaction between the liquid and the solid surface creates a complex problem, which should be addressed while designing a storage tank. Under any external excitation, the behaviour of these two materials will be different. The design engineer should consider both these behaviours. The major factor to be considered in the design of a liquid storage tank is liquid sloshing. The sloshing may exert high pressure on the side walls of the tank, which may lead to damage to the structure, as shown in Fig. 1.1. Hence, the accurate estimation and control of liquid sloshing is essential.

1.2 SLOSHING OF LIQUID

The sloshing is one of the important criteria to be addressed while designing a liquid storage tank. The free surface fluctuations of low frequency range occurring in partially

filled liquid containers subjected to external excitation are known as ‘sloshing’. The sloshing becomes a major cause of damage under certain conditions of external excitation. The free surface conditions will become complex enough, and can not be defined using the linear theory. The role of nonlinearity in defining the crest and trough of the sloshing liquid is inevitable. The sloshing liquid may impact the tank roof and tank walls, and sometimes, it may get mixed with the cover gas (Sanapala et al. 2016). The impact of sloshing liquid on tank walls may lead to high hydrodynamic pressure in addition to hydrostatic pressure. Under severe conditions, this may cause a damaging effect on the liquid tanks. Therefore, liquid sloshing is a complex phenomenon and is a major concern in the fields of civil, mechanical, nuclear engineering and aerospace engineering.



(a)



(b)

Fig. 1.1. (a) Sloshing Damage to Oil Storage Tanks during 2011 Tohoku, Japan Earthquake (Hatayama 2013) (b) Damage on the roof of a tank due to excessive sloshing (Manser et al. 2017).

1.2.1 Liquid-tank models

The road tankers, which aid in liquid transportation, are also triggering the research importance in the area of liquid sloshing. Under resonant conditions, the sloshing liquid is a potential source of danger in these vehicles, which may lead to an explosion causing loss of property and human life. The study of liquid sloshing started several decades ago. Since then, several models defining the behaviour of liquid inside the container started to pop up in the view of researchers. Among these models, the one defined by Housner (1963) got

worldwide attention. Housner considered the liquid-tank system as a single degree of freedom system, as shown in Fig. 1.2, if it has no free surface. However, in the case of partially filled containers, the approximation of the single mass model fails. So Housner considered such a system as a two degree of freedom system as shown in Fig. 1.3.

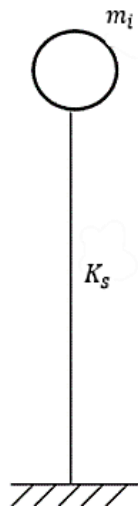


Fig. 1.2 Single lumped mass model.

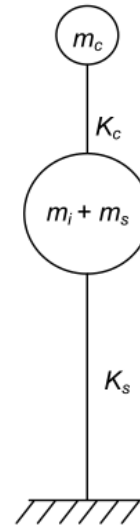


Fig. 1.3 Two mass model.

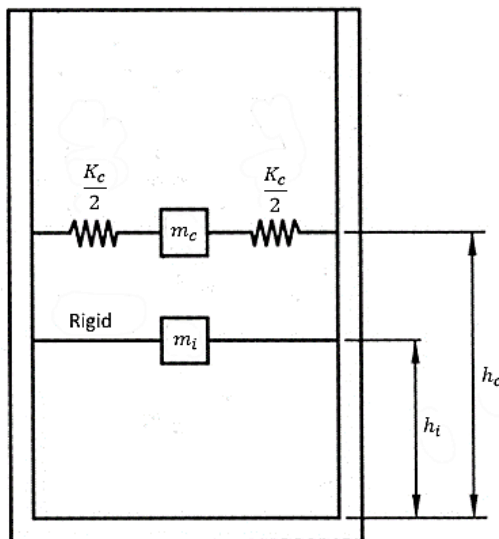


Fig. 1.4 Spring-mass model for ground supported tank as per IS 1893 (part 2):2014.

In this model, the liquid mass will be considered to be of two parts, namely impulsive mass (m_i) and convective mass (m_c). ' m_s ' is the sum of the mass of the empty container of elevated tank and one-third mass of staging. ' K_c ' and ' K_s ' are the spring stiffness in convective mode and lateral stiffness of elevated tank staging, respectively. The liquid mass in the lower region of the tank, which is rigidly attached to the tank, is considered as the impulsive mass, and the one in the upper region of the tank is considered as the convective mass. The impulsive mass of liquid will vibrate along with the tank wall, whereas the convective mass vibrates independently. The spring-mass model of the ground supported tank as per IS 1893 (part 2):2014, showing the impulsive and convective masses, is shown in Fig. 1.4. The depths of impulsive and convective mass of liquid are represented as ' h_i ' and ' h_c ' respectively.

1.2.2 Fluid-structure interaction

Since the position of the free surface of the liquid varies nonlinearly with time, the study of the motion of liquid is difficult to solve analytically as well as numerically. The problem will become more complex while considering the fluid-structure interaction. Under external excitations, the impulsive mass of liquid accelerates along with the tank wall at high frequency ranges, whereas the convective mass of liquid accelerates independently at low frequency ranges. In most numerical simulations, the interaction between the two different media ends up in large-scale numerical matrix systems (Cho and Song 2001). The establishment of interaction between the structure and the liquid is a prerequisite since it affects the behaviour of liquid motion. The previous studies included the fluid-structure interaction by using different models, such as the Eulerian approach, Lagrangian approach, Eulerian-Lagrangian approach and added mass approach.

1.2.3 Control of liquid sloshing

The estimation of sloshing associated force is important since the exceedance of a certain level of induced force will lead to a dangerous situation in terms of the stability of the system. The induced force due to sloshing liquid will depend on various parameters, such

as the tank dimension, liquid depth, excitation frequency, amplitude of excitation and flexibility of the tank. If the induced force is higher than a certain prescribed maximum value, then some kind of suppression should be introduced to control the dynamic motion of the liquid. In the case of small containers, the liquid viscosity adds to the need of suppressing the sloshing motion, whereas, for large containers, the damping due to the liquid viscosity will not be adequate to meet the need for suppression of sloshing.

In such situations, anti-slosh devices play an important role. Baffle plates, floating cans, floating lids and mats are some of the dynamic motion suppression tools. Recently, baffle plates are being used in road tankers as sloshing control tools. The baffle plates are internal barriers which restrict the free movement of liquid and thus reduce the sloshing. It reduces the frequency of sloshing and the pressure on the side walls. The baffles can be used effectively to damp liquid sloshing near resonance. Many studies are being carried out on the configuration of baffle plates to develop an effective anti-slosh device. The baffle plates improve the stiffness of the liquid storage tank as well. Because of ease of installation, the disc-type baffles are commonly used in liquid storage tanks. Recently, the perforated baffle plates are being used as an improvement over the conventional baffle plates due to the advantage of weight reduction.

1.3 PROBLEM IDENTIFICATION

In the present scenario of frequent natural and man-made calamities worldwide, the accurate estimation and control of sloshing in storage tanks are important. Many studies and recent news reported the damage to the liquid storage containers due to the heavy pressure exerted during sloshing. The damage to the liquid tanks may harm the environment and even human life because the stored liquid can sometimes be a toxic chemical. Therefore, there is an urgent requirement to develop an effective anti-slosh device that can suppress the liquid sloshing effectively.

The present research work focuses on the development of an effective configuration of a perforated baffle plate as an anti-slosh device. The effect of various geometric

configurations of perforated baffle plates on the slosh response of liquid tanks is studied under seismic and pitch excitations in the time domain. For this purpose, transient simulations are carried out using Computational Fluid Dynamics (CFD). The dynamic characteristics of the cylindrical liquid tanks are studied by considering tank models of aspect ratio in the range of 0.1 to 1.9. Further study is carried out under seismic ground motions by generating a rectangular tank model of real tank dimension with an aspect ratio of 0.25 along the x -direction and 0.5 along the y -direction. The study continued under pitch excitation by generating a rectangular tank model with an aspect ratio of 1.0 along the x -direction and 2.0 along the y -direction.

1.4 ORGANIZATION OF THE THESIS

The research thesis has seven chapters, which are organized as follows:

Chapter 1: Introduction

This chapter presents a brief overview of liquid sloshing, the modelling approaches, fluid-structure interaction, major slosh control methods and the motivation for the present research work.

Chapter 2: Literature Review

This chapter discusses previously reported literature on liquid sloshing. Focus has been given to the various modelling and analysis techniques of liquid tanks and the major findings on baffle plates as an anti-slosh mechanism. A brief summary of the literature is included to identify the research gap for the study.

Chapter 3: Objectives and Scope of the study

Major objectives and the scope of the study are included in this chapter.

Chapter 4: Methodology

This chapter elaborates on the detailed methodology followed to accomplish the framed objectives of the study. The techniques of numerical and experimental analysis adopted for the study, including the details of various models, are discussed.

Chapter 5: Modal analysis of liquid storage tanks

The free vibration characteristics of the liquid tanks with and without baffle plates are discussed in this chapter.

Chapter 6: Identification of an effective configuration of perforated baffle plate

This chapter elaborates in detail the slosh response of the liquid tanks under seismic as well as pitch excitations. Parametric studies on the effects of various geometric configurations of perforated baffle plates are included and developed an effective perforated baffle configuration for slosh damping. Additionally, this chapter contains experimental validation of the developed configuration of the perforated baffle plate.

Chapter 7: Conclusions

This chapter covers a brief summary of the research work that has been carried out. Major conclusions comprising the necessary recommendations for the use of the developed configuration of perforated baffle plate are also discussed.

1.5 SUMMARY

Sloshing is a major problem that may damage the liquid storage tanks under severe conditions. Therefore accurate estimation and control of liquid sloshing are important. Nonlinear free surface conditions and fluid-structure interaction make the problem of liquid sloshing complex. Considering the harmful effects on environment and human life, there is an urgent requirement to develop an effective anti-slosh device that can suppress the liquid sloshing effectively.

CHAPTER 2

LITERATURE REVIEW

2.1 OVERVIEW

Sloshing is the free surface fluctuation of low-frequency range, occurring in partially filled liquid containers subjected to external excitation. It is an important criterion to be addressed while designing a liquid storage tank. Under severe conditions, it may damage the liquid tanks resulting in irreplaceable loss. The dynamic boundary conditions along with fluid-structure interaction (FSI) are the two important criteria in this area of research. The pressure on the free surface of the liquid should be uniform to satisfy the dynamic boundary conditions, which can be obtained from Bernoulli's equation. The position of the free surface of the liquid medium will be unknown at any instant of time under external excitations. Therefore, the seismic design of a liquid tank should consider the nonlinear sloshing effects, which will be more than that of linear predictions. The amplitude of water surface time histories grows linearly at the initial stage and later under the influence of dissipation or forced frequency beat pattern forms (Lepelletier and Raichlen 1988). Lepelletier and Raichlen (1988) also noted the inadequacy of linear theory near resonance.

Moreover, the development of earlier models of liquid tanks was based on the concept of rigid tanks (Housner 1963) and the dynamic response of contained liquid only (Haroun 1983). Later, the Alaska earthquake in 1964 exposed the importance of considering of vibrational characteristics of such structures. To include all these effects, different modelling approaches have been developed by previous researchers, namely added mass approach (Dogangun et al. 1996), equivalent spring-mass system (Livaoglu and Dogangun 2006), Lagrangian approach (Dogangun and Livaoglu 2004), Eulerian approach (Kumar and Maity 2016) and Eulerian-Lagrangian approach (Donea et al. 1982; Nomura and Hughes 1992). Besides these, Rawat et al. (2019) used Coupled Acoustic-Structure (CAS)

and Coupled Eulerian-Lagrangian (CEL) approaches to study the dynamic behaviour of the liquid. The common modelling approach adopted by most of the International codes is the one proposed by Housner (1963).

2.2 MODELLING APPROACH

The early studies on storage tanks were started at the time of Westergaard (1931). The behaviour of the storage tank is complex due to the uncertain shape and free surface conditions of contained liquid. During vibration, the free surface of the liquid changes and thus, modelling becomes difficult. In the 1950s single lumped mass model in which the total weight of the tank is assumed to be concentrated at the top of the columns, was suggested by Chandrasekaran and Krishna (1954). The earlier Indian seismic code IS1893 also followed the concept of a single degree of freedom system. But this concept is valid only if the tank is full and for the tank structure with the support of uniform rigidity throughout (Livaoglu and Dogangun 2006).

The widely used modelling approach which is used by most of the International codes is the one proposed by Housner (1963). Housner introduced a mathematical model for a rigid tank to study the dynamic behaviour of a tank. According to this approach, a closed tank is considered to be a single degree of freedom system if it is completely filled or empty. Whereas, it is essential to consider it as a two degree of freedom system if it contains a free surface, which will cause sloshing in the tank. Housner (1955) provided simplified formulae for hydrodynamic pressure in the tank subjected to horizontal acceleration. The impulsive mode represents that part of liquid which will act in unison with the rigid tank, whereas the convective mode represents that part of liquid which will undergo sloshing motion. Based on the mathematical model developed by Housner (1963), the code IS 1893-1984 was revised in 2014 to help the designers with the seismic design of liquid storage tanks. As compared to IS 1893-1984, the revised code considered the liquid storage tank as a two-degree of freedom system.

2.3 APPROACHES FOR MODELLING FLUID-STRUCTURE INTERACTION

The interaction between the contained liquid and the tank structure is a paramount factor which needs to be considered while determining the slosh-induced forces. Many researchers used the equivalent spring-mass system to characterize the dynamic behaviour of liquid storage tanks. In this system, the impulsive mass is represented by ' m_i ' which is rigidly attached to the tank wall, while convective mass is represented by ' m_c ', which is attached to the tank wall by springs (Livaoglu and Dogangun 2006). Only one convective mode is considered by Housner (1963), but later studies included higher modes also (Bauer 1981).

Apart from the spring-mass model, there are different ways to deal with fluid-structure interaction problems, namely added mass approach (Dogangun et al. 1996), the Eulerian-Lagrangian approach (Donea et al. 1982; Nomura and Hughes 1992), Lagrangian approach (Dogangun and Livaoglu 2004) and Eulerian approach (Mandal and Maity 2016). Among these, the added mass approach is the simplest one, where the mass matrix will be increased to account for the effect of fluid without any change in stiffness and damping matrices (Livaoglu and Dogangun 2006). The Arbitrary Lagrangian-Eulerian (ALE) (Kilic 2009) method consists of three domains spatial, material and referential domain. The spatial and material domains are generally regarded as in motion, while the referential domain is defined as fixed throughout. Besides these, some other hydrocodes are also used to study the dynamic behaviour of liquid, namely Coupled Acoustic-Structure (CAS) and Coupled Eulerian-Lagrangian (CEL) approach (Rawat et al. 2019). The CAS approach is based on the linear wave theory, and it uses the Helmholtz equation as the governing equation for acoustic waves in terms of pressure as an independent variable. Since the acoustic element has only a pressure degree of freedom at each node, it reduces the computational time significantly. This approach assumes no material flow, and hence, there will not be any mesh distortion. The CEL approach is based on nonlinear theory, and it uses the Lagrangian element to model the tank wall and the Eulerian element to model the liquid.

2.4 MODAL CHARACTERISTICS

The method of fixed-interface modal synthesis was used by Daniel (1980) to get an efficient solution for the fluid-structure Eigenvalue problem. He also suggested the use of hard-walled fluid modes to consider the compressibility of the fluid. (Gupta and Hutchinson 1988) introduced a complementary Rayleigh's quotient to find the fundamental frequency of a cylindrical tank using variational principles. They observed that the frequency of sloshing was independent of tank wall flexibility. Tang (1994) considered a cylindrical tank with two liquids for the free vibration study. A combination of Lagrange's equation and the Rayleigh-Ritz procedure was used to obtain the governing equation of the liquid-tank system with two liquids. Cho et al. (2002) observed lower frequency values for the fluid-structure interaction problems while considering the compressibility of the fluid. Jung et al. (2006) suggested a theoretical formulation for the modal characteristics of a thin-walled conical frustum shell. They carried out the numerical simulation of this system using ANSYS 5.6 software adopting FLUID80 and SHELL63 elements. The lower modes were observed to be affected by the inclusion of liquid than the higher modes. Jung et al. (2009) studied the annulus effect on the natural frequencies and observed that the axisymmetric models are efficient in investigating the modal characteristics. Manshadi and Maheri (2010) observed that progressive corrosion affects the dynamic characteristics of cylindrical tanks. Jung et al. (2011) investigated the effect of fluid on the response of a pressurizer. Amiri and Sabbagh-Yazdi (2012) found that the frequency values corresponding to the circumferential mode are affected by the roof of the tank. Belostosky et al. (2014) demonstrated fluid-structure interaction problems using the Navier-Stokes equation and also provided a picture of sloshing liquid utilizing the advantages of the software ANSYS and ABAQUS. Cherif and Ouissi (2016) adopted a hierarchical finite element method for the free vibration analysis of a cylindrical rigid tank. It uses the 'p' refinement of the finite element method instead of 'h' refinement.

2.5 LIQUID SLOSHING

The damage to the oil storage tanks due to the Earthquake in Niigata, Japan, in 1964 inspired the researchers to consider the importance of sloshing (Sakai 1984). The sloshing in a cylindrical tank was studied by Balendra (1982), and he suggested analytical expression for free surface displacements. The frequency of the sloshing motion of liquid inside the tank is smaller than that of the liquid-tank system (Haroun and Tayel 1985). Hence it does not interact with the frequency of the liquid tank system. Chen et al. (1996) developed an innovative method to transform the nonlinear sloshing problem from the physical domain to the computational domain in which the problem can be analysed by the finite difference method. They considered the Crank-Nicolson time marching scheme for the study and included a second-order dissipation term in the system to filter out the high-frequency waves. The sloshing effects were studied in terms of sloshing amplitude, base shear and overturning moment. When a liquid tank is subjected to a base excitation record with long-period components, severe sloshing will occur.

The seismic design of a liquid tank should consider the nonlinear sloshing effects, which will be more than that of linear predictions. Though the linear theory is accurate in predicting peak hydrodynamic forces, it is non-conservative in predicting the secondary peaks of the hydrodynamic forces. Lepelletier and Raichlen (1988) identified six key parameters which influence the water surface elevation at any given time ' t ', in a given tank of length ' L '. The water surface time histories based on dispersive and dissipative theory were symmetric about the mean water level. Initially, the amplitude grows linearly later, under the influence of dissipation or forced frequency beat pattern forms. Due to dissipation, the steady-state condition results in time. However, the experimental model indicated the inadequacy of linear theory near resonance. This is due to the presence of nonlinearities.

The Marmara earthquake on 17 August 1999 clearly depicted the effect of sloshing on the liquid storage tanks (Kilic 2009). It caused severe damage on the upper level of the tank,

including damage to the tank walls and the roof. Kianoush and Ghaemmaghami (2011) employed the linear free surface boundary conditions to simulate the sloshing behaviour in a liquid tank. However, under strong seismic excitations and turbulence effects (Chandrasekaran and Madhavi 2014a, 2015b), the sloshing amplitude will increase, leading to more complicated boundary conditions. The sloshing in a tank without any anti-sloshing device is usually damped by viscous forces. For the sloshing behaviour of liquid, 0.5% of critical damping is applied (IS1893(Part2) 2014; ACI 350.3-06 2006; Eurocode 8 2006). The liquid in the tank behaves violently under a large amplitude of excitation (Akyildiz et al. 2013). The degrees of nonlinearities are directly affected by the frequency of excitation and the rolling amplitude. As the fill depth increases, the liquid absorbs the disturbances and thus reduces the sloshing. Therefore, fluctuations due to sloshing motion will be less under the large depth of liquid.

The site-source distance of the earthquake affects the performance of the tank-liquid system (Shakib and Alemzadeh 2017). The vertical component of ground motion increases the sloshing response for near-fault and far-fault records. Under near-fault conditions, when the directivity pulse has substantial content near the second convective mode, it may result in more sloshing height than expected (Kalogerakou et al. 2017). This is one of the reasons for post-earthquake damage observed in many tank roofs located in the proximity of active faults. The response of the second convective mode under near-fault conditions is three times larger than that of far-fault conditions. Kim et al. (2018) employed an image filter processing algorithm to measure the slosh response of the liquid tanks. The image filtering technique was applied to the image captured using a camcorder to reduce the noise and light reflection on the image so that it facilitates the measurement of the water level. Hejazi and Mohammadi (2019) noted that the sloshing wave height under horizontal and horizontal plus vertical earthquake excitation was almost the same. Based on the CAS approach, Rawat et al. (2019) calculated the sloshing displacement from the correlation $p = \rho_L g h$; where ' h ' is the sloshing displacement, ' ρ_L ' is the density of the liquid, and ' g ' is the acceleration due to gravity. According to the CEL approach, the sloshing displacement is given by the sum of the Eulerian volume fraction along the vertical height.

Rawat et al. (2019) considered the normal vertical velocity of the liquid as zero when the liquid-tank system was subjected to horizontal excitation. Another important boundary condition they considered was the pressure on the free surface of the liquid, which is equal to the atmospheric pressure or simply pressure is zero.

2.6 ANALYTICAL APPROACH

Housner (1955) presented simplified formulae for evaluating hydrodynamic pressure on fluid tanks for both impulsive and convective modes. The study considered a rectangular tank, which is symmetrical in both X-Y and Z-Y planes. The horizontal acceleration of the container in the X direction will cause the fluid acceleration in X and Y directions, while the fluid acceleration in the Z direction will obviously be zero. When the container wall is subjected to acceleration, the fluid itself may set into oscillations and may exert pressure on the tank wall. With these concepts, Housner formulated equations for free surface oscillations and the fundamental frequency of vibration as well. The expressions revealed that the effect of fluid pressure on tank walls is the same as that when a small fraction of fluid is rigidly connected to the tank wall at a height ($\sqrt[3]{g} \times h$) from the bottom of the tank for both rectangular and cylindrical containers. The study also extended to an elliptical tank, composite tank, rectangular dam, and flexible retaining tank walls. Housner (1963) investigated the dynamic properties of the tanks with the free water surface. Following the 1960 Chilean earthquake, Housner suggested simplified equations for the dynamic properties of storage tanks. The modelling approach and the formulae for the dynamic characteristics of the tank suggested by Housner form the basis for today's research in the area of storage tanks.

Goudarzi et al. (2010) developed an analytical model based on the linear wave theory. The analytical model was validated using experimental data. The method of separation of variables and the superposition principle were used by Wang et al. (2012, 2013) to obtain an analytical solution for the potential function of the liquid domain in a cylindrical container subjected to lateral excitation. This was made possible by initially dividing the

liquid domain into several sub-domains. The dynamic response equation was obtained by introducing the potential functions into the free surface wave equation. Wang et al. (2019) obtained the analytical solution of the response of liquid in the tank subjected to pitching excitation by using Stokes-Joukowski potential. The dynamic response equation can be obtained by substituting the Stokes-Joukowski potential into the kinematic and dynamic boundary conditions on the free surface.

2.7 NUMERICAL APPROACH

The nonlinear dynamic boundary condition arising out of varying free surface of the liquid medium makes these kinds of problems difficult to solve numerically and analytically (Nakayama and Washizu 1981). Nakayama and Washizu (1980) introduced the pseudo-variational principle to the fluid problem, which is discretized by the finite element technique. This method enabled the researchers to depict the dynamic boundary condition without much difficulty. The Arbitrary Lagrangian-Eulerian finite element method (ALE) is used for the transient fluid-structure interaction study by Donea et al. (1982). The primary objective of using the ALE finite element method was to develop a numerical tool for fluid-structure interaction problems. The study used the numerical time integration method for the analysis.

The finite elements were used by Balendra (1982) for the seismic study of cylindrical storage tanks. The tank wall was idealized as a thin shell. The liquid was discretized into finite elements. The computer code SAMMSOR-11 was used for the generation of the shell. The shell structure and the liquid were generated using a ring element with four degrees of freedom and an annular ring element with liquid dynamic pressure as the only degree of freedom, respectively. The study suggested design charts for hydrodynamic pressure, shear and overturning moments at the foundation, the stress resultants of the shell and the free surface displacements. Haroun (1983) wrote a computer program for calculating the natural frequencies and mode shapes of a liquid-shell system. In 1985 Haroun and Tayel carried out a numerical study of an axisymmetric partially filled liquid

tank by modelling the shell as finite elements. The fluid region was considered analytically. An added mass matrix was introduced in the matrix of shell motion to incorporate the effect of liquid dynamic pressure during vibration. The shell nodal displacements or the Eigenvectors were the direct results of the computer program written for the numerical analysis. Other parameters like shell axial bending moment, hydrodynamic pressure distribution along the tank wall and shell axial forces were calculated using the Eigenvectors obtained. Nomura and Hughes (1992) used added mass and added damping coefficients for the numerical verification of the proposed solution procedure for fluid-rigid body interaction problems. The viscosity was taken into consideration in the calculation of added damping coefficients, while the evaluation of added mass did not require the consideration of viscosity. Since the use of Lagrangian description for the entire fluid medium may cause vortex shedding, which will lead to severe mesh distortion, a mixed concept of Lagrangian and Eulerian descriptions was employed for their study. The same concept of the added mass matrix was later used by many researchers, namely Lay (1993) and Amabili et al. (1996).

Nakayama and Washizus (1981) studied the nonlinear sloshing problems by applying the boundary element method. For the study, the problem was first formulated mathematically, and then the governing equation except the dynamic boundary condition was transformed into an integral equation by using Green's formula. Later Galerkin method was used to reduce the dynamic boundary condition. The study revealed the appropriateness of the boundary element method to study the unsteady sloshing motion of the liquid. Haroun (1983) used the Lagrangian function to represent the free surface condition of liquid. Since the boundary solution technique is limited to homogeneous linear problems, the study used variational formulation based on Green's theorem. Lepelletier and Raichlen (1988) carried out a numerical study for nonlinear oscillations in rectangular tanks. The study used the one-step integration scheme for first-order differential equations of the nonlinear kind. The finite element analysis of the welded storage tank has been carried out by James and Raba (1991) by using axisymmetric solid elements. Lay (1993) developed a numerical model for singly and doubly curved tanks. The study was based on the combined finite-element-

boundary-element numerical procedure. The tank structure was modelled by using shell elements, while the effect of the fluid region was included by the concept of boundary-element. Zhao et al. (2018) adopted a similar procedure by developing an equivalent fluid mass matrix by the boundary-element method, and then it was combined with the shell structure matrix.

Malhotra and Veletsos (1994) considered several storage tanks to study numerically the uplifting of laterally excited storage tanks. The study was carried out by changing the area of contact of the base plate, the nonlinearities associated with membrane action and plastic yielding in the base plate. The uplifting significantly reduced the hydrodynamic pressure; however, the axial stresses in the tank wall increased. Dogangun et al. (1996) programmed the formulation of the three-dimensional Lagrangian fluid element, which was incorporated into the structural analysis program SAPIV. The study considered hydrodynamic pressure and displacement as key parameters. They carried out both static and dynamic analyses, and the results were compared with that of the analytical methods developed by Hoskins and Jacobsen (1934). Both results were in good coordination. The hydrodynamic pressure on the flexible tanks was larger compared to that of rigid tanks, and the variation in hydrodynamic pressure was found to be rapid up to mid-height, and then it was reduced.

Newmark's predictor–multicorrector algorithm was used by Pal et al. (1999) for the numerical modelling of composite cylindrical tanks. The procedure was applied to both rigid and flexible tanks considering sloshing. The step-by-step integration scheme was used by many researchers to solve the generated equations of motion (Haroun and Abou-Izzeddine (1992), Pal et al. (2001), Kianoush and Ghaemmaghami (2011), Mandal and Maity (2016)). Cho et al. (2002) developed a pre-processor for generating finite meshes. They observed mode shapes by using a user interface module developed based on Patran Command Language (PCL). Biswal et al. (2006) adopted the mixed Eulerian–Lagrangian scheme to study the nonlinear sloshing response in a cylindrical tank with the rigid baffle by applying the finite element code in Fortran 90. The Runge–Kutta method allows

representing the response in the time domain. Kilic (2009) used the Eulerian approach to model the fluid domain and Belytschko-Tsay shell elements to model the rigid tank structure. Out of various Eulerian approaches, the pressure-based Eulerian approach has the advantage of only one unknown per node (Mandal and Maity 2016).

Kruntcheva (2007) used Shell63 and Fluid80 elements to model the tank-fluid structure in ANSYS 1997. The coupling between the fluid and the structure represents the same displacement in a direction normal to the fluid-solid interface. The holographic images were used for the analysis of responses. Singal et al. (2014) carried out a study on the kerosene-filled tank model, which was meshed using ANSYS ICEM-CFD 12 software. The pressure-based solver was used for the transient simulation of the problem, with a fractional step algorithm as the pressure-velocity coupling method. Brar and Singh (2014) also carried out a CFD analysis on the elliptical oil transportation tank. A 2-D model of the petrol truck, with a capacity of 15000 litres, was generated in COMSOL multi-physics, considering a scale factor of 1:3. The triangular mesh was considered for the study. In order to measure the maximum pressure exerted on the tank initially, the fluid was set free to move. Then the container was subjected to linear instability by applying sudden retardation, which led to additional pressure on the tank walls. Hosseinzadeh et al. (2014) used SHELL181 and FLUID80 elements to generate the tank-liquid system using ANSYS software. Hejazi and Mohammadi (2019) used four noded fluid elements for the linear modelling of sloshing in ANSYS (2D) with no net flow rate. The seismic behaviour of the tank was simulated with Newmark's method considering the rigid tank. Kangda et al. (2019) studied the sloshing frequency and sloshing mass of an annular tank with a centrally placed circular obstruction using ANSYS software. The fluid medium was modelled using FLUID80 elements.

Mandal and Maity (2016) used the MATLAB environment to evaluate the hydrodynamic response under liquid sloshing. After computing the acceleration of the fluid particle from hydrodynamic pressure, the velocity of the fluid particle can be evaluated based on Gill's time integration scheme. Different types of software used for the finite element modelling

of liquid storage tanks, namely LS-DYNA (Kilic 2009), ANSYS APDL (Kruncheva 2007; Kangda et al. 2019), ANSYS Workbench FLUENT (Singal et al. 2014; Mocilan et al. 2016), OpenFOAM (Sanapala et al. 2016; Sanapala et al. 2018; Demirel and Aral 2018), ADINA (Eswaran et al. 2009; Kotrasova 2017; Wang et al. 2019), SAP2000, STAAD, Abaqus (Rawat et al. 2019). In order to study the position of the interface between two or more fluids, the Volume of Fluid (VOF) method was employed by many researchers (Chandrasekaran and Madhavi 2014b, 2015c; Singal et al. 2014; Mocilan et al. 2016; Iranmanesh and Passandideh-Fard 2017; Chu et al. 2018). The solver ‘interDyMFoam’ works based on the volume of fluid method (Sanapala et al. 2016). Hejazi and Mohammadi 2019 adopted Reynolds-averaged Navier–Stokes equations (or RANS) for the nonlinear modelling of two immiscible fluids. The volume fractions of these fluids were tracked by using the VOF method. This method relies on the fact that the two fluids are not interpenetrating. Thus, the volume fraction of each phase sum up to unity. They employed the finite volume method to solve the equations numerically, and the SIMPLE algorithm was incorporated for pressure-velocity coupling.

The Abaqus software was used by Rawat et al. (2019) to study the ground-supported rigid storage tanks subjected to seismic excitation. The FEM approaches, such as linear wave theory-based Coupled Acoustic-Structural (CAS) and nonlinear wave theory based Coupled Eulerian-Lagrangian (CEL), were considered for the Fluid-Structure Interaction study of the tank. The CAS approach uses an acoustic element to model the liquid and Lagrangian elements to model the tank wall. The normal motion at the acoustic-structure interface and the pressure of the acoustic element can be related using the boundary impedance. In this approach, the liquid was modelled using the 3-D acoustic continuum element (AC3D8R) and the tank wall was modelled using 3-D rigid three-node triangular and four-node quadrilateral discrete elements (R3D3 and R3D4). The surface-based tie constraint allows both surfaces to remain in contact throughout the simulation process. In the case of the CEL approach, the interaction between the liquid and the tank is established by using some general contact algorithm. And this approach does not require any additional solver to analyse the liquid region. The volume fraction tool in each Eulerian element is

used to trace the free surface of the liquid. 3-D eight-node Eulerian continuum elements (EC3D8R) were used to model the liquid region, and 3-D rigid four-node bi-linear quadrilateral discrete rigid elements (R3D4) were used to model the rigid tank. The comparison of these approaches with the experimental method depicts some minor deviation in the results of sloshing displacement because of the contact condition and the simulation technique used for the numerical analysis. Though the computational time requirement in the CAS approach was less, the CEL approach was more accurate in terms of sloshing displacement.

2.8 EXPERIMENTAL STUDIES

Vibration tests on full-scale tanks were carried out by Haroun (1983). Seismometers were used to measure the vertical motion and the amount of rocking at the base. The responses of single deck and double deck type floating roof liquid tanks were studied by Sakai et al. (1984). Lepelletier and Raichlen (1988) used the wave generator-wave plate assembly for the experimental study on the rectangular tank under steady-state and transient conditions. Water surface elevation was measured by resistance wave gauges in conjunction with an oscillograph. Pal et al. (2001) investigated the slosh dynamics of liquid-filled containers experimentally. The shake table facility of 1.2mx1.4m was utilized by Maleki and Ziyaeifar (2007) to carry out a series of experiments on cylindrical tanks fitted with baffles. Two ring baffles and a vertical blade baffle were used for the study. The wave amplitude decay method was selected to measure the slosh damping. The Hydraulic Institute of Stuttgart University carried out a series of tests to verify the analytical results on the hydrodynamic damping ratio of liquid sloshing (Goudarzi et al. 2010). The experiments were carried out on a shake table with a rectangular tank made of acrylic glass of thickness of 2cm. The ultrasonic wave gauges were used to measure the wave amplitude response of the tank.

The nonlinear behaviour of liquid sloshing was studied by Akyildiz et al. (2013) experimentally under pitch oscillations. The ring baffle of plexiglass material was used with a width of 5 cm and 10 cm. The piezoresistive type pressure transducers were used to

measure the pressure at various points. The 15 kW DC motor allowed the tank to rotate freely about the transverse axis through the centre of the tank. The experiments were conducted under periodic rotational motion with 4° and 8° . A shake table of 4 m \times 4 m at CSIR-SERC, Chennai, was used by Chaduvula et al. (2013) for the experimental study on an elevated steel water tank under combined horizontal, vertical and rocking motions for a synthetic earthquake excitation for 0.1g and 0.2g acceleration. The study used a cylindrical tank of 1:4 scale with a natural frequency 8.24 Hz. 8 numbers of accelerometers and 2 numbers of pressure transducers were used to measure the output response.

Brar and Singh (2014) developed a scaled-down model of an oil transportation truck, and the system was studied under a to and fro motion by attaching it with a guide mechanism. Linear movement was applied to the tank by varying the speed of the motor. The output response was measured in terms of pressure by attaching pressure gauges to various points of the tank. The study observed some variation in the results of CFD analysis and experiment. This variation is attributed to changes in the boundary condition, material properties, friction and loading conditions during the experiment. The shake table test on a 19.2 m diameter steel cylindrical tank was conducted by Hosseinzadeh et al. (2014) using three earthquake records as base motion. A flat ring baffle was used to control the sloshing motion of the liquid. An 8-channel data acquisition system with 4 accelerometers, 2 LVDT, and 2 strain-gauges was used to study the output response. The sloshing motion was recorded using a digital HD camera. The Fast Fourier Transform (FFT) and transfer functions between input and output acceleration were used to evaluate the frequency of the impulsive mode. The half-power bandwidth method was used to determine the damping values. The forced and free vibration parts of sloshing amplitude time histories were the references for finding the damping and frequency values of convective mode.

The frequency response of rectangular containers fitted with various internal objects was studied by Nayak and Biswal (2015). A shake table of 1 m \times 1 m with a control unit of frequency range 0.40-2.20 Hz was used for the study. The tank model was made of a Perspex sheet with the assumption of a rigid tank. Three baffle configurations, namely

bottom-mounted, surface-piercing and submerged block baffle, were selected and fixed to the tank with the help of stainless steel rods. The test was conducted by varying aspect ratio, the relative height of the baffle and the liquid depth. A lateral sine sweep test was carried out with and without baffle. Hosseini et al. (2017) carried out a shake table test on the floating-roof Plexiglas tank at the International Institute of Earthquake Engineering and Seismology (IIEES). The floating-roof and the Suspended Annular Baffle (SAB) were installed at three distances, such as 0.7, 0.5, and 0.2 m, from the roof of the tank. 0.5 mm thick steel plate was used for the floating-roof, and two widths, 0.07 and 0.11 m, were considered for SAB. Unidirectional shake table capable of producing harmonic sine motion with amplitude up to 3cm as well as single-component earthquake motion with main components from Kocaeli, Turkey earthquake of 1999, Loma Prieta earthquake of 1989 and Chi-Chi, Taiwan earthquake of 1999 were used for the study.

The sloshing response of the cylindrical tank was studied by Kim et al. using a shake table in 2018. Five accelerometers were installed at various heights from the bottom of the tank to evaluate the acceleration response. Two SONY HDR-CX130 digital camcorders were used to capture images of sloshing. Initially, to study the dynamic characteristics of the tank, a white noise test was conducted. The seismic excitation test was conducted using the El Centro seismic wave. Radnic et al. (2018) also carried out a shake table test on three rectangular tanks of different stiffness. The bottom of the tank was fixed to the top of the shake table. The hydrostatic and hydrodynamic pressure, horizontal displacement and transverse horizontal strain of the tank wall were considered as parameters for the study. The motion of the tank-liquid system was monitored using two digital cameras. The shake table set-up was employed by many researchers for the experimental study of the tank-liquid system, namely Hosseinzadeh et al. (2014), Chu et al. (2018) and Hejazi and Mohammadi (2019). The test was conducted by Hejazi and Mohammadi (2019) with a sway amplitude of 0.1g to 0.8g. The frequency range was 0.5 to 14Hz from below the natural frequency to near and above it. The shaking table deck, roof, and walls of the tank are fitted with piezoresistive pressure transmitters and four accelerometers. All the data

were recorded simultaneously with a data acquisition system. They considered the induced maximum pressure as a major parameter.

2.9 EFFECT OF BAFFLE ON THE PERFORMANCE OF TANK-LIQUID SYSTEM

Due to the increase in the demand to control the sloshing liquid, researchers developed various anti-slosh elements. Baffle plates are one of the well-applied anti-slosh elements. The frequency response of a rectangular container fitted with various internal objects has been studied by Nayak and Biswal (2015). It is noted from the study that the baffles will act as energy dissipaters on account of flow separation effects. In the case of road tankers fitted with baffle, it will easily dissipate kinetic energy, thus reducing sloshing. They used the method of logarithmic decay of wave amplitude to analyse the hydrodynamic slosh damping. As the height of the baffle increases, the reduction in sloshing also increases (Nayak and Biswal 2015; Sanapala et al. 2016; Chu et al. 2018). It indicated an increase in the damping ratio with a relative height of baffle. The damping effect of surface-piercing type baffle configuration was more than that of bottom-mounted and submerged type. Incorporating an internal baffle is a kind of simplest solution to control the free surface elevation and slosh force (Sanapala et al. 2018).

The parametric Eigen characteristics of a baffled cylindrical liquid-storage tank by the coupled structural-acoustic finite element method showed that the frequency of the liquid-tank system decreases with an increase in the number of baffles (Cho et al. 2002, 2005). The flexibility of the baffle plate will not affect the sloshing frequency parameters of the liquid for the larger thickness of the baffle plate (Biswal et al. 2003). The fundamental frequency of the system decreases with an increase in the length of the vertical baffle (Hasheminejad and Mohammadi 2011). However, it did not affect symmetrical modes (Hasheminejad and Aghabeigi 2012). If the combination of the surface-piercing type and the bottom-mounted baffle is used, the fundamental sloshing frequency increases while other frequencies decrease slowly (Wang et al. 2016).

Besides these, the amplitude of sloshing is another important response parameter investigated by many researchers. The amplitude of sloshing in a liquid tank with a flexible baffle will be more than that of a rigid baffle, though it is less than that of a without baffle condition (Biswal et al. 2004). Since the liquid below the first baffle behaves like a rigid mass, the baffle installed below the first baffle will not be much effective in reducing the slosh amplitude (Biswal et al. 2006). Moreover, the amplitude of sloshing reduces with the introduction of a vertical baffle near the surface (Xue and Lin 2011; Hasheminejad et al. 2014).

Younes et al. (2007) investigated the effect of different combinations of baffles in reducing the amplitude of sloshing. Many parallel studies have been reported by previous researchers using different configurations of vertical baffle plates to reduce the liquid sloshing (Panigrahy et al. 2009; Akyildiz 2012; Xue et al. 2012, 2017). The baffle plate located at the centre of the tank increases the damping ratio effectively and causes a reduction in the pressure acting on the sidewalls of the tank (Akyildiz and Ünal 2005). The vertical baffle plate in the middle of the tank is also effective in reducing the sloshing fluctuations of the free surface (Liu and Lin 2009; Sanapala et al. 2016). The pressure exerted on the walls due to sloshing was reduced due to the incorporation of baffles in the tank (Brar and Singh 2014). A reduction in sloshing height of 20% to 30% for single baffled tanks and about 45% for double baffled tanks were observed by (Hasheminejad et al. 2014).

The ring baffles are effective in reducing the sloshing effect of liquid (Maleki and Ziyaeifar 2007; Akyildiz et al. 2013). This arrangement enhances the energy dissipation rate of fluid during the flow over the baffle. The ring baffles reduce the velocity impact and vertical motion of liquid effectively (Eswaran et al. 2009). The horizontal baffle also reduces the vertical component of velocity, while the vertical baffle reduces the horizontal component of velocity. The introduction of the horizontal baffle in the liquid domain divided it into two parts, namely the sloshing part, which will be above the baffle plate and the rigid part, which will be below the baffle plate (Wang et al. 2012, 2013). Hence, it will cause a discontinuity in the pressure distribution along the wall. Hosseini et al. (2017) reported that

the Suspended Annular Baffle (SAB) effectively reduces the sloshing motion in floating-roof liquid storage tanks. It helps to reduce the swirling of the floating-roof and improve the damping ratio by almost six times that of no floating roof condition. But for higher excitation levels, the reduction in the sloshing values was less as SAB also moves upward with the roof, and it takes more time to reach back to the original position. And before SAB reaches the original position roof again moves upward. The SAB placed in the impulsive part of the impounded liquid is effective in reducing sloshing height. The effectiveness of the ring in developing slosh damping increases if it is installed near the free surface of the liquid (Cho et al. 2005; Wang et al. 2012; Sanapala et al. 2018; Wang et al. 2019).

The perforated baffle plates have been used as an improvement over the solid baffle plates to control the liquid sloshing. In the case of a one-baffled tank, the fundamental frequency decreases uniformly with a decrease in the baffle inner-hole diameter (Cho et al. 2002). Damping of slosh response improves with an increase in the number of baffles (Younes et al. 2007; Chu et al. 2018). The effectiveness of perforated baffles in reducing the slosh response was studied by experimental and numerical methods by various researchers (Xue and Lin 2011; Xue et al. 2012; Kumar and Sinhamahapatra 2013; Xue et al. 2013). Jin et al. (2014) experimentally investigated the effectiveness of the horizontal perforated baffle plates in controlling the sloshing liquid. Wang et al. (2019) reported a decrease in the surface wave height with a reduced inner hole radius of the baffle plate in the case of a cylindrical tank with multiple baffles. In the case of tanks fitted with perforated vertical baffle plates, the open-area ratio (area of perforation measured considering an infinitesimal strip of fluid) is the major parameter that affects the liquid sloshing (Bellezi et al. 2019).

2.10 RESPONSE UNDER HORIZONTAL AND VERTICAL EXCITATIONS

Under horizontal excitation, the tank wall will experience the hydrodynamic pressure due to the superposition of long-period components of the convective fluid and the short-period components of the impulsive fluid (Haroun and Abou-Izzeddine 1992). The fundamental frequency increases until the height to radius ratio of the tank reaches around 1.7. Beyond

this point, the frequency decreases. If this ratio is held constant and the shear wave velocity is increased, the frequency also increases.

The vertical excitation in a horizontally loaded tank will result in amplified hoop tensile stress (Haroun and Abou-Izzeddine 1992). Since the experimental studies show that the sloshing is minimum under arbitrary vertical excitation, the liquid free surface can be neglected. The consideration of the effect of soil reduces the response of the system compared to that of a rigid foundation. Also, if the tank is slender, the response will be less. The vertical ground acceleration has a more significant effect on the convective part of the response than it has on the impulsive part (Moslemi and Kianoush 2012). The heave motion of the vessel represents the vertical excitation of the liquid-tank system (Zhao et al. 2018). Although the linear theory does not support the sloshing motion due to vertical excitation, the resonant sloshing can occur under certain excitation when the nonlinearity is considered. In the case of near-field earthquakes, the liquid pressure induced on the tank wall can be increased under vertical seismic excitation, but the effect is not significant in the case of sloshing wave height (Hejazi and Mohammadi 2019). The vertical displacement of the free surface depends on the spectral response acceleration at the natural mode of sloshing.

2.11 RESPONSE UNDER ROCKING AND HARMONIC EXCITATIONS

Under rocking excitation, the maximum hydrodynamic pressure occurs at a plane normal to the axis of rocking (Veletsos and Tang 1986). The maximum impulsive pressure occurs away from the bottom of the tank in the case of tall tanks, whereas in the case of broad tanks, it varies monotonically from top to bottom. The moment immediately above the base is due to the hydrodynamic pressure at the wall of the tank, whereas the foundation moment is due to the effect of hydrodynamic pressure at the base also. As shear wave velocity increases, the rocking acceleration response decreases (Haroun and Abou-Izzeddine 1992). The rocking response of a tall tank is more than that of broad tanks. The sloshing responses, including amplitude and phase, are dependent upon the location of the centre of rotation

under rotational excitation (Zhao et al. 2018). The frequency properties of sloshing under rotational excitation are the same as that of horizontal excitation.

The free water surface elevation will be significant if the harmonic excitation period is close to the first period of free oscillation of water. And also, the hydrodynamic forces and pressure on the tank wall are more than that of hydrostatic values by several times (Radnic et al. 2018). The hydrodynamic forces increase with the amplitude of the harmonic excitation.

2.12 RESPONSE UNDER SEISMIC EXCITATION

There are several recorded earthquakes which affected even the emergency response efforts (Soroushnia et al. 2011). Chile 1960, Niigata 1964 (Sakai et al. 1984), 1971 San Fernando, 1978 Izu-Oshima and Miyagi are a few examples of devastating earthquakes which triggered more research importance in the area of storage structures. The behaviour of the fluid–tank–soil system will be affected by the frequency characteristics of the earthquake record (Kianoush and Ghaemmaghami 2011). The site-source distance of the earthquake affects the performance of the tank-liquid system (Shakib and Alemzadeh 2017). The vertical component of ground motion increases the sloshing response for near-fault and far-fault records. Under near-fault conditions, when the directivity pulse has substantial content near the second convective mode, it may result in more sloshing height than expected (Kalogerakou et al. 2017). This is one of the reasons for post-earthquake damage observed in many tank roofs located in the proximity of active faults. It was also reported that the response of the second convective mode under near-fault conditions is three times larger than that of far-fault conditions.

Under earthquake excitation, linear and nonlinear hydrodynamic pressures are of almost the same magnitude. Significantly higher water waves occur under real and artificial earthquake excitation even for low base acceleration (Radnic et al. 2018). Tabas (1978), Kobe (1995), Imperial Valley (1979) and Chi-Chi (1999) are some of the earthquake records used for the study on liquid tanks (Hejazi and Mohammadi 2019). Kobe and Tabas

have most of the peak ground acceleration for the horizontal component; however, the Imperial Valley earthquake has a high vertical to horizontal PGA ratio. Chi-Chi (1999) has two station codes, TCU52 and TCU68. Within the range of 14-16sec, the TCU68 has maximum horizontal and vertical accelerations. TCU52 has the maximum horizontal acceleration in 13sec, in which the vertical component is negligible. The seismic excitation causes high sloshing amplitude, which will, in turn, lead to the high hydrodynamic pressure on the tank wall (Rawat et al. 2019). The distribution of this pressure will be affected nonlinearly by surface pressure and sloshing displacement.

2.13 IMPULSIVE AND CONVECTIVE COMPONENTS OF RESPONSE

The coupling between the shell vibrational modes and the liquid sloshing modes is weak enough to consider the tank wall to be rigid for the evaluation of convective pressure (Haroun, 1983; Hashemi et al. 2013). The impulsive pressure should be evaluated by considering the liquid-shell system and neglecting the sloshing. The meridional stresses due to water as a live load are not much significant. Hence, it can be assumed to be zero except at the base (James and Raba 1991). In the case of a steel water tank, the actual maximum stress in a panel will be equal to the hoop stress in the next lower level.

As the liquid depth to inner lateral dimension ratio increases, the impulsive mass of the liquid tank system also increases (Kumar et al. 2016). The convective components of base shear, base moment and overturning moment are less compared to impulsive components. For lower tank length, the hydrodynamic pressure on the tank wall increases due to the increased tendency of the fluid to rotate inside the tank (Mandal and Maity 2016). The hydrodynamic pressure on the tank wall decreases as the stiffness of the tank wall reduces (Radnic et al. 2018). Similarly, the lateral displacement and stress on the tank wall increase as the stiffness of the tank wall decreases. The major component of hydrodynamic pressure is the impulsive pressure component, which has a parabolic distribution along the tank wall (Rawat et al. 2019). The maximum value of impulsive pressure was observed at the bottom of the tank, whereas the maximum value of convective pressure was observed at the top of

the tank. These observations show that the calculation of hydrodynamic pressure is not affected by the nonlinearity of the sloshing displacement. If the aspect ratio is less, the distribution of total pressure along the height of the tank will be parabolic, and the contribution of convective hydrodynamic pressure at the base will be more. However, in the case of the higher aspect ratio, the distribution of total pressure along the height of the tank will be uniform. The excitation amplitude affects the sloshing wave height and pressure induced on the tank wall directly (Hejazi and Mohammadi 2019). The time period of sloshing is increased with a decrease in fill depth, and consequently, the spectral response acceleration of the Tabas record decreases. Near the free water surface, the value of convective pressure will be significant and will be more dependent on the spectral response acceleration of the fundamental sloshing period.

2.14 EFFECT OF ROOF

There will be a slight reduction in the values of the natural frequencies due to the additional mass of the roof (Haroun 1983). The interaction between the roof and the contained liquid was theoretically analysed by using the concept of fluid-elastic vibration by Sakai (1984). The bending rigidity was assumed to be uniform throughout the roof for ease of analysis. The first natural frequency of single deck and double deck roofs were the same, whereas, for higher orders, the value of natural frequency for double deck was less than that of a single deck roof. The floating roof hardly influences the first sloshing mode. It helps to improve the damping ratio of the fluid-roof system by 2.5 times (Sakai 1984).

2.15 SEISMIC CODES FOR LIQUID TANKS

The international codes used for the design of liquid tanks are ACI 350.3, Eurocode-8, and New Zealand standard (Hashemi et al. 2013), API 650 and AWWA 100 (Haroun 1983). These codes are based on the mechanical model suggested by Housner (1963). Jaiswal et al. (2003) reviewed various international codes for the seismic design of liquid tanks, namely ACI 350.3, Eurocode 8, NZSEE guidelines, API 650 and AWWA standards. The review includes various aspects like time period, hydrodynamic forces and sloshing wave

height. A brief review of the limitations of the Indian seismic code is also included. Most of the international codes did not consider the effect of vertical excitation. Also, the provisions for soil flexibility and buried tanks are given only in qualitative terms. The expression for hydrodynamic force in all the codes is based on mechanical analogues. Jaiswal and Jain (2005) pointed out the limitations of IS1893:1984 and suggested some modified provisions along with the commentaries for the seismic analysis of liquid tanks. Provisions for ground-supported tanks, soil flexibility, P- δ effect and response reduction factors are some of the suggested points.

Kamara (2010) illustrated the design of concrete tanks in accordance with ACI 350-06, which was adapted from ACI 318-02. The international codes, namely ACI 350.3, Eurocode 8 and the New Zealand standard, considered wall flexibility and included the corresponding increase in the acceleration coefficients (Hashemi et al. 2013). But the effect was not accurately addressed. Kumar et al. (2016) stated that the convective time period based on Draft IS 1893 Part 2, ACI 350.3 and Eurocode 8 are almost the same; however, the impulsive period is slightly higher when calculated based on Eurocode 8. Liu (2018) presented a review on seismic analysis of concrete tanks in high seismic zones based on ACI 305.3. The study also explained Housner's assumptions, which are included in the design code using a finite element model analysis in SAP2000.

2.16 SUMMARY AND RESEARCH GAPS

From the detailed review of the literature, it is observed that sloshing is the major criterion to be addressed in the study of the structural performance of liquid storage tanks. The high level of hydrodynamic pressure which will get induced on the tank wall should be controlled to account for the stability of the tank-liquid system. Recently, the baffle plates have been used as an anti-slosh device. The reviews on literature reveal that the effectiveness of baffle plates depends on the geometric characteristics, in addition to the location and the number of baffle plates. Perforated baffle plates add the advantages of weight reduction in addition to the slosh response damping. And the use of the perforated

baffle plate has not been effectively addressed so far. Moreover, even a slight reduction in the slosh response is significant considering the damages it may cause if the tank structure collapse. Therefore, the performance improvement of the liquid tank equipped with perforated baffle plates is important. In view of the research gaps identified, this study focuses on the development of an effective configuration of perforated baffle plate for improved slosh damping in liquid storage tanks.

CHAPTER 3

OBJECTIVES AND SCOPE OF THE STUDY

3.1 GENERAL

The problem of liquid sloshing is a major concern in various fields such as storage and transportation of various liquids including harmful chemicals, moving vehicles, spacecraft and various fluid-based mechanical systems. Therefore, considering the safety of life and the environment, the quantification and control of slosh-induced responses are of great concern in various fields. Increasing demand for safety in various fluid-based applications provided the thrust for the present study.

3.2 OBJECTIVES

The main objectives of the present study are as follows:

1. To study the free vibration characteristics of the liquid tanks with and without perforated baffle plates.
2. To examine the influence of geometry and location of perforated baffle plates on slosh response of liquid tanks.
3. To develop an effective configuration of the baffle plate.
4. To verify experimentally the effectiveness of the developed configuration of the perforated baffle plate.

3.3 SCOPE OF THE STUDY

The liquid sloshing is a significant factor that should be considered while designing the liquid storage tanks. Previous literature reported even the collapse of the liquid storage tanks due to the sloshing of liquid. Therefore, quantification and control of liquid sloshing

are of utmost importance in this area of research. The present research work focuses on the development of an effective configuration of the perforated baffle plate as an anti-slosh device. The study commenced with the analysis of frequency characteristics of liquid storage tanks, considering cylindrical as well as rectangular tanks. In the case of cylindrical tanks, the study focused on the impulsive frequency values due to the discrepancies noticed in these frequency values from that obtained based on the standard codal provisions. A parametric study is carried out on 560 models of cylindrical tanks with aspect ratio, the thickness of the tank wall, Young's modulus of the material, depth of the liquid and the density of the liquid as the parameters. IS 1893(Part 2):2014, ACI 350.3 and Eurocode-8 are the standard codes of practices considered for the study. The study also analysed the frequency values of rectangular tanks with and without baffle plates under impulsive as well as convective modes of vibration.

The effects of various geometric configurations of perforated baffle plates on the slosh response of rectangular liquid tanks are studied under seismic and pitch excitations in the time domain. For this, transient simulations are carried out using Computational Fluid Dynamics (CFD). Three seismic ground motions of Imperial Valley (1979), El Centro (1940) and Kobe (1995) ground motions with low, intermediate and high frequency ranges, respectively, are selected for the study. The analysis is carried out for the tank models with single and multiple baffle plates. Slosh responses under different configurations of perforated baffle plates are observed by considering the percentage of perforation of the baffle plate, inter perforation distance, size of the perforations, alignment of perforations, the offset distance of the perforated baffle plate, the distance between the perforated baffle plates, and the vertical position of the perforated baffle plate as the parameters. The slosh responses are observed in terms of free surface elevation, hydrodynamic pressure, turbulence kinetic energy, turbulence eddy dissipation, velocity streamlines, power spectral density corresponding to the free surface elevation and the free surface deformation. The experimental validation of the developed configuration of the perforated baffle plate is done by carrying out a shake table test. The slosh responses are analysed in terms of pressure and free surface elevation.

CHAPTER 4

METHODOLOGY

4.1 GENERAL

The liquid-tank system differs from other engineering structures mainly because of the interaction between the two types of elements, namely solid and liquid. Though the modelling of the liquid retaining tanks considering this interaction is difficult to carry out, it should be done with great accuracy in order to obtain a good simulation of a real state problem. Since the mathematical calculation of the solid-liquid interaction under transient loading is tedious work, the finite element modelling gained great acceptance in the simulation of real-field complex problems.

4.2 NUMERICAL ANALYSIS OF LIQUID TANKS

A 2-D schematic diagram of the rectangular tank with perforated baffle plates is shown in Fig. 4.1 to represent the geometric details. The reference frame is assumed to be located at the free surface, confirming symmetry about zx and zy planes. The elevation of the free surface, the acoustic domain, and the acoustic domain boundary are represented as ' η ', ' Ω_f ' and ' Γ_f' ', respectively. Two vertical baffle plates are located symmetrically about zy plane.

4.2.1 Governing equations

The Navier-Stokes equations of fluid momentum and flow continuity govern the fluid motion in the tank. Considering ' v_x, v_y, v_z ' as components of the velocity vector in x, y and z direction, ' ρ ' as the density of the liquid, ' p ' as the pressure, ' μ_e ' as the effective viscosity and ' t ' as time, the Navier-Stokes equations can be expressed as (Tryggesson 2007):

$$\frac{\partial \rho v_x}{\partial t} + \frac{\partial(\rho v_x v_x)}{\partial x} + \frac{\partial(\rho v_y v_x)}{\partial y} + \frac{\partial(\rho v_z v_x)}{\partial z} = -\frac{\partial p}{\partial x} + \frac{\partial}{\partial x} \left(\mu_e \frac{\partial v_x}{\partial x} \right) + \frac{\partial}{\partial y} \left(\mu_e \frac{\partial v_x}{\partial y} \right) + \frac{\partial}{\partial z} \left(\mu_e \frac{\partial v_x}{\partial z} \right) + F_b \quad (4.1)$$

$$\frac{\partial \rho v_y}{\partial t} + \frac{\partial(\rho v_x v_y)}{\partial x} + \frac{\partial(\rho v_y v_y)}{\partial y} + \frac{\partial(\rho v_z v_y)}{\partial z} = -\frac{\partial p}{\partial y} + \frac{\partial}{\partial x} \left(\mu_e \frac{\partial v_y}{\partial x} \right) + \frac{\partial}{\partial y} \left(\mu_e \frac{\partial v_y}{\partial y} \right) + \frac{\partial}{\partial z} \left(\mu_e \frac{\partial v_y}{\partial z} \right) + F_b \quad (4.2)$$

$$\frac{\partial \rho v_z}{\partial t} + \frac{\partial(\rho v_x v_z)}{\partial x} + \frac{\partial(\rho v_y v_z)}{\partial y} + \frac{\partial(\rho v_z v_z)}{\partial z} = -\frac{\partial p}{\partial z} + \frac{\partial}{\partial x} \left(\mu_e \frac{\partial v_z}{\partial x} \right) + \frac{\partial}{\partial y} \left(\mu_e \frac{\partial v_z}{\partial y} \right) + \frac{\partial}{\partial z} \left(\mu_e \frac{\partial v_z}{\partial z} \right) + F_b \quad (4.3)$$

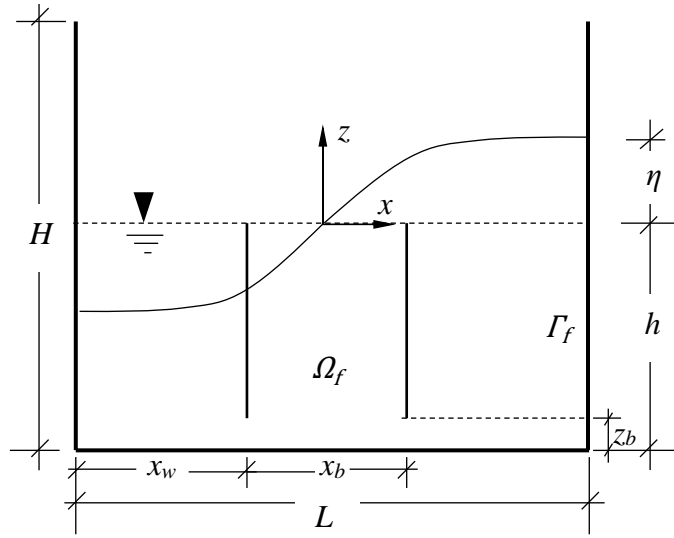


Fig. 4.1 Schematic diagram of liquid tank with baffle plates.

Considering a liquid motion, there are two types of forces, such as surface forces and body forces. The surface forces are represented by the first two terms on the right hand side of the Navier stokes equation and body forces are represented by ‘ F_b ’. The term on the left hand side of the Navier stokes equation that causes nonlinearity in the sloshing problem is called convective term (Tryggesson 2007). The continuity equation can be represented as follows (Tryggesson 2007):

$$\frac{\partial \rho}{\partial t} + \frac{\partial(\rho v_x)}{\partial x} + \frac{\partial(\rho v_y)}{\partial y} + \frac{\partial(\rho v_z)}{\partial z} = 0 \quad (4.4)$$

4.2.2 Boundary conditions

The coupling conditions on the interface ‘ Γ_I ’ between the fluid and the structure are given by (ANSYS 2013):

$$\bar{\sigma}(\bar{u}_S)\hat{n} + p\hat{n} = 0 \quad (4.5)$$

$$\hat{n} \cdot \bar{u}_S - \hat{n} \cdot \bar{u}_f = 0 \quad (4.6)$$

where, ‘ \bar{u}_S , ‘ $\bar{\sigma}(\bar{u}_S)$, ‘ \hat{n} and ‘ \bar{u}_f ’ represent the displacement in solid, solid stress tensor, outward normal unit vector and the displacement in acoustic fluid respectively. Under the seismic excitation, the sloshing surface of the liquid is assumed to be at an elevation of ‘ η ’. In this case, the pressure for the sloshing surface is expressed as:

$$p = \rho g \eta \quad (4.7)$$

where, ‘ g ’ is the acceleration due to gravity. Applying the velocity and the momentum conservation equations along with Eq. (4.7), the boundary condition for the sloshing surface can be expressed as (Moslemi and Kianoush 2012):

$$\frac{1}{\rho} \frac{\partial p}{\partial z} = -\frac{1}{\rho g} \ddot{p} \quad (4.8)$$

where, ‘ \ddot{p} ’ is the second derivative of pressure. The convective component of response can be obtained by applying the boundary condition given in Eq. (4.8). To obtain the impulsive component of response, the Eq. (4.8) should be replaced with the following condition at the free surface (Moslemi and Kianoush 2012).

$$p(x, y, z, t) = 0 \quad (4.9)$$

4.2.3 Finite element formulation

Numerical modelling is carried out by considering the liquid tank as a multi-degree of freedom system, and it can be expressed as follows:

$$[M]\{\ddot{u}\} + [C]\{\dot{u}\} + [K]\{u\} = \{F^a(t)\} \quad (4.10)$$

where, $[M]$ is the mass matrix, $[C]$ is the damping matrix, $[K]$ is the stiffness matrix and $\{F^a(t)\}$ is the load vector of the liquid tank system. The spatial variation of displacement is represented by ‘ u ’. In the case of liquid-storage tanks, the damping is due to the two components of mass, namely, impulsive and convective. As per the International codes of practice (IS1893(Part2) 2014; ACI 350.3-06; Eurocode 8 the damping is taken as 0.5% of critical under convective mode and 5% of the critical under impulsive mode.

Based on the governing equations, the acoustic wave equation can be expressed as follows (ANSYS Inc 2013):

$$\begin{aligned} \nabla \cdot \left(\frac{1}{\rho_0} \nabla p \right) - \frac{1}{\rho_0 c^2} \frac{\partial^2 p}{\partial t^2} + \nabla \cdot \left[\frac{4\mu}{3\rho_0} \nabla \left(\frac{1}{\rho_0 c^2} \frac{\partial p}{\partial t} \right) \right] \\ = - \frac{\partial}{\partial t} \left(\frac{Q}{\rho_0} \right) + \nabla \cdot \left[\frac{4\mu}{3\rho_0} \nabla \left(\frac{Q}{\rho_0} \right) \right] \end{aligned} \quad (4.11)$$

where, ‘ ρ_0 ’ is the mean fluid density, ‘ c ’ is the speed of sound in a liquid medium, ‘ μ ’ is the dynamic viscosity and ‘ Q ’ is the mass source in the continuity equation. The finite element formulation corresponding to the acoustic wave equation is obtained using the Galerkin procedure (Bathe 2014). For this, Eq. (4.11) is multiplied by testing function ‘ w ’ and integrated over the volume of the domain. The normal velocity on the acoustic domain boundary is applied to yield the weak form of the Eq. (4.11). The spatial variation of pressure (p) and displacement (u) can be represented in terms of shape function as:

$$P = \{N\}^T \{p_e\} \quad (4.12)$$

$$u = \{N'\}^T \{u_e\} \quad (4.13)$$

where, the nodal components of pressure and displacement are represented by ‘ p_e ’ and ‘ u_e ’, respectively. ‘ $\{N\}$ ’ and ‘ $\{N'\}$ ’ are the element shape functions corresponding to the pressure and the displacement. Applying the second time derivative of the variables p and u in the weak form of Eq. (4.11), the finite element form of the wave can be expressed as:

$$\begin{aligned}
& \iiint_{\Omega_f} \frac{1}{\rho_0 c^2} \{N\} \{N\}^T dv \{\ddot{p}_e\} + \iiint_{\Omega_f} \frac{4\mu}{3\rho_0^2 c^2} [\nabla N]^T [\nabla N] dv \{\ddot{p}_e\} + \\
& \iiint_{\Omega_f} \frac{1}{\rho_0} [\nabla N]^T [\nabla N] dv \{p_e\} + \oint_{\Gamma_f} \{N\} \{n\}^T \{N'\}^T dS \{\ddot{u}_{e,f}\} \\
& = \iiint_{\Omega_f} \frac{1}{\rho_0} \{N\} \{N\}^T dv \{\dot{q}\} + \iiint_{\Omega_f} \frac{4\mu}{3\rho_0^2} [\nabla N]^T [\nabla N] dv \{q\}
\end{aligned} \tag{4.14}$$

where, ‘ dv ’ is the volume differential of the acoustic domain ‘ Ω_f ’, ‘ dS ’ is the surface differential of the acoustic domain boundary ‘ Γ_f ’, ‘ n ’ is the outward unit vector, and ‘ q ’ is the nodal mass source vector. The second time derivative of the nodal displacement of the fluid particles is represented by ‘ $\ddot{u}_{e,f}$ ’. Eq. (4.14) can be written in matrix form as analogous to the equation of motion as follows:

$$[M_f] \{\ddot{P}_e\} + [C_f] \{\dot{P}_e\} + [K_f] \{P_e\} + \bar{\rho}_0 [R]^T \{\ddot{u}_{e,f}\} = \{f_f\} \tag{4.15}$$

where,

$$[M_f] = \bar{\rho}_0 \iiint_{\Omega_f} \frac{1}{\rho_0 c^2} \{N\} \{N\}^T dv, \text{ acoustic fluid mass matrix} \tag{4.15.a}$$

$$[C_f] = \bar{\rho}_0 \iiint_{\Omega_f} \frac{4\mu}{3\rho_0^2 c^2} [\nabla N]^T [\nabla N] dv, \text{ fluid damping matrix} \tag{4.15.b}$$

$$[K_f] = \bar{\rho}_0 \iiint_{\Omega_f} \frac{1}{\rho_0} [\nabla N]^T [\nabla N] dv, \text{ fluid stiffness matrix} \tag{4.15.c}$$

$$[R]^T = \oint_{\Gamma_f} \{N\} \{n\}^T \{N'\}^T dS, \text{ fluid boundary matrix} \tag{4.15.d}$$

$$\{f_f\} = \bar{\rho}_0 \iiint_{\Omega_f} \frac{1}{\rho_0} \{N\} \{N\}^T dv \{\dot{q}\} + \bar{\rho}_0 \iiint_{\Omega_f} \frac{4\mu}{3\rho_0^2} [\nabla N]^T [\nabla N] dv \{q\}, \text{ fluid load vector} \tag{4.15.e}$$

where, the acoustic fluid mass density constant is represented by ' $\bar{\rho}_0$ '. The Fluid-structure interaction (FSI) effect is incorporated into the wave equation by using the kinetic conditions relating the solid stress to the fluid pressure imposed at the interface. For this, the load vector is separated into the fluid pressure load ' $\{f_f\}$ ' and the resultant of all other forces ' $\{f_s\}$ '. The present study simulated the liquid sloshing using a commercial CFD solver, Fluent. The FSI may be flagged by specifying the FSI label without a value on the fluid elements at the interface, which will couple the structural motion and fluid pressure at the interface. In this study, the structural parts, including the tank and the baffle plates, are discretized using SOLID187, which is a ten-node element with three degrees of freedom at each node. The liquid medium is discretized using FLUID220, which is a twenty-node acoustic element with four degrees of freedom at each node. Therefore, the FSI interface is automatically flagged because the acoustic elements are adjacent to solid structural elements (ANSYS 2012). The pressure-velocity coupling is done using the PISO (Pressure-Implicit with Splitting of Operators) algorithm.

The numerical modelling of the free surface is carried out by considering the Volume of Fluid (VOF) method. For this, two Eulerian phases are considered, and the distribution of liquid is computed for each cell by solving the following transport equation at each time step (Eswaran et al. 2009):

$$\frac{\partial(\alpha_v)}{\partial t} + v\nabla(\alpha_v) = 0 \quad (4.16)$$

where, ' α_v ' is the volume fraction and ' v ' is the velocity vector. Eq.(4.16) is solved using an explicit time discretization approach. In each cell, the computed volume fraction should satisfy the following equation (Thiagarajan et al. 2011):

$$\sum_{i=1}^n \alpha_{vi} = 1 \quad (4.17)$$

where, ‘ i ’ is the number of phases. The turbulence modelling is done using the standard k - ε model. Here, ‘ k ’ and ‘ ε ’ are the turbulence kinetic energy and the dissipation rate, respectively. It consists of two equations as follows (Launder and Spalding 1974):

$$\frac{\partial(\rho k)}{\partial t} + \nabla \cdot (\rho k v) = \nabla \cdot (\mu + \mu_t/\sigma_k) \nabla k + 2\mu_t \hat{S}\hat{S} - \rho\varepsilon \quad (4.18)$$

$$\frac{\partial(\rho\varepsilon)}{\partial t} + \nabla \cdot (\rho\varepsilon v) = \nabla \cdot (\mu + \mu_t/\sigma_\varepsilon) \nabla \varepsilon + (2C_{1\varepsilon}\mu_t\hat{S}\hat{S} - C_{2\varepsilon}\rho\varepsilon)\varepsilon/k \quad (4.19)$$

where, ‘ k ’ is the turbulence kinetic energy, ‘ \hat{S} ’ is the rate of deformation, and ‘ ε ’ is the dissipation rate. The turbulent viscosity ‘ μ_t ’ can be estimated as:

$$\mu_t = \rho C_\mu \frac{k^2}{\varepsilon} \quad (4.20)$$

In the case of standard k - ε model, the coefficients are as follows (Launder and Spalding 1974):

$$\sigma_k = 1, \sigma_\varepsilon = 1.3, C_{1\varepsilon} = 1.44, C_{2\varepsilon} = 1.92, C_\mu = 0.09.$$

Considering the Fluid pressure load at the interface along with the sloshing effects, the modified elemental equation of motion is expressed as:

$$([M_f] + [S_f])\ddot{p}_e + [C_f]\dot{p}_e + [K_f]p_e + \bar{\rho}_0[R]^T\ddot{u}_e = [f_f] \quad (4.21)$$

The subscript ‘ f ’ represents the acoustic fluid matrices. The matrix ‘ $[S_f]$ ’ is the acoustic sloshing mass. Considering the structural load at the interface, the dynamic elemental equation of the structure can be expressed as:

$$[M_S]\{\ddot{u}_e\} + [C_S]\{\dot{u}_e\} + [K_S]\{u_e\} - [R]\{p_e\} = \{f_S\} \quad (4.22)$$

The subscript ‘S’ corresponds to the compatible structural elements in the model. The complete assembled form of finite element discretized equation considering FSI conditions along with sloshing effects is obtained by combining Eq. (4.21) and Eq. (4.22) as:

$$\begin{aligned} \begin{bmatrix} [M_S] & 0 \\ \bar{\rho}_0[R]^T & [M_f] + [S_f] \end{bmatrix} \begin{Bmatrix} \{\dot{u}_e\} \\ \{\ddot{p}_e\} \end{Bmatrix} + \begin{bmatrix} [C_S] & 0 \\ 0 & [C_f] \end{bmatrix} \begin{Bmatrix} \{\dot{u}_e\} \\ \{\dot{p}_e\} \end{Bmatrix} + \begin{bmatrix} [K_S] & -[R] \\ 0 & [K_f] \end{bmatrix} \begin{Bmatrix} \{u_e\} \\ \{p_e\} \end{Bmatrix} \\ = \begin{Bmatrix} \{f_s\} \\ \{f_f\} \end{Bmatrix} \end{aligned} \quad (4.23)$$

4.3 MODAL ANALYSIS OF LIQUID STORAGE TANKS

4.3.1. Dynamic characteristics of cylindrical tanks

The study of dynamic characteristics is a prerequisite for understanding the dynamic behaviour of liquid tanks under seismic loading. Therefore, different parameters that may influence the frequency characteristics of cylindrical liquid tanks are analysed by generating 560 three-dimensional finite element models of liquid tanks. These models are developed by varying the aspect ratio (H/D), the thickness of the tank wall (t_w), Young’s modulus of material (E), depth of liquid (h) and the density of the liquid (ρ). The range and the interval of these parameters are selected based on the general design guidelines as per the Indian standards and the total computation time. The study considered liquid tank models with a height of 8 m and a full depth of liquid of 7 m, as shown in Fig. 4.2. The analysis is carried out on the tank models with an aspect ratio ranging from 0.1 to 1.9. The thickness of the tank wall is varied from 0.3 m, 0.4 m and 0.5 m for all the models. The material properties assigned for the models are given in Table. 4.1.

The depth of liquid is varied as the multiple of $1/6^{\text{th}}$ of fully filled condition. The modulus of elasticity for concrete is taken as $5000\sqrt{f_{ck}}$ (IS 456 2000), where f_{ck} is characteristic compressive strength. Poisson’s ratio is taken as 0.15.

Table. 4.1. Material properties

Grade of concrete	M30, M40
Density and Poisson's ratio of concrete	2500 kg/m ³ and 0.15
Density of liquid	Water: 1000 kg/m ³ , Petrol: 748.9 kg/m ³ and Mercury: 13590 kg/m ³

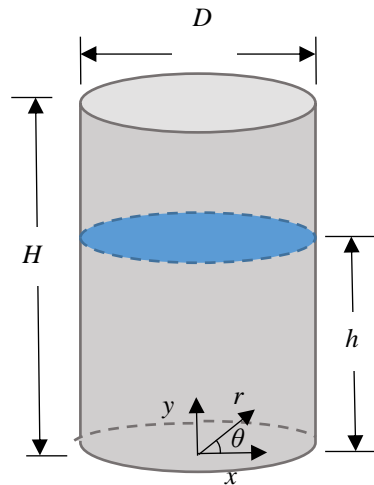


Fig. 4.2 Geometry of circular tank.

A detailed parametric study is carried out considering the aspect ratio (H/D), the thickness of the tank wall (t_w), Young's modulus of material (E), depth of liquid (h) and density of the liquid (ρ) as the parameters. An average deviation of 30% was observed for the impulsive frequency values estimated based on IS1893(Part2):2014, ACI350.3 and Eurocode-8 compared to the finite element results obtained using ANSYS Mechanical APDL software. However, the convective frequency values are found to be in good agreement with those obtained based on codal provisions. Therefore, the study further focused on the impulsive frequency of cylindrical tanks. Accordingly, in the further sections, the impulsive frequency is simply mentioned as frequency only. Also, the codes

of practices are represented as IS, ACI and EN8, corresponding to IS1893(Part2):2014, ACI350.3 and Eurocode-8, respectively. The formulae given in these standard codes of practice for the estimation of natural period of the liquid tanks are tabulated in Table. 4.2.

Table. 4.2. Formulae for natural period of liquid tanks

Sl. No.	International code	*Natural period (T_0)	
		Impulsive mode	Convective mode
1	IS1893(Part2):2014	$C_i \frac{h\sqrt{\rho}}{\sqrt{t/D} \sqrt{E}}$ where, ' C_i ' is the coefficient of time period for impulsive mode.	$C_c \sqrt{\frac{D}{\rho}}$ where, ' C_c ' is the coefficient of time period for convective mode.
2	ACI 350.3	$\frac{2\pi}{\omega_i}$ where, $\omega_i = C_l \times \frac{1}{h} \sqrt{\frac{10^3 E}{\rho_c}}$ where, ' C_l ' is the coefficient to determine the natural frequency and ' ρ_c ' is the mass density of concrete.	$\frac{2\pi}{\omega_c}$ where, $\omega_c = \frac{\lambda}{\sqrt{D}}$ $\lambda = \sqrt{3.68g \tanh [3.68(h/D)]}$
3	Eurocode-8	$C_i \frac{\sqrt{\rho} h}{\sqrt{s/R} \sqrt{E}}$ where 's' is the equivalent uniform thickness of tank wall.	$C_c \sqrt{R}$

*Natural period (T_0) = $1/f$, where ' f ' is the natural frequency in Hz.

The major assumptions made for the study are as follows:

- The origin is located at the top of the tank, confirming symmetry about yz and yx planes (with y -axis upwards).
- The base of the tank models is assumed to be rigidly restrained in all directions.
- The height of the tank is kept constant for all the models.
- The full depth of liquid is considered to be 7 m.
- The impulsive mode shapes considered are of the cantilever type.

The whole domain of the liquid tank is discretised using 4-noded SHELL181 and 8-noded FLUID30 elements. The mesh size of each model is finalised based on the mesh convergence test with a maximum and a minimum number of elements as 286457 and 1024. The fluid-structure interface is included in the models by applying the FSI label for the fluid element at the interface. The impulsive components of response can be obtained by applying the conditions for pressure at the free surface instead of the FREE flag. The modal analysis is carried out using the unsymmetric mode extraction method because the modelling of the tanks is done considering the coupling between the elements. The natural frequency values for all the models are noted based on the participation factor and mode shapes. All the impulsive mode shapes considered are of cantilever type modes corresponding to the circumferential wave number equal to 1. These types of modes do not alter the cross-section of the tank while vibrating.

A database is developed with all the parameters considered for the parametric study, the frequencies obtained from FEA and using formulae given in the International codes of practice. This database is further analysed using SPSS software by carrying out Artificial Neural Network (ANN) simulation and nonlinear regression analysis to assess the contribution of different parameters in the frequency. 70% of the data was used for training the model, and the rest of the randomly selected 30% of data was kept for testing. The study developed coefficients ' α ' and ' β ', and the prediction equations are established for

the estimation of the impulsive frequency of cylindrical tanks by augmenting the existing equations in standard codes with the missing parameters.

4.3.2 Dynamic characteristics of rectangular tanks

The frequency characteristics of rectangular liquid tanks are analysed by generating finite element models of the tank with and without baffle plates. For this, a three-dimensional rectangular tank of length (L) of 20 m and breadth (B) of 10 m is considered. The height of the tank wall (H) is considered to be 5 m. The depth of liquid (h) is 4 m. The baffle plates are assumed to be of the surface-mounted type with a height of 4 m, which is installed at 0.5 m above the bottom of the tank. The frequency characteristics are analysed for the tank models with single as well as multiple baffle plates of with and without perforations. The perforated baffle plates are generated with perforations in the range of 5% to 30%.

The tank structure is generated by using concrete material with a density of 2500 kg/m³ and Poisson's ratio of 0.15. The finite element modelling is done by using SOLID187 elements for the tank structure and FLUID220 elements for the liquid medium. The modal analysis is carried out on the generated liquid tank models, and the frequency values are observed under the first three modes of vibration, considering impulsive and convective conditions. The tank models are designated as ' $T_{\%}^{b_n}$ ', where ' b_n ' is the number of baffle plates, represented as tally marks, and '%' is the percentage of perforation of the baffle plate.

4.4 DEVELOPMENT OF AN EFFECTIVE CONFIGURATION OF PERFORATED BAFFLE PLATE

Considering the need for an effective anti-slosh device, a detailed methodology is developed based on the following assumptions.

- The origin is located at the top of the tank, confirming symmetry about yz and yx planes (with y -axis upwards).

- The base of the tank models is assumed to be rigidly restrained in all directions.
- Baffle plates are modelled as thin rigid structural element, attached to the walls of the tank.
- Size of the baffle plates are kept constant.
- The perforations are circular in shape.

4.4.1. Analysis of geometric configuration of perforated baffle plates under seismic ground motion

The effect of the geometric configuration of the perforated baffle plate on the slosh response of a rectangular tank is studied by considering the vertical perforated baffle plate as the anti-slosh element. A three-dimensional rectangular tank of length (L) of 20 m and width (B) of 10 m is considered for the study, as shown in Fig. 4.3(a). The height of the tank wall (H) is considered to be 5 m. The depth of liquid (h) is 4 m. The bottom of the tank is assumed to be rigidly restrained in all directions. The reference frame is assumed to be located at the free surface, confirming symmetry about zx and zy planes. Water is considered as the filled liquid with a density of 1000 kg/m^3 and a bulk modulus of 2.2 GPa. The probes are located at point-a and point-b, where the slosh responses are measured in terms of elevation of sloshing surface and hydrodynamic pressure, respectively.

The study is carried out considering single as well as multiple vertical baffle plates with and without perforations. The liquid tank models used for the analysis are given in Table.4.3. The baffle plates are modelled as a wall with a height of 4 m. The bottom of the baffle plates is kept 0.5 m above the rigid base of the tank. A general layout of the perforated baffle plate is shown in Fig. 4.3(b). The perforations are made about the geometric centre of the baffle plate. The dimension and the vertical position of the baffle plate are selected based on the previously reported studies (Akyildiz 2012; Jung et al. 2012; Hasheminejad et al. 2014; Nayak and Biswal 2015). The dynamic response of the liquid medium is simulated by carrying out the pressure-based transient analysis using the VOF

model. ANSYS Fluent (Livaoglu et al. 2012) is used as the solver for the dynamic analysis. The earthquake records can be classified into three categories based on the ratio of peak ground acceleration to peak ground velocity, namely; low ($PGA/PGV < 0.8$), intermediate ($0.8 < PGA/PGV < 1.2$) and high ($PGA/PGV > 1.2$) (Tso et al. 1992; Nayak 2013). The present study is carried out under three earthquake motions, namely; Imperial Valley (1979), El Centro (1940) and Kobe (1995) corresponding to low ($PGA/PGV = 0.476 \text{ g-sec-m}^{-1}$), intermediate ($PGA/PGV = 0.883 \text{ g-sec-m}^{-1}$) and high frequency ranges ($PGA/PGV = 1.245 \text{ g-sec-m}^{-1}$), respectively. All the earthquake records are scaled to a PGA value of 0.3 g. The acceleration time history records of these three ground motions for 15 sec are shown in Fig. 4.4. The details of ground motion records are tabulated in Table 4.4.

Initially, the study analysed the slosh response of a rectangular tank fitted with a single vertical baffle plate. The effectiveness of perforated plates to control the slosh response is observed by considering the percentage of perforation of the baffle plate, clear spacing of the perforations and the offset distance of the perforated baffle plate as the parameters. At first, the slosh response of the unbaffled tank is studied under the three ground motions considered. Subsequently, a vertical baffle plate with the percentage of perforation in the range of 5% to 35% is installed in the middle of the tank. After determining the optimum range of perforation, the effect of clear spacing of perforations (b) on the slosh response is investigated. The slosh responses of these tank models are compared with that of the unbaffled tank as well. Additionally, the changes in the slosh response under different horizontal positions of the perforated baffle plate are observed by varying the offset distance of the baffle plate as the ratio of $x_w/l = 0.2$ to 1, where ' x_w ' represents the horizontal distance or the offset distance of the baffle plate from the left wall, and ' l ' is half the length of the tank wall, parallel to the ground motion.

Table. 4.3. Models generated for seismic analysis

Tank with single baffle plate		Tank with multiple baffle plates	
Name of model	Percentage of perforations (%)	Name of model	Percentage of perforations (%)
T	0	T	0
T'_0	0	T'''_0	0
T'_{10}	10	T'''_5	5
T'_{15}	15	T'''_{10}	10
T'_{17}	17	T'''_{11}	11
T'_{20}	20	T'''_{12}	12
T'_{25}	25	T'''_{13}	13
T'_{30}	30	T'''_{14}	14
T'_{35}	35	T'''_{15}	15
-	-	T'''_{16}	16
-	-	T'''_{17}	17
-	-	T'''_{18}	18
-	-	T'''_{19}	19
-	-	T'''_{20}	20
-	-	T'''_{25}	25
-	-	Case 1	17 (Centrally aligned)
-	-	Case 2	17 (Centrally aligned on the upper half)
-	-	Case 3	17 (Left aligned on the upper half)
-	-	Case 4	17 (Right aligned on the upper half)
-	-	Case 5	17 (Alternate arrangement of case 3 and case 4)
-	-	Case 5a	15(Alternate arrangement of case 3 and case 4)
-	-	Case 5b	10(Alternate arrangement of case 3 and case 4)
-	-	Case 5c	5 (Alternate arrangement of case 3 and case 4)

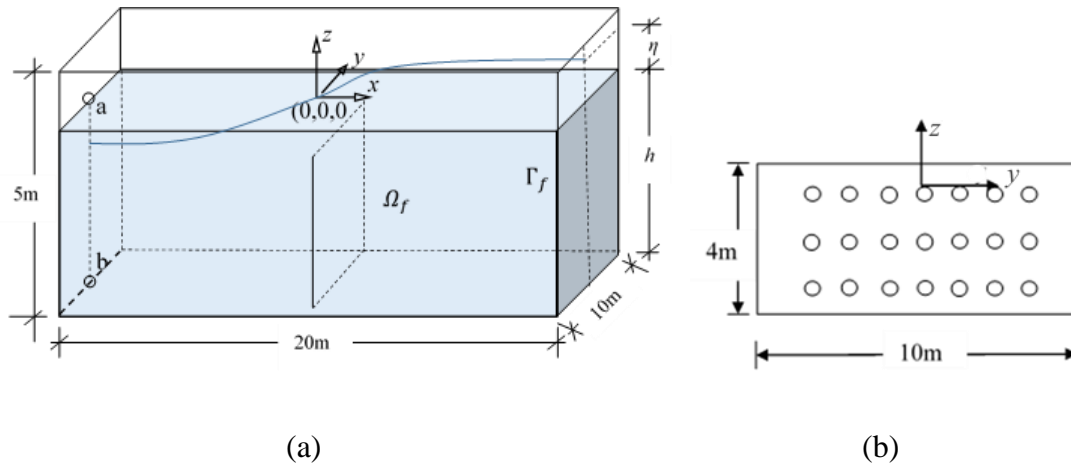


Fig. 4.3 Geometric configuration of (a) tank (b) 15% perforated baffle plate.

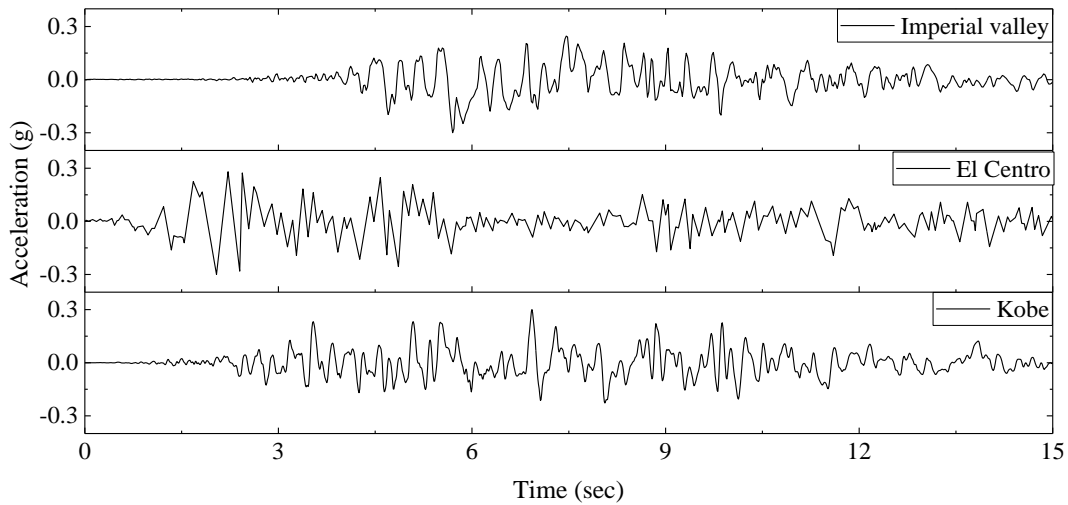


Fig. 4.4 Time history records of ground motions.

Table. 4.4. Details of ground motion records used

Name of Earthquake (Year)	Recording Station	Component
Imperial Valley (1979)	Holtville post office	S45W
El Centro (1940)	El Centro, California	S00E
Kobe (1995)	Kakogawa, Japan	CUE90

Later, the slosh responses of the rectangular tank with multiple baffle plates are investigated by considering the parameters such as the percentage of perforations and alignment of perforations, which are the major influencing parameters of the slosh suppression mechanism of the perforated baffle plates (Chen et al. 2016; Bellezi et al. 2019). In this case, the study considered three baffle plates with percentage of perforations ranging from 5% to 25%. Based on the alignment of perforations, the tank models are categorised into five cases as shown in Fig. 4.5. Different cases of perforations considered are; case 1: Centrally aligned, case 2: Centrally aligned on the upper half, case 3: Left aligned on the upper half, case 4: Right aligned on the upper half, case 5: Alternate arrangement of case 3 and case 4.

4.4.1.1 Mesh convergence study

In order to establish the numerical accuracy of the simulation, the mesh convergence study is conducted for all the models with different configurations of the perforated baffle plate. A representative sketch showing the mesh convergence in terms of the free surface elevation of the tank model fitted with a 15% perforated baffle plate under El Centro ground motion, measured at point-a, is shown in Fig. 4.6. Considering the finer mesh as the basis, the percentage error was estimated as 1.53%, 3.44% and 9.28%, corresponding to the element sizes of 0.11 m, 0.12 m and 0.13 m, respectively. Therefore, further study is carried out for the tank models by considering a mesh size of 0.12 m.

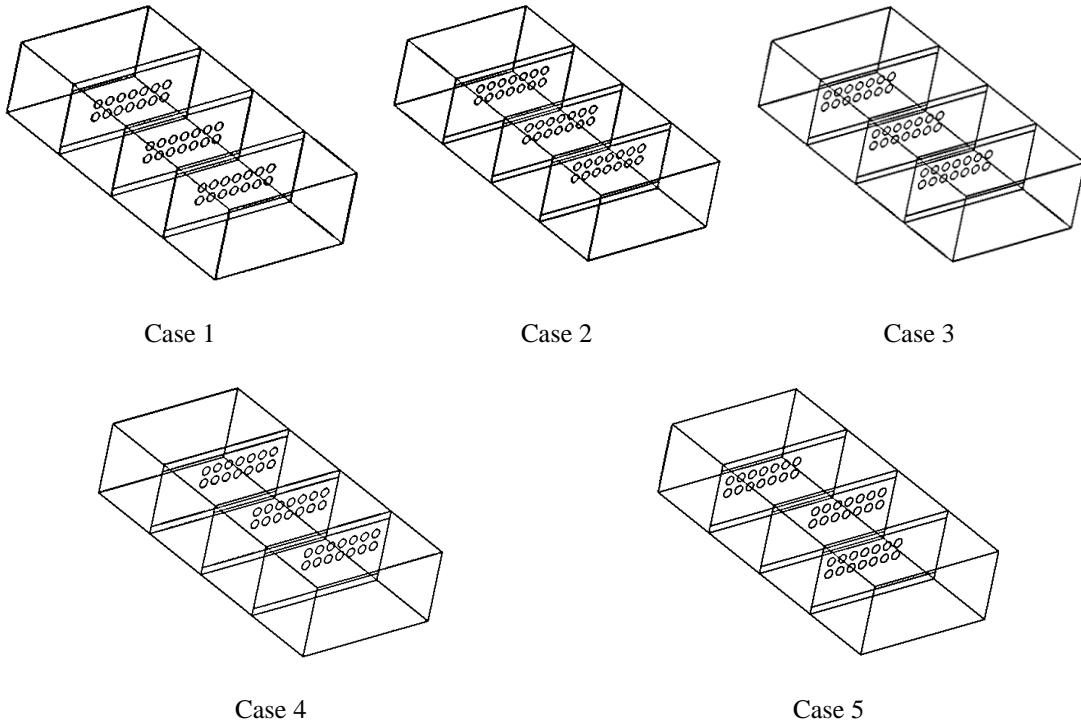


Fig. 4.5 Different alignment of perforations analysed under seismic ground motions.

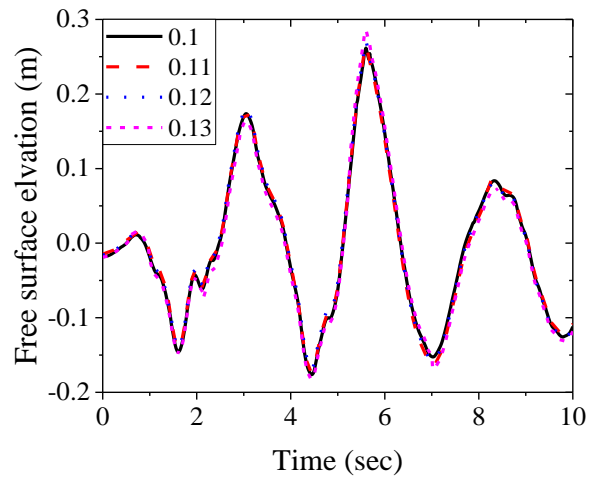


Fig. 4.6 Mesh convergence in terms of free surface elevation under seismic ground motion.

4.4.2. Analysis of geometric configuration of perforated baffle plates under pitch excitation

The study investigates the slosh response of the liquid medium in a rectangular tank with a plan area of 0.4 m x 0.2 m. The height of the tank (H) is considered to be 0.4 m with a varying fill depth of liquid (h). The tank is assumed to be fixed at the bottom. Two vertical baffle plates are installed symmetrically at the centre of the tank, as shown in Fig. 4.7(a), to damp the slosh response. The liquid tank models used for the analysis are given in Table. 4.5.

The dimensions of the baffle plates are 0.2mx0.2m, which are assumed to be invariable. The total length of the tank (L) can be expressed as; $L= x_b+2x_w$, where ' x_b ' is the distance between the baffle plates and ' x_w ' is the distance of the baffle plate from the tank wall. The vertical distance of the base of the baffle plate from the base of the tank is represented as ' z_b '. The slosh response of a rectangular tank under pitch excitation is analysed to investigate the slosh damping caused by the perforated baffle plates of various configurations considered. For this, a rectangular tank of given geometry is subjected to a pitch excitation of $\theta(t) = \theta_0 \sin \omega t$. Here ' θ_0 ' is the amplitude of excitation, which is taken as 8° . The excitation frequency ' ω ' is considered to be equal to the natural frequency of the liquid (ω_n), which is calculated as (Faltinsen and Timokha 2009):

$$\omega_n^2 = g \frac{n\pi}{L} \tanh\left(\frac{n\pi}{L} h\right) \quad (4.24)$$

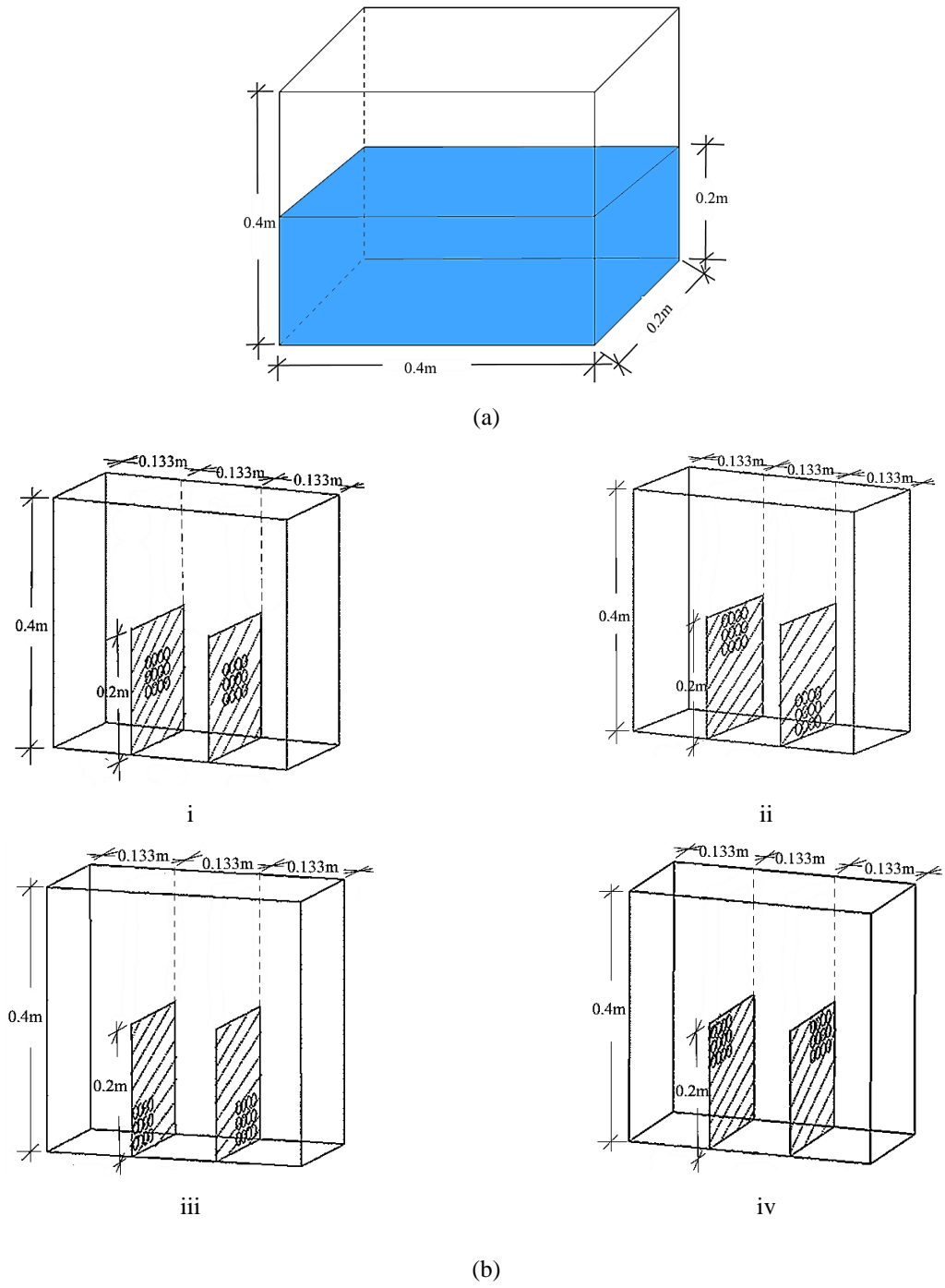


**Fig. 4.7 Model details (a) Geometry of liquid tank with baffle plate
 (b) Alignment of perforations (i) Case 1 (ii) Case 2 (iii) Case 3 (iv) case 4.**

Table. 4.5. Models generated for analysis under pitch excitation

Name of model	No. of baffle plates	Percentage of perforations (%)
T	0	0
T''_0	2	0
T''_5	2	5
T''_{10}	2	10
T''_{15}	2	15
T''_{20}	2	20
T''_{25}	2	25
T''_{30}	2	30
Case 1	2	10 (Baffle plates with central perforations)
Case 2	2	10 (Successive baffle plates with top and bottom aligned central perforations)
Case 3	2	10 (Successive baffle plates with left and right aligned perforations at the bottom)
Case 4	2	10 (Successive baffle plates with left and right aligned perforations at the top)
Case 4 (5%)	2	5 (Successive baffle plates with left and right aligned perforations at the top)

where ‘ g ’ is the acceleration due to gravity, and ‘ n ’ is the mode number. To develop an effective configuration of the perforated baffle plate, a detailed parametric study is carried out, and variations in the slosh responses are observed under convective and impulsive modes. The area of perforations, inter perforation distance, size of the perforations, the distance between the perforated baffle plates, alignment of perforations, and the vertical position of the perforated baffle plate are considered as the parameters of the study. The effects of these parameters are investigated considering the fill depth of liquid as 0.2 m. Correspondingly, the frequency of the liquid for the first mode ($n=1$) is calculated as 8.403 rad/sec, which is taken as the excitation frequency.

The simulation is carried out for 15 sec. Different configurations of perforated baffle plates with respect to the alignment of perforations are given in Fig. 4.7(b). Here, four different configurations of perforated baffle plates are depicted as case 1: baffle plates with central perforations; case 2: successive baffle plates with top and bottom aligned central perforations; case 3: successive baffle plates with left and right aligned perforations at the bottom; case 4: successive baffle plates with left and right aligned perforations at the top. Additionally, the effects of fill depth of liquid, frequency and amplitude of input motion on the slosh response are also analysed. The responses of the liquid are observed in terms of free surface elevation, hydrodynamic pressure, turbulence kinetic energy, velocity streamlines, power spectral density, and free surface deformation.

4.4.2.1 Mesh convergence study

The mesh convergence study is carried out on all the tank models with different configurations of baffle plates. Different models are generated by varying the mesh size of the elements. Pressure-based transient analysis is carried out for 15 sec by applying a pitch excitation of $\theta(t) = \theta_0 \sin\omega t$. The amplitude of excitation is kept equal to 8° , with the excitation frequency being equal to the natural frequency of the liquid. A representative mesh convergence study on a tank model with a 10% perforated baffle plate having centrally oriented perforations is shown in Fig. 4.8, in terms of free surface elevation, measured at point (-0.2, 0, 0). Based on the finer mesh (0.004 m), percentage deviations of the peak values of the free surface elevations are calculated as 0.77%, 4.65%, and 9.95%, corresponding to the element sizes of 0.005 m, 0.006 m, and 0.007 m, respectively. Therefore, further study is carried out on this model by keeping the mesh size as 0.006 m, which is adequate to depict the slosh responses at required points with minimum computational time.

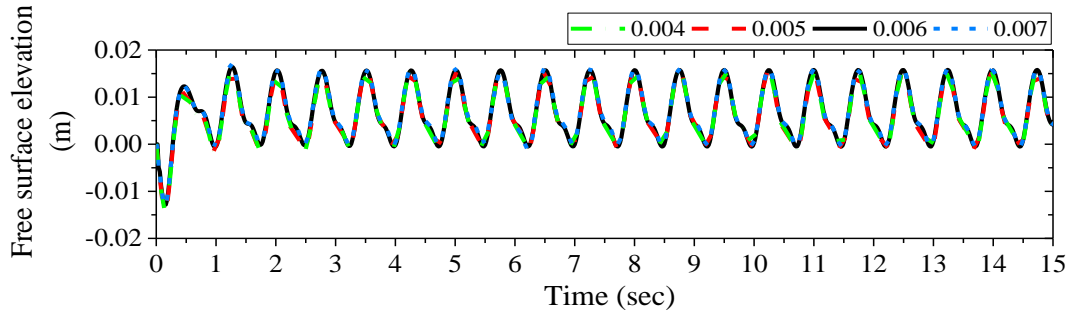


Fig. 4.8 Mesh convergence in terms of free surface elevation under pitch excitation.

4.4.2.2 Validation of numerical procedure

The simulation procedure adopted for solving the liquid sloshing is validated considering the experimental work conducted by Xue and Lin (2011). Among all the different models considered in this work, the experimental model shown in Fig. 4.9 is used for validation, in addition to an un baffled tank model. The models are subjected to an external harmonic load of $x = -a \cos \omega t$, where $a = 0.1$ m and $\omega = 3.5317$ rad/sec. The water depth is considered to be 0.18 m for both models.

The natural frequency of the tank model without the baffle plate is 6.4029 rad/sec (Xue and Lin 2011). The modal acoustic analysis of the corresponding finite element model resulted in a natural frequency of 6.4276 rad/sec, which is in close agreement with the natural frequency of the experimental model given in the reference work. Additionally, the transient analysis is carried out considering the pressure-based solver for the same liquid tank model. A reduction of 55% is observed in the free surface elevation of the liquid medium with the introduction of a vertical baffle plate. A similar reduction was also reported in the experimental results of Xue and Lin (2011), which is shown in Fig. 4.10. The trend of the numerical simulation results is in close agreement with the experimental results in terms of both amplitude and phase.

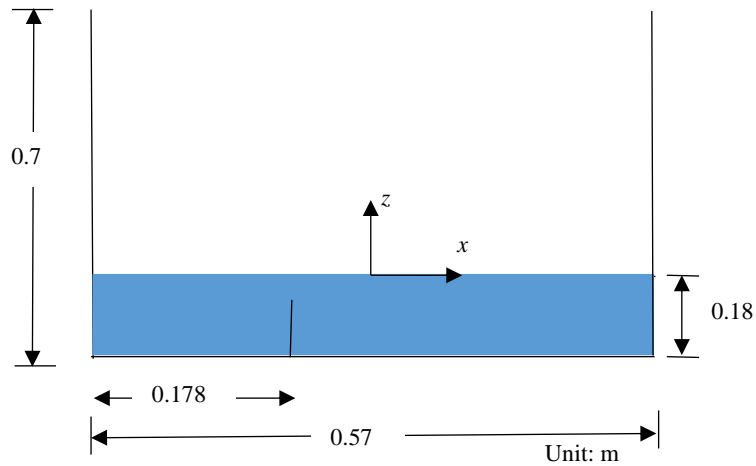


Fig. 4.9 Configuration of liquid tank model based on Xue and Lin (2011).

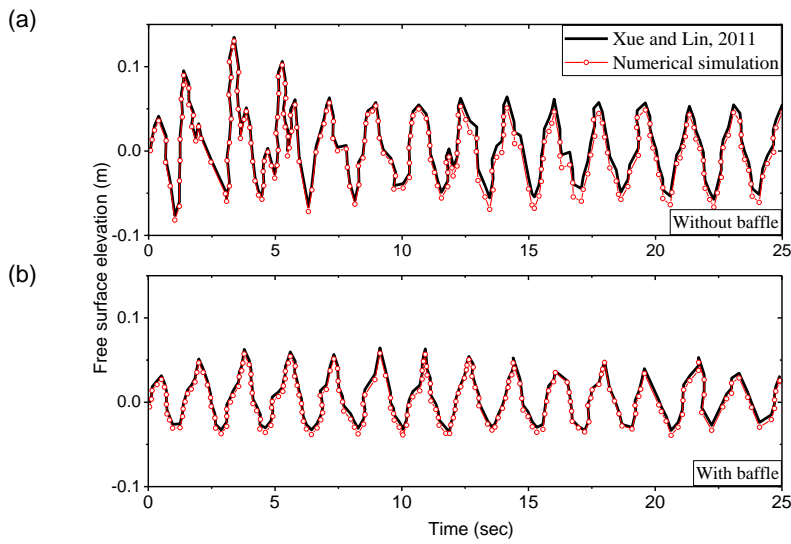


Fig. 4.10 Comparison of numerical results with experimental data from Xue and Lin (2011) (at $x=-0.275$ m).

Subsequently, the validation of the numerical simulation procedure is carried out in terms of pressure response by considering the experimental data obtained from Xue et al. (2012). The line sketch of the tank model generated for the numerical validation is shown in Fig.

4.11. The tank model is equipped with a vertical baffle plate with a square orifice of the length of 80 mm. The depth of liquid is assumed as 280 mm.

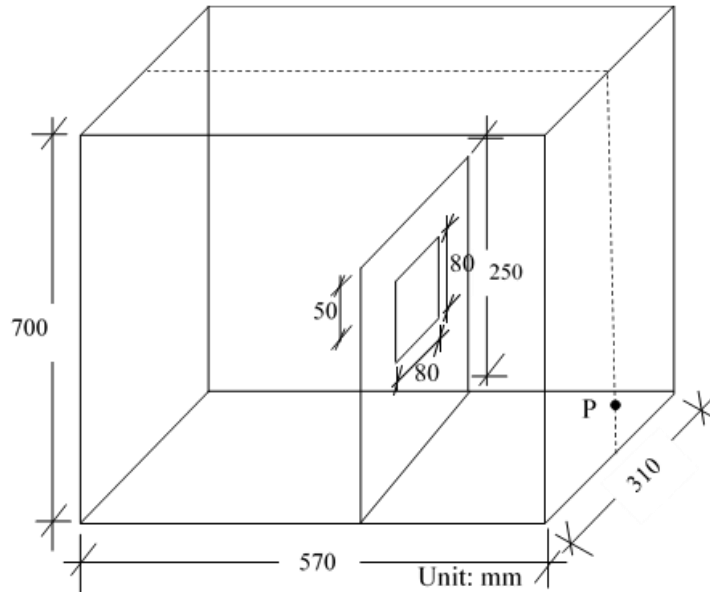
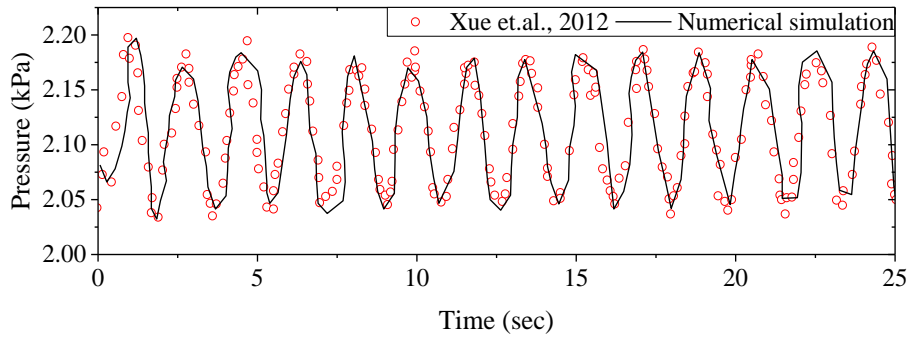
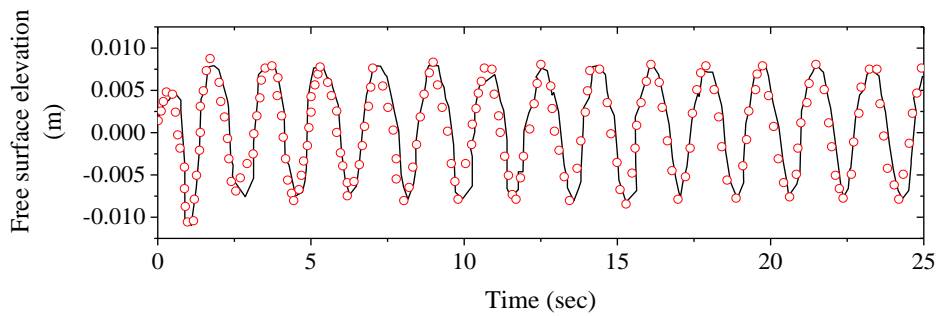


Fig. 4.11 Geometric details of validation model (based on Xue et al. 2012).

The natural frequency of the tank model is calculated as 7.0247 rad/sec using Eq. (4.24). The tank model is excited with surge oscillations; $x = -a \cos \omega t$; where ‘ a ’ and ‘ ω ’ are assumed as 15 mm and $0.5\omega_0$, respectively. 3D grid is generated for the numerical model with the mesh size of $\Delta x = \Delta y = 5 \text{ mm}$ and $\Delta z = 2 \text{ mm}$. The hydrodynamic pressure at the probe, P on the wall (located at 65 mm above the bottom of the tank) is compared with that of experimental results, as shown in Fig. 4.12(a). Additionally, the free surface elevation measured at a wave gauge (located at 10 mm away from the left tank wall) is shown in Fig. 4.12(b). The numerical results are in good agreement with the experimental data. Therefore, the numerical procedure adopted in this study is capable of simulating the slosh response of a rectangular tank with vertical baffle plates, considering the nonlinearity caused by the free surface boundary conditions.



(a)



(b)

Fig. 4.12 Validation of numerical simulation based on experimental data from Xue et al. 2012 (a) Hydrodynamic pressure (b) Free surface elevation.

4.4.3 Experimental evaluation of developed configuration of perforated baffle plate

The experimental evaluation is carried out by conducting a shake table test on a rectangular tank with and without baffle plates. The length, width and height of the tank model are 0.4 m, 0.2 m and 0.4 m, respectively. The baffle plates with a height of 0.3 m and a width of 0.2 m are used for the study. The tank and the baffle plates are fabricated with plexiglass material of 10 mm thickness. Three uniformly spaced vertical slits are made to ensure the seating of baffle plates in the tank. Water is considered as the filled liquid with a depth of 0.2 m. The experiments are carried out by introducing solid as well as perforated baffle

plates in the tank. The study used centrally perforated baffle plates with perforations of 5%, 10% and 15% in addition to the developed configuration of the perforated baffle plate. The perforated baffle plates with the zig-zag blocking alignment of perforations are fabricated with 5% perforations. The model details are given in Table. 4.6.

The test setup consists of a shake table with a cylindrical cam arrangement, shake table control panel, datalogger, sensors and necessary DC power supplies, as shown in Fig. 4.13.

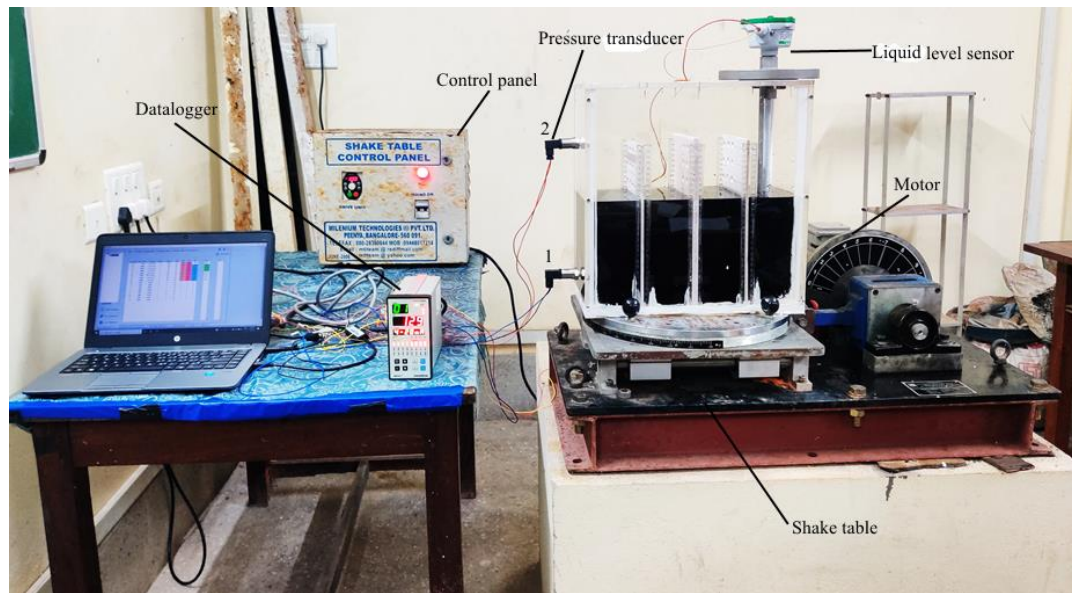


Fig. 4.13 Test setup.

Table. 4.6. Models fabricated for experimental study

Name of model	No. of baffle plates	Percentage of perforations (%)
T	0	0
T_0'''	3	0
T_5'''	3	5
T_{10}'''	3	10
T_{15}'''	3	15
$T_{5-zig-zag}'''$	3	5 (Zig-zag blocking alignment)

A horizontal shake table of 30 kg payload capacity with a maximum amplitude of motion of 10 mm is employed for the study. The shake table control panel enable to adjust the frequency of excitation of the shake table. Data logging is enabled using a Masibus make 8-channel scanner of model 85XX+. The tank is rigidly fixed on the shake table, which can be moved to and fro in the horizontal direction by a motor. Two pressure transducers are fitted at the height of 0.05 m and 0.3 m from the bottom of the tank. A liquid level transmitter is placed at a distance of 0.06 m from the right tank wall. Input configuration is done for 4-20 mA to enable data logging. The frequency of excitation is kept at 1.7 Hz. The amplitudes of motion of the shake table considered are 5 mm and 10 mm. The slosh responses are measured in terms of pressure and free surface elevation.

4.5 SUMMARY

The methodology followed for the development of an anti-slosh mechanism that damp the slosh response effectively is detailed in this chapter. The geometric configurations of the liquid tank models and the details of external excitations to evaluate the sloshing response primarily in terms of free surface elevation and the hydrodynamic pressure are elaborated. The test setup for the investigation of the developed configuration of the perforated baffle plate is explained as well, along with a detailed experimental procedure.

CHAPTER 5

MODAL ANALYSIS OF LIQUID STORAGE TANKS

5.1 GENERAL

The dynamic characteristic is a significant factor that affects the behaviour of a liquid tank under seismic excitation. Therefore, accurate quantification of the fundamental frequency of a liquid storage tank is of prime importance. However, the studies validating the accuracy of the currently used frequency estimation methods of liquid tanks are found to be less. This chapter deals with the numerical analysis of dynamic characteristics of liquid tanks and its comparison with the current codes of practices.

5.2 DYNAMIC CHARACTERISTICS OF CYLINDRICAL TANKS

A parametric study has been conducted to evaluate the effects of the aspect ratio of the tank, depth of liquid, the thickness of the tank wall, the density of the filled liquid and the material property of the tank structure on the free vibration characteristics of the cylindrical liquid tanks.

5.2.1 Effect of aspect ratio of the tank

The fundamental frequency values of tanks made of M30 grade concrete for different aspect ratios are shown in Fig. 5.1(a) for various liquid depth conditions. It is evident from the figure that the natural frequency of the system is directly proportional to the aspect ratio of the tank. In particular, for the tanks having an aspect ratio of 0.9 and below, the increase in the frequency values with an increase in the aspect ratio is significant. This fact is clear in the case of the tank with an aspect ratio of 0.3, which has a maximum increase of 2.96 times in the frequency value as compared to the tank with an aspect ratio of 0.1. The effect of an increase in liquid depth up to half-filled conditions is to decrease the frequency of the tank, which is significant for the tank with an aspect ratio of 1.0 and below. This reduction

in frequency value is more evident for the tank with an aspect ratio of 0.5 with a maximum reduction of 39%. An increase in liquid depth above the half-filled level has less effect on the frequency of the liquid tank. The liquid tanks with an aspect ratio above 1.0 show a slight increment (<10%) in the frequency values for the increase in the aspect ratio. Also, the variation of frequency values with an increase in the liquid depth for these tanks is a smooth curve.

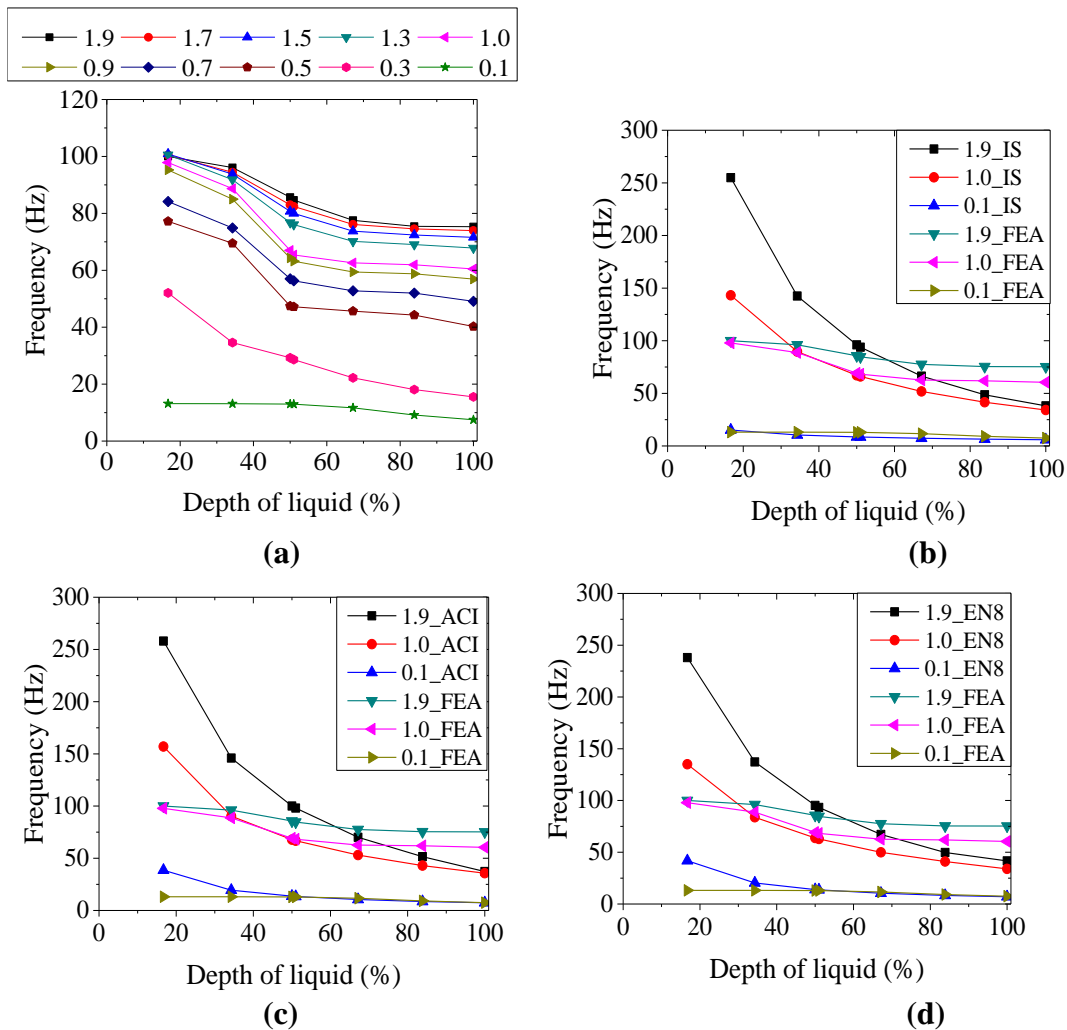


Fig. 5.1 (a) Variation of frequency with aspect ratio; Comparison of frequency for different aspect ratio (b) FEA and IS (c) FEA and ACI (d) FEA and EN8.

Fig. 5.1 (b), (c) and (d) show the representative comparison of the fundamental frequency of the liquid tanks with aspect ratios of 1.9, 1.0 and 0.1 obtained from FE analysis with the equivalent values obtained using the International codes, namely IS, ACI and EN8. In these figures, 1.9_IS, 1.9_ACI, 1.9_EN8, and 1.9_FEA represent the variation of frequency for a liquid tank with an aspect ratio of 1.9, obtained based on IS, ACI, EN8 and FE analysis, respectively. Similarly, the variation of frequency of the tanks with aspect ratios of 1.0 and 0.1 are also depicted in the corresponding figures.

The expressions for fundamental frequency given in all the three codes of practice overestimate the frequency values up to the half-filled condition and then underestimate these values thereafter till the fully-filled condition, except for the tanks with the lowest aspect ratio. Considering the liquid tank with an aspect ratio of 1.9, all the three international codes of practice overestimate the fundamental frequency value by more than 1.5 times than that value obtained from FE analysis at the lowest liquid depth condition. This implies the presence of more number of internal modes which are omitted by the codes of practice. At fully-filled condition, these codes of practice underestimate the frequency value by 50%. However, at the half-filled condition, the frequency values estimated based on both the codes of practice and the FE analysis tend to match. In the case of the tanks with an aspect ratio of 0.1, the natural frequency values are found to be in good comparison with the values based on IS irrespective of liquid depths, whereas the natural frequencies match well with ACI and EN8 based values for 1/3rd fill condition and more. However, ACI and EN8 values show a variation of more than 1.9 times in the natural frequency values for lower liquid depth conditions. The general trend of variation in frequency values for tanks with the other seven aspect ratios in the range of 0.1 to 1.9 is found to be the same as that of frequency values observed for tanks having aspect ratios 0.1, 1.0 and 1.9. The same procedure was followed for the tank models generated using M40 grade of concrete also. The trend lines of frequency of these models also fall in line with that of models generated using M30 grade of concrete. The general pattern of these frequencies demarcates the models with an aspect ratio below 1.0, which shows more increment in the frequency values with an increase in the aspect ratio. It is worth noting that the aspect ratio

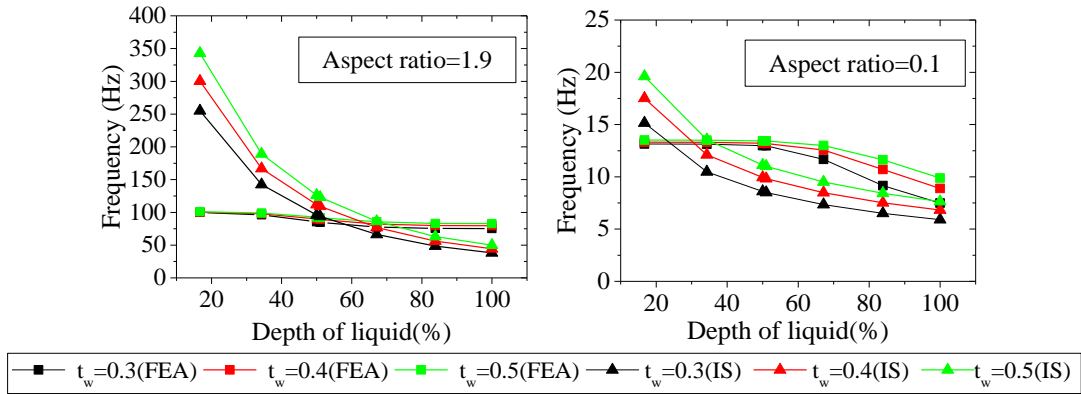
of a tank is a major factor that affects the frequency characteristics of the liquid-tank system. The codal formulae are reliable for a tank of the aspect ratio of 0.1 when filled to 1/3rd or more.

5.2.2 Effect of thickness of tank wall

The frequency values of FE models with different wall thicknesses of 0.3 m, 0.4 m and 0.5 m are compared with those obtained based on standard codal provisions in Fig. 5.2 for the tanks with an aspect ratio of 1.9 and 0.1.

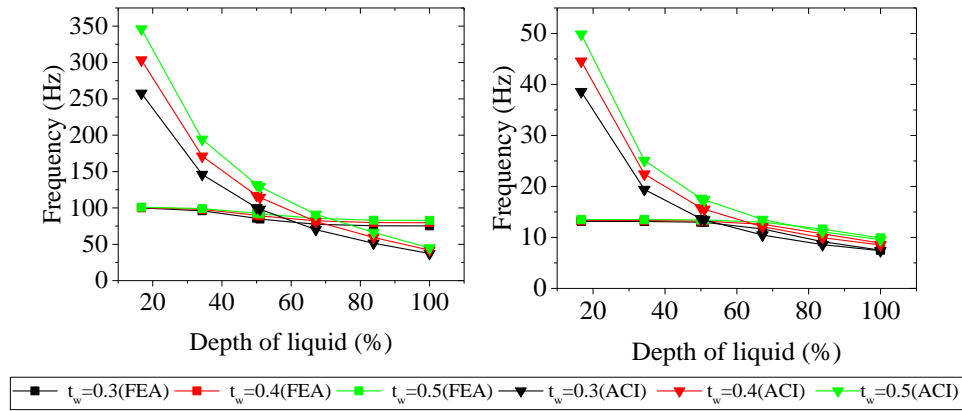
In the figure, the curves 1.9_0.3, 1.9_0.4 and 1.9_0.5 represent the frequency values of tanks with an aspect ratio of 1.9 and thickness of 0.3 m, 0.4 m and 0.5 m, respectively. Similarly, the frequency values of tanks with aspect ratio 0.1 and thickness 0.3 m, 0.4 m and 0.5 m are represented by 0.1_0.3, 0.1_0.4, 0.1_0.5 respectively. From the graph, it is evident that the frequency values are directly proportional to the thickness of the tank wall. For the liquid depth up to 25% of the full tank depth, the increase in the frequency with the thickness of the tank wall is negligible. Similarly, the tanks with other aspect ratios in the given range were also analysed, and a similar trend is observed for all the models.

A maximum deviation of 60% is observed from the code-based values for the tank models with an aspect ratio of 1.9 and tank wall thickness of 0.3 m, and this deviation increases to 70% for the tanks with a wall thickness of 0.5 m. These conditions are the same in the case of both IS, ACI and EN8 codes of practice. In contrast, a close adherence with the frequency values obtained from the codes is observed for the tank models with an aspect ratio of 0.5 and below under all the three values of tank wall thicknesses considered. Moreover, in the case of tank models filled up to half the depth of liquid, the frequency values obtained from the FE analysis match with those values obtained based on the current codes of practice considered, irrespective of the thickness of the tank wall.



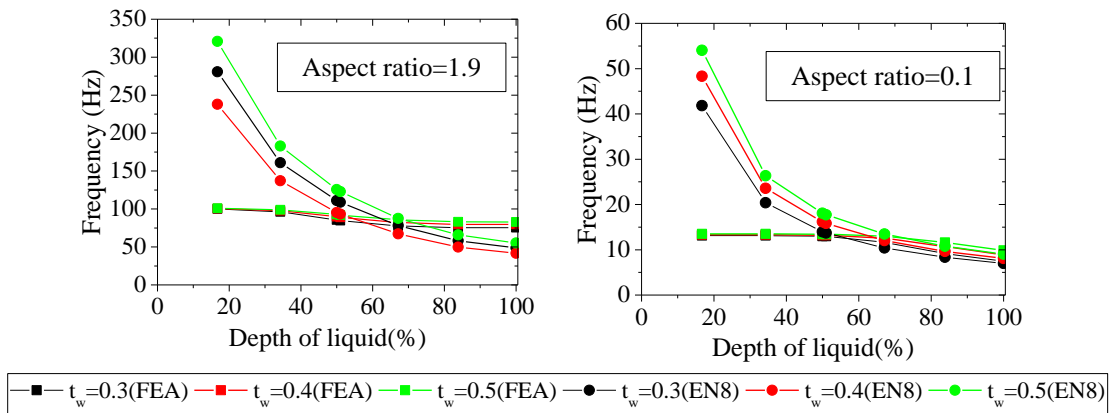
(a)

(b)



(c)

(d)



(e)

(f)

Fig. 5.2 Comparison of frequency values for different wall thickness

(a),(b) FEA and IS (c),(d) FEA and ACI (e),(f) FEA and EN8.

5.2.3 Effect of density of filled liquid

Fig. 5.3 compares the frequency of tank models (Aspect ratio of 1.9) filled with different liquids to those obtained based on standard codal provisions. In the given figure, the 1.9_Petrol, 1.9_Water and 1.9_Mercury indicate the natural frequency of the tank models with an aspect ratio of 1.9 at different depths of liquid. Similarly, the frequency values of tank models with an aspect ratio of 0.1 at different depths of liquid is indicated as 0.1_Petrol, 0.1_Water and 0.1_Mercury. Since the density of water and petrol differ much less, the frequency of the tank with petrol as the filled liquid is comparable with that of the tank with water as the liquid, with a slight variation of only 3.4% at full tank condition for the tank model with an aspect ratio of 1.9. Mercury, which is a high-density liquid, reduced 68% of the frequency at the lowest liquid depth condition and 85% of the frequency at full tank condition as compared to the frequency of the same tank containing water as the liquid because of increased impulsive mass.

For the model with an aspect ratio of 0.1, the frequency of the tank filled with mercury differs from that of the tank filled with water by 16% at the lowest liquid depth and 73% at the highest liquid depth conditions. However, the frequencies of the tank filled with water and petrol are comparable as in the case of the tank with an aspect ratio of 1.9. Additionally, it is noted that the deviation of FEA based frequency values from that obtained based on codes decreases with an increase in the density of the filled liquid. It is valid in the case of both IS and EN8 based frequency values. However, considering the ACI code, the expression for the estimation of the impulsive frequency of cylindrical tanks is devoid of the term density of the filled liquid. Therefore, the frequency values will not change with the density of the filled liquid.

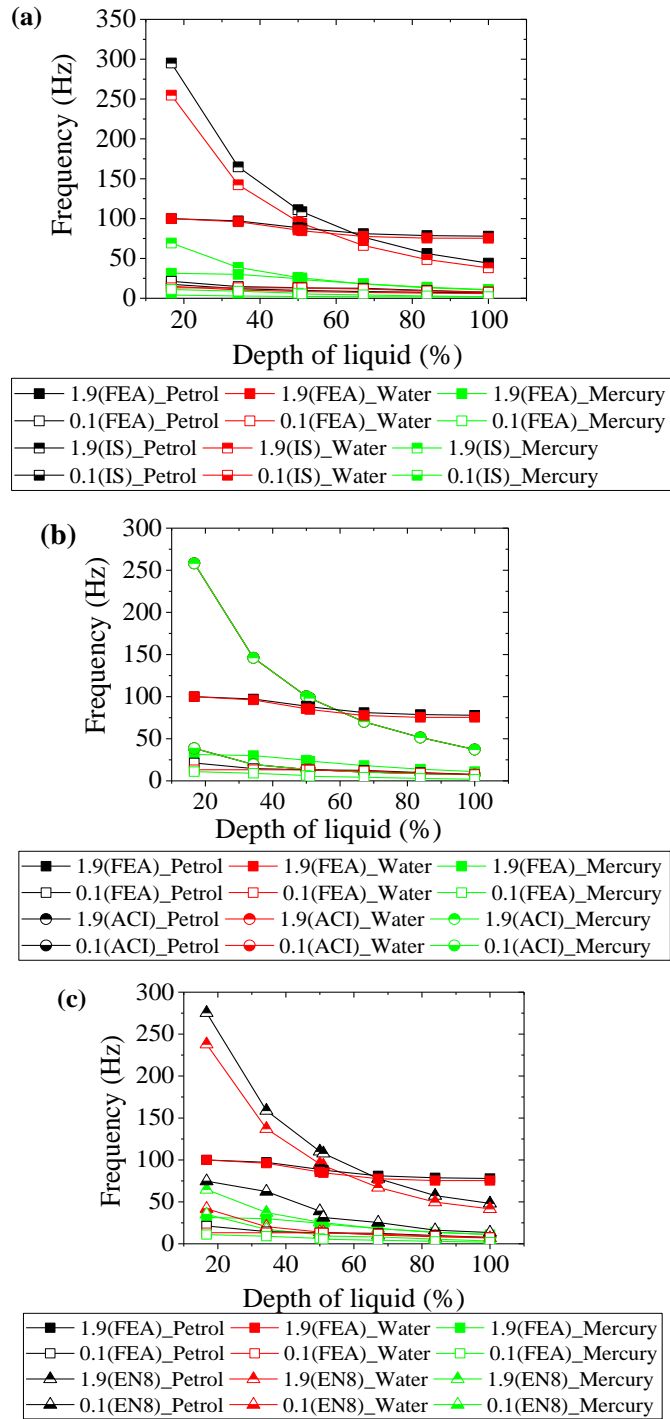


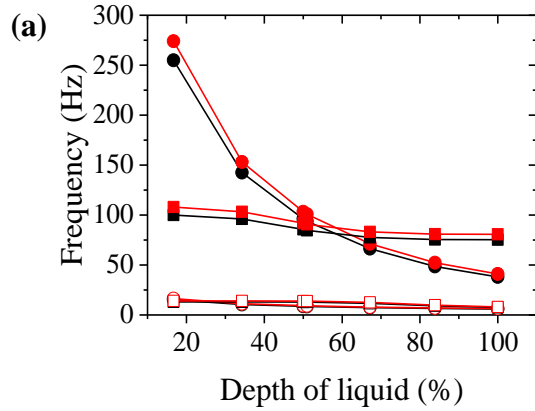
Fig. 5.3 Comparison of frequency values for different liquids (a) FEA and IS (b) FEA and ACI (c) FEA and EN8.

5.2.4 Effect of material property

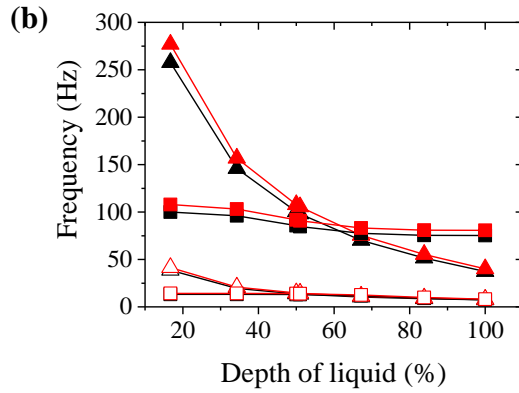
The natural frequencies of the liquid tanks made of M30 and M40 grades of concrete are compared in Fig. 5.4. The change in the grade of concrete directly influences the Young's modulus of the material. Therefore, the effect of the grade of concrete of construction is studied by changing the Young's modulus of the material. It is evident from the figure that the modal characteristics of the tank are directly affected by the variation in the value of Young's modulus. The higher grade of concrete results in higher frequency values. However, this effect is negligible for wider tanks or the tank with the lowest aspect ratio of 0.1 (i.e. lowest value considered for analysis). Additionally, it is noted that the deviation of FEA based frequency values from that obtained based on codes of practices are almost the same under different grades of concrete.

5.2.5 Formulation of modification coefficients

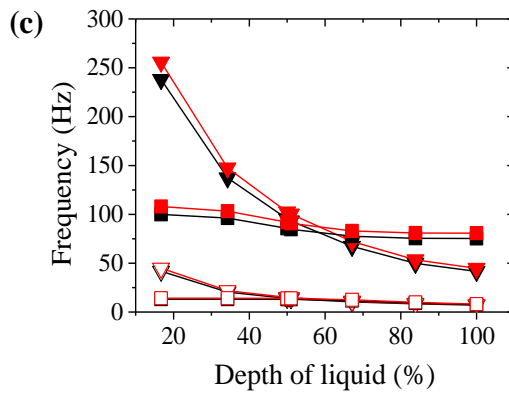
The comparison of frequency values obtained from the FE analysis and that of codal expressions reveals an average deviation of 30%. It is more evident from the Pearson correlation coefficient (r_{XY}) of 0.772, 0.702 and 0.766 for frequency values based on IS, ACI and EN8 codes of practices, respectively. Additionally, based on the parametric study, it is worth to note that the aspect ratio is the major influencing factor that affects the impulsive frequency of cylindrical tanks. Therefore, based on the observations, the full database is split into two, considering the aspect ratio as the ruling parameter. Further, analysis is carried out for these two cases, namely Case 1: tanks with the aspect ratio less than or equal to 1 ($H/D \leq 1$) and Case 2: tanks with the aspect ratio greater than 1 ($H/D > 1$).



● 1.9(IS)_M30 ● 1.9(IS)_M40 ■ 1.9(FEA)_M30 ■ 1.9(FEA)_M40
 ○ 0.1(IS)_M30 ○ 0.1(IS)_M40 □ 0.1(FEA)_M30 □ 0.1(FEA)_M40



▲ 1.9(ACI)_M30 ▲ 1.9(ACI)_M40 ■ 1.9(FEA)_M30 ■ 1.9(FEA)_M40
 △ 0.1(ACI)_M30 △ 0.1(ACI)_M40 □ 0.1(FEA)_M30 □ 0.1(FEA)_M40



▼ 1.9(EN8)_M30 ▼ 1.9(EN8)_M40 ■ 1.9(FEA)_M30 ■ 1.9(FEA)_M40
 ▽ 0.1(EN8)_M30 ▽ 0.1(EN8)_M40 □ 0.1(FEA)_M30 □ 0.1(FEA)_M40

Fig. 5.4 Comparison of frequency for different grades of concrete (a) FEA and IS (b) FEA and ACI (c) FEA and EN8.

In order to improve this correlation between the frequency values observed from FEA and those calculated from the International codes, the generated database is analysed by developing ANN models with two hidden layers. The input parameters are selected based on the parametric study as; the frequency value obtained from the corresponding code(f_{code}), aspect ratio(H/D), the ratio of the depth of liquid to the total height of tank (h/H) and the ratio of the depth of liquid to the diameter of the tank (h/D). The frequency obtained from FE analysis (f_{FEA}) is used as the dependent variable. Only 70% of the data is used for training the model, and the rest of the randomly selected 30% of data is kept for testing in the preliminary study. Representative NN diagrams generated for the analysis considering IS code expressions are shown in Fig. 5.5(a) and Fig. 5.5(b), respectively. The first and the second hidden layers consist of three and two units, respectively. The training and testing of the input database are carried out with a relative error of 0.035 and 0.028, respectively. Also, the significance values of variables considered are less than 0.05, representing a statically significant relationship between the variables considered. The hyperbolic tangent is used as the activation function for both the hidden layers and the outer layer.

The Pearson correlation between predicted value ($f_{P,IS}$) and actual f_{FEA} is 0.987 for Case 1 and 0.975 for Case 2. Also, the significance values of variables are less than 0.05 for both these cases. The same procedure is repeated by considering the frequency values obtained from ACI (f_{ACI}) and EN8 (f_{EN8}) as one of the independent variables instead of ' f_{IS} '. The Pearson correlation coefficients obtained for the NN models with f_{ACI} as one of the independent variables are 0.989 and 0.990 for Case 1 and Case 2, respectively. In this model, Young's modulus (E), density (ρ) and the height of the tank (H) are also considered as independent variables. Similarly, for the NN model with f_{EN8} as the input, the Pearson correlation obtained for Case 1 and Case 2 are 0.986 and 0.979, respectively. These correlations are illustrated as scatter plots in Fig. 5.6. These scatter plots with $r_{XY}>0.9$ emphasize the good possibility of predicting the frequency values of the tanks as close to the f_{FEA} values by augmenting f_{IS} or f_{ACI} or f_{EN8} using a function formulated by the parameters h/D , H/D and h/H .

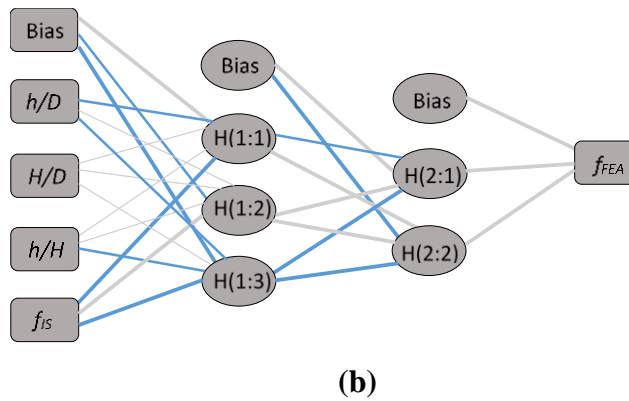
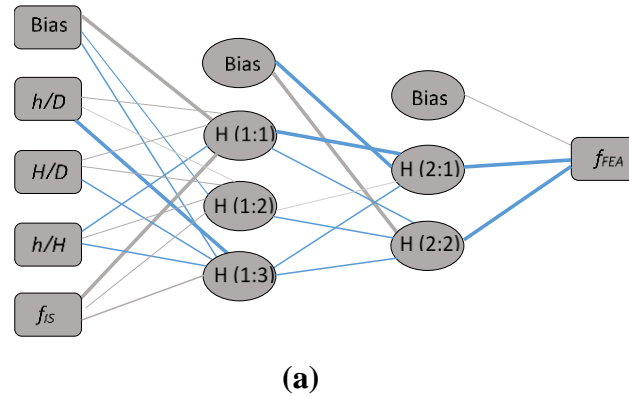


Fig. 5.5 ANN models Considering IS code of practice: (a) case 1 (b) case 2.

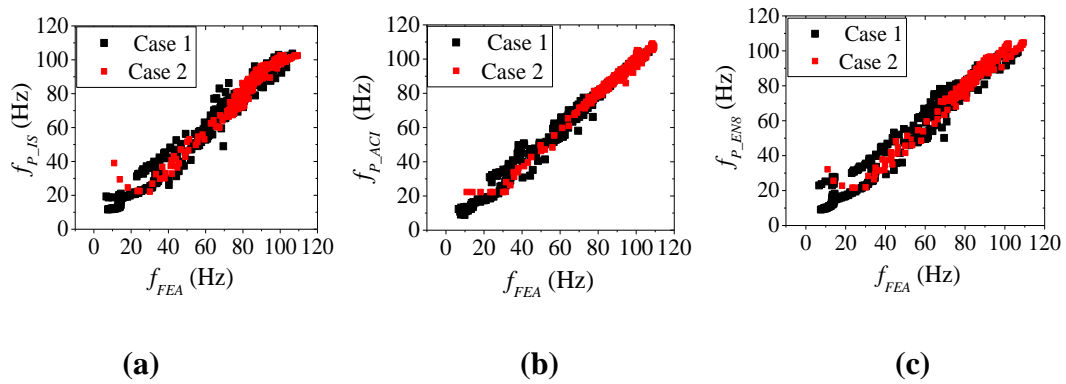


Fig. 5.6 Scatter plots based on ANN analysis (a) f_{P_IS} and f_{FEA} (b) f_{P_ACI} and f_{FEA} (c) f_{P_EN8} and f_{FEA} .

To generate an expression that predicts the frequency values of the tanks as close to the f_{FEA} values, the nonlinear regression analysis is carried out on the split database, and the formulae given in the International codes are modified. Unlike the linear regression

analysis, nonlinear regression considers the regression model as a nonlinear function of one or more independent variables. The parameters considered, to predict the relationship between f_{FEA} and $f_{(Code)}$ are H/D, h/H and h/D. All the variables are considered as ratio in order to avoid any dimensional irregularity. In the case of ACI 350.3, the effects of density of the liquid (ρ) is also included in the prediction model, which was not considered in the codal expression. The independent variables are selected by observing the corresponding significance value. Intensive regression analysis based on intricate trial and error method have been carried out considering 70% of the data. Modification coefficients, ' α and β ' are suggested to improve the accuracy of the estimation of the fundamental impulsive frequency of cylindrical liquid tanks. The accuracy of the relationship was tested using the remaining randomly selected 30% of the data. Based on the modification coefficients, the predicted value of frequency can be estimated as follows:

Case 1: Cylindrical tanks with aspect ratio less than or equal to 1

$$f_P = \alpha \times f_{code} \quad (5.1)$$

Case 2: Cylindrical tanks with aspect ratio greater than 1

$$f_P = \beta \times f_{code} \quad (5.2)$$

where, ' f_P ' is the predicted value of frequency. Modification coefficients, ' α and β ' are tabulated in Table 5.1. The scatter plots showing the relationship between the predicted values of frequency (f_{P-IS}) and the actual value of frequency for the two cases are shown in Fig. 5.7 for the three codes of practices considered. All scatter plots represent $r_{XY} > 0.9$, indicating an acceptable relationship.

The applicability of these equations is tested by estimating the frequencies of randomly selected tank geometries. A separate set of tanks with aspect ratios ranging from 0.7 to 1.9 that were not considered previously in this study are selected. All the 46 finite element models of circular liquid tanks are generated using ANSYS Mechanical APDL software,

and modal analysis is performed. The fundamental frequencies are estimated based on the formulae given in the codes of practice, finite element analysis, and the modified formulae. The correlation plot between the predicted value of frequency and those obtained based on FEA represents $r_{XY} > 0.9$, as illustrated in Fig. 5.8. The tank models are observed to satisfy the modified expressions formulated in this study.

Table 5.1 Modification coefficients

<i>IS1893(Part2):2014</i>	
$\alpha_{IS} = \frac{2.351 \times 0.83^{(H/D)} \times \left(\frac{h}{H}\right)^{0.6}}{\tanh^{-1}\left(\frac{H}{D}\right)^{h/D}}$	$\beta_{IS} = \frac{2.565 \times 0.729^{(H/D)} \times \tanh^{-1}\left(\frac{h}{H}\right) \times \left(\frac{h}{H}\right)^{1.7}}{\tanh^{-1}\left(\frac{H}{D}\right)^{h/D}}$
<i>ACI 350.3</i>	
$\alpha_{ACI} = \frac{2.351 \times 0.83^{(H/D)} \times \left(\frac{h}{H}\right)^{0.6}}{\tanh^{-1}\left(\frac{H}{D}\right)^{h/D}}$	$\beta_{ACI} = \frac{2.565 \times 0.729^{(H/D)} \times \tanh^{-1}\left(\frac{h}{H}\right) \times \left(\frac{h}{H}\right)^{1.7}}{\tanh^{-1}\left(\frac{H}{D}\right)^{h/D}} \times \left[\frac{\sqrt{E}}{\rho g H} \right]$
<i>Eurocode-8</i>	
$\alpha_{EN8} = \frac{1.958 \times 1.062^{(H/D)} \times \left(\frac{h}{H}\right)^{0.6}}{\tanh^{-1}\left(\frac{H}{D}\right)^{h/D}}$	$\beta_{EN8} = \frac{2.756 \times 0.706^{(H/D)} \times \tanh^{-1}\left(\frac{h}{H}\right) \times \left(\frac{h}{H}\right)^{1.7}}{\tanh^{-1}\left(\frac{H}{D}\right)^{h/D}}$

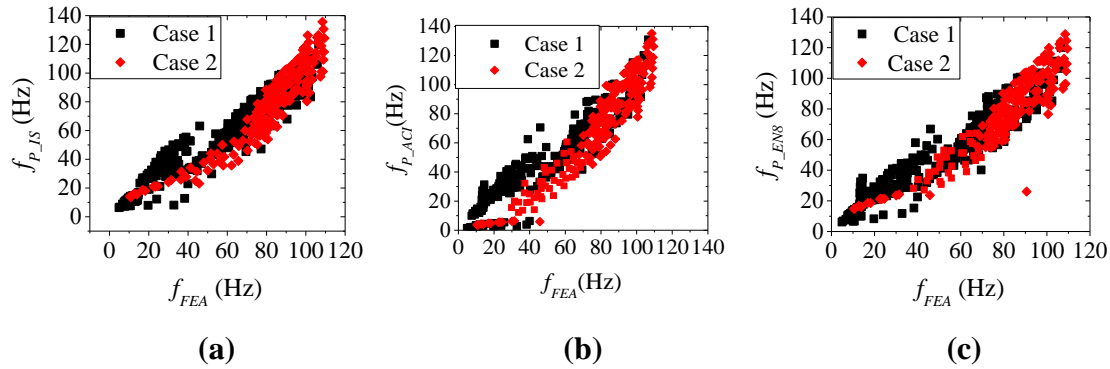


Fig. 5.7 Scatter plots based on regression analysis (a) f_{P_IS} and f_{FEA} (b) f_{P_ACI} and f_{FEA} (c) f_{P_EN8} and f_{FEA} .

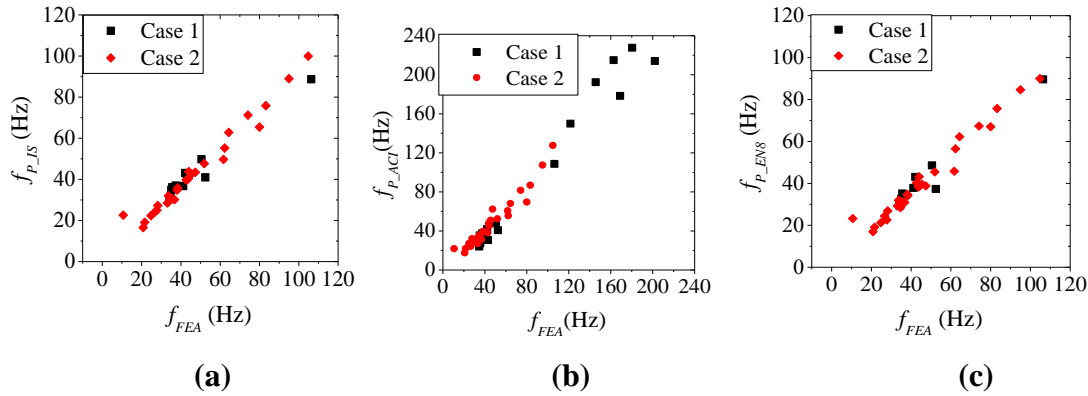


Fig. 5.8 Scatter plots based on applicability check (a) f_{P_IS} and f_{FEA} (b) f_{P_ACI} and f_{FEA} (c) f_{P_EN8} and f_{FEA} .

5.3 DYNAMIC CHARACTERISTICS OF RECTANGULAR TANKS

The dynamic characteristics of the tank models with and without baffles are analysed using the combined principles of acoustic modelling and finite element analysis. In addition to the solid baffle, the baffle plates with perforations are considered as well. The numerical model generated for the free vibration analysis is validated by comparing the natural frequency values of the unbaffled tank with those obtained based on the standard codes of practices, namely IS1893 (Part2):2014 and ACI 350.03, as given in Table 5.2. The frequency values computed based on the finite element analysis (FEA) and the codes of practices (IS1893 (Part2):2014 and ACI 350.03) are in good agreement with each other.

Table 5.2 Comparison of natural frequency of vibration

Mode	Frequency (Hz)		
	FEA	IS1893	ACI
Impulsive	15.585	16.627	15.651
Convective	0.147	0.148	0.148

Initially, the study considered the tank fitted with a single baffle plate. Table 5.3 shows the frequency values corresponding to the first three modes of vibration under impulsive and convective conditions.

Table 5.3 Frequency of tank models with and without single baffle plate

Models	Frequency (Hz)					
	Impulsive			Convective		
	Mode 1	Mode 2	Mode 3	Mode 1	Mode 2	Mode 3
T	15.585	15.835	22.576	0.147	0.257	0.257
T'_0	11.223	20.124	22.561	0.125	0.258	0.260
T'_5	9.315	18.513	19.651	0.123	0.216	0.237
T'_{10}	8.579	15.274	15.983	0.126	0.235	0.259
T'_{15}	6.424	14.930	15.264	0.139	0.258	0.260
T'_{20}	5.674	14.452	15.243	0.140	0.258	0.260
T'_{25}	5.947	14.351	15.244	0.141	0.258	0.260
T'_{30}	6.396	14.830	15.307	0.143	0.258	0.260

The dynamic interaction of the structural vibration mode and the liquid sloshing mode is negligible due to the large difference in the frequency ranges, which is evident from the natural frequency values. It confirms the observation of Haroun (1983) on the fundamental

frequency of the liquid containers. Under external excitation, the movement of the impulsive and convective mass of liquid is affected by the perforated baffle plate, causing blockage and additional vortices. It will shift the frequency values for the first mode as well as for the higher modes. The frequency values reduce by 28% and 15% under impulsive and convective modes, respectively, with the introduction of a solids baffle plate in the tank. The frequency values are further reduced with the use of the perforated baffle plate instead of the solid baffle plate. However, the frequency values increase when the perforations of the baffle plate increase beyond a certain higher value, which indicates the tendency of these tank models to behave like an unbaffled tank.

Table 5.4 Frequency of tank models with and without multiple baffle plate

Models	Frequency (Hz)					
	Impulsive			Convective		
	Mode 1	Mode 2	Mode 3	Mode 1	Mode 2	Mode 3
T	15.585	15.835	22.576	0.147	0.257	0.257
T_0'''	5.087	5.380	5.498	0.008	0.150	0.186
T_5'''	6.207	6.353	6.515	0.108	0.189	0.237
T_{10}'''	6.996	7.135	7.268	0.119	0.208	0.248
T_{15}'''	7.127	7.598	7.856	0.123	0.217	0.257
T_{20}'''	8.239	8.358	8.466	0.127	0.225	0.257
T_{25}'''	8.846	9.243	10.576	0.140	0.237	0.271
T_{30}'''	9.614	11.674	13.546	0.143	0.267	0.284

The frequency values of tank models fitted with multiple baffle plates are shown in Table. 5.4. A major downward shift in the frequency values is observed with the introduction of solid baffles in the tank. A maximum shift in the frequency values is noted for the natural frequency of the sloshing liquid with a reduction of 94% as compared to the unbaffled case.

In the case of impulsive mode, the natural frequency is reduced by 67% for the tank with the solid baffle compared to the unbaffled tank. However, the frequency values under the impulsive and convective modes shift slightly upwards with the inclusion of perforations in the solid baffle. The frequency values increase further with the increase in the percentage of perforation of the baffle plate under the impulsive and convective modes of vibration. This increasing trend in the frequency values confirms the tendency of the tank models to attain a near-natural frequency value of an unbaffled tank at a higher density of perforations. Additionally, it is noted that the frequency values corresponding to the second and third modes of vibration increase at a higher rate with the increase in the percentage of perforation of the baffle plate. Therefore, under higher modes of vibration, the frequency values reach that of the unbaffled tank at a lower density of perforations. The liquid sloshing shifts the centre of mass of the liquid, which is a major factor affecting the slosh-induced responses (Sanapala et al. 2018). The maximum shift in the centre of mass occurs, corresponding to the sloshing mode number, $n=1$. Therefore, the primary mode of vibration of the liquid should be considered as the basis for the investigation of the slosh responses in the liquid tank.

5.4 SUMMARY

Modification coefficients for the formulae given in the standard codal practices are developed for the accurate estimation of the impulsive frequency of the cylindrical tanks. The introduction of the baffle plate reduces the fundamental frequency of rectangular tanks. The dynamic interaction of the structural vibration mode and the liquid sloshing mode is negligible due to the large difference in the frequency ranges under the convective and impulsive modes. Use of multiple baffle plates increases the impulsive frequency of the rectangular tanks; however, it decreases the convective frequency compared to the single baffled tanks.

CHAPTER 6

IDENTIFICATION OF AN EFFECTIVE CONFIGURATION OF PERFORATED BAFFLE PLATE

6.1 GENERAL

The liquids are being used in various fields such as civil, mechanical, chemical and aerospace. The nature of this liquid can vary from potable water to highly toxic chemicals. Therefore, it can cause highly detrimental effects on nature and life if any damage occurs to the liquid storage tanks. Considering these detrimental effects, there is an urgent need to develop an effective configuration of the perforated baffle plate to damp the liquid sloshing to the maximum possible extent. For this, the present research work carried out a numerical simulation of liquid tank models with and without baffle plates under seismic ground motions as well as pitch excitation. Based on the observations, an effective baffle configuration is suggested, and it is validated experimentally using a laboratory model.

6.2 ANALYSIS OF GEOMETRIC CONFIGURATION OF PERFORATED BAFFLE PLATES UNDER SEISMIC GROUND MOTION

The free surface elevation (η) is a major response that can be directly observed during seismic excitation. This response is causative of the resulting damages. The elevation of the liquid medium of the unbaffled tank with a natural frequency of 0.138 Hz under the excitation of the three different earthquakes is shown in Fig. 6.1. The unpredictable variation in the free surface elevation in the time domain makes the sloshing problem highly nonlinear. This is evident from the random nature of the free surface fluctuations of the liquid medium under the seismic excitations. The Imperial Valley earthquake creates larger fluctuations of the free surface level compared to the other two earthquakes. Apparently, it is due to the near-resonant effect (Hejazi and Mohammadi 2019) under low frequency ground motions with a dominant frequency of 0.395 Hz compared to the cases

under the other two ground motions considered. In the near-resonant region, the free surface motion will be highly nonlinear (Faltinsen and Timokha 2009), which is evident from the temporal variation of the free surface under the Imperial Valley earthquake, as illustrated in Fig. 6.1.

On the other hand, the Kobe ground motion produces a far-resonant region, which causes a highly irregular surface with a less peak surface elevation compared to the response under Imperial Valley ground motion. The frequency content of the El Centro earthquake falls in between that of the Imperial Valley and Kobe earthquakes. Consequently, the trend of the free surface elevation under the El Centro earthquake is intermediate to that under Imperial Valley and Kobe earthquakes with respect to the peak value of surface elevation and the number of peaks. The trend of these free surface elevations is consistent with the results of Y.S. Choun (2012).

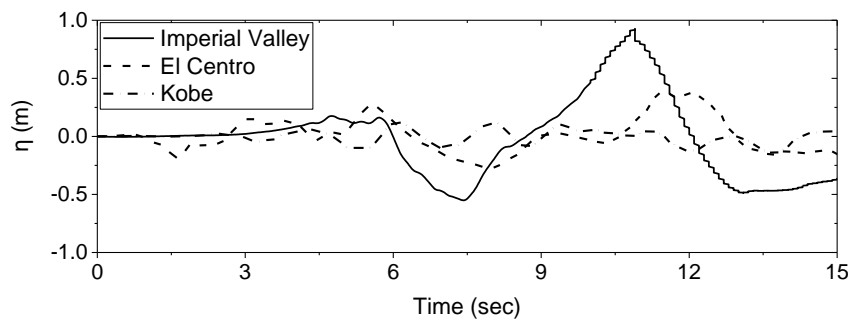
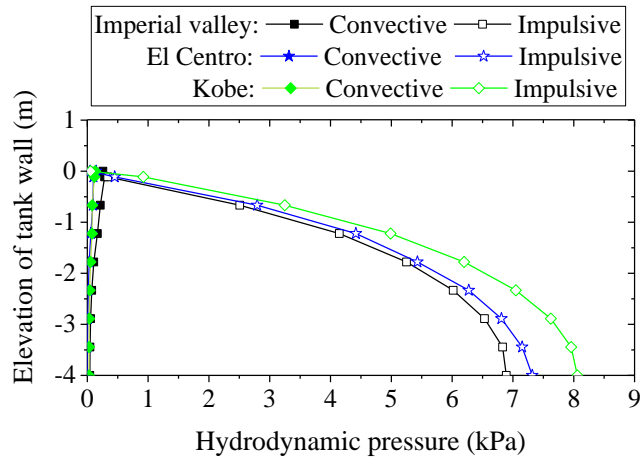


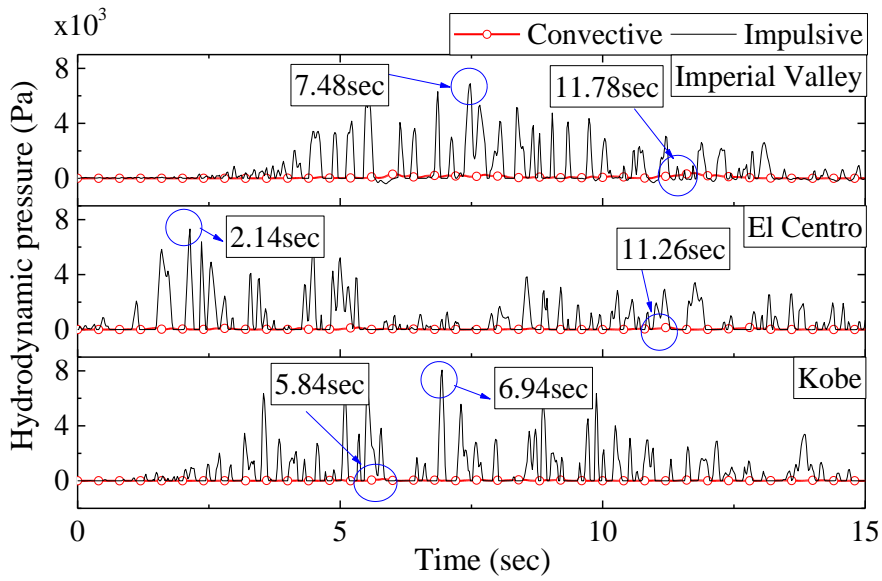
Fig. 6.1 Free surface elevation at a point (-10, 0, 0) on left wall of the unbaffled tank.

The hydrodynamic pressure exerted on the tank wall due to the sloshing liquid is another important response to be considered in the safety assessment of liquid tanks. Fig. 6.2(a) shows the variation of maximum pressure along the height of the tank for the unbaffled tank under the seismic excitations of different frequency ranges. It can be noted that the impulsive component of pressure dominates the convective component for the given tank

model. The trend of variation of the pressure components of the liquid tank confirms the results of Kianoush and Ghaemmaghami (2011) and Rawat et al. (2019).



(a)



(b)

Fig. 6.2 Variation of hydrodynamic pressure for tank model ‘T’

(a) along height of the tank wall (b) in time domain.

The probability of the existence of two near-resonant conditions corresponding to the impulsive and convective modes of vibration under the seismic ground motion is evident from Fig. 6.2(a). The convective response is more under Imperial Valley ground motion, whereas the impulsive response is more under the Kobe earthquake, which is a high-frequency ground motion. These two amplified response characteristics are due to the two different near-resonant conditions.

The temporal variations of hydrodynamic responses under the convective and impulsive modes of vibration, measured at point-a and point-b, respectively, are given in Fig. 6.2(b). The time corresponding to the maximum responses varies depending upon the mode of vibration and the frequency content of the external excitation. The turbulence kinetic energy of the sloshing liquid corresponding to the maximum wave height is shown in Fig. 6.3. Here, the horizontal distance measured from the centre of the tank is represented as ' x ', and the half the length of the tank is represented as ' l '. Under all three cases of ground motions, the maximum kinetic energy of the sloshing liquid occurs near the middle of the tank. The need for an anti-slosh mechanism in the middle of the tank is apparent from these observations. Additionally, a double peak pattern and more fluctuations are noted under Imperial Valley ground motion, representing a violent sloshing due to the near-resonant effect under convective mode. The undulations of the energy curve reduce as the frequency content of the ground motion changes from near-resonant to far-resonant conditions.

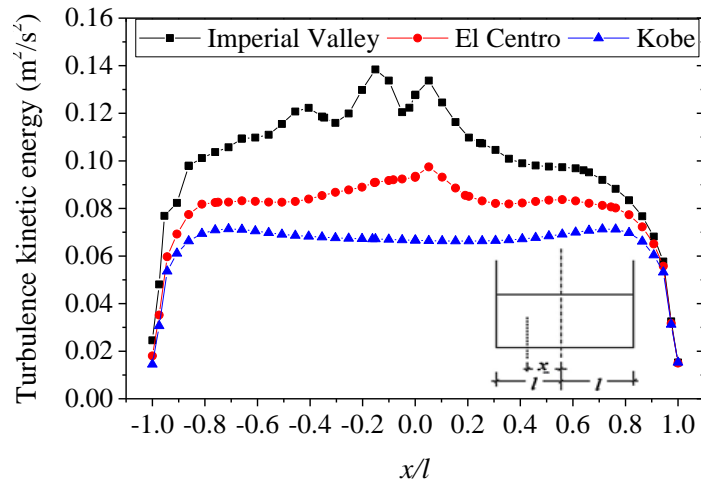


Fig. 6.3 Variation of turbulence kinetic energy along the length of the tank.

6.2.1 Analysis of slosh response of the tank fitted with single baffle plate

In this section, a parametric study is carried out on the tank models fitted with a single baffle plate, considering the percentage of perforation, clear spacing of perforations and the offset distance of the perforated baffle plate as the parameters. The numerical simulations are conducted under seismic ground motions of different PGA/PGV ratios.

6.2.1.1 Effect of percentage of perforation of baffle plate

The presence of any anti-slosh mechanism reduces the elevation of the free surface of the liquid medium by providing increased damping (Franklin T. Dodge 2000). The representative sketches of the damped free surface elevation (η) of the liquid medium due to the installation of the perforated baffle plate under the excitation of the three given ground motions are shown in Fig. 6.4.

The major parameter that affects the effectiveness of the perforated baffle plate is the percentage of perforation provided (Bellezi et al. 2019). The solid vertical baffle reduces the peak surface elevation by 22%, 46% and 11% under low, intermediate and high frequency ground motions, respectively, compared to that of the unbaffled tank. This

reduction in the free surface elevation improves with the replacement of the solid baffle with the perforated baffle. The peak surface elevation (η_{max}) reduces with an increase in the percentage of perforation of the baffle plate under low frequency seismic excitation. However, this reduction is interrupted beyond a perforation of 17% with a slight increment in the peak surface elevation. Beyond 17% perforation, the peak surface elevation changes randomly. The flow tends to reach the initial steady-state rapidly with an increase in the percentage of perforation beyond 17%. The trend in the behaviour of the tank under intermediate frequency excitation is similar to that under low frequency excitation, though there is a direct relationship between the percentage of perforation and the peak surface elevation. Particularly, under intermediate frequency excitations, the peak surface elevation increases slightly with the increase in the percentage of perforation provided. Beyond 30% perforation, the surface elevation tends to be that of an unbaffled tank in the case of both low and intermediate frequency excitations.

Unlike liquid sloshing under low and intermediate frequency ground motions, the flow under high frequency ground motion is devoid of sudden peak elevations. However, it contains several low amplitude peaks. In this case, the peak surface elevation changes directly with the percentage of perforation, as in the case of the intermediate frequency ground motion. In addition, the peak surface elevation reaches that of the unbaffled tank for perforation of 25% onwards.

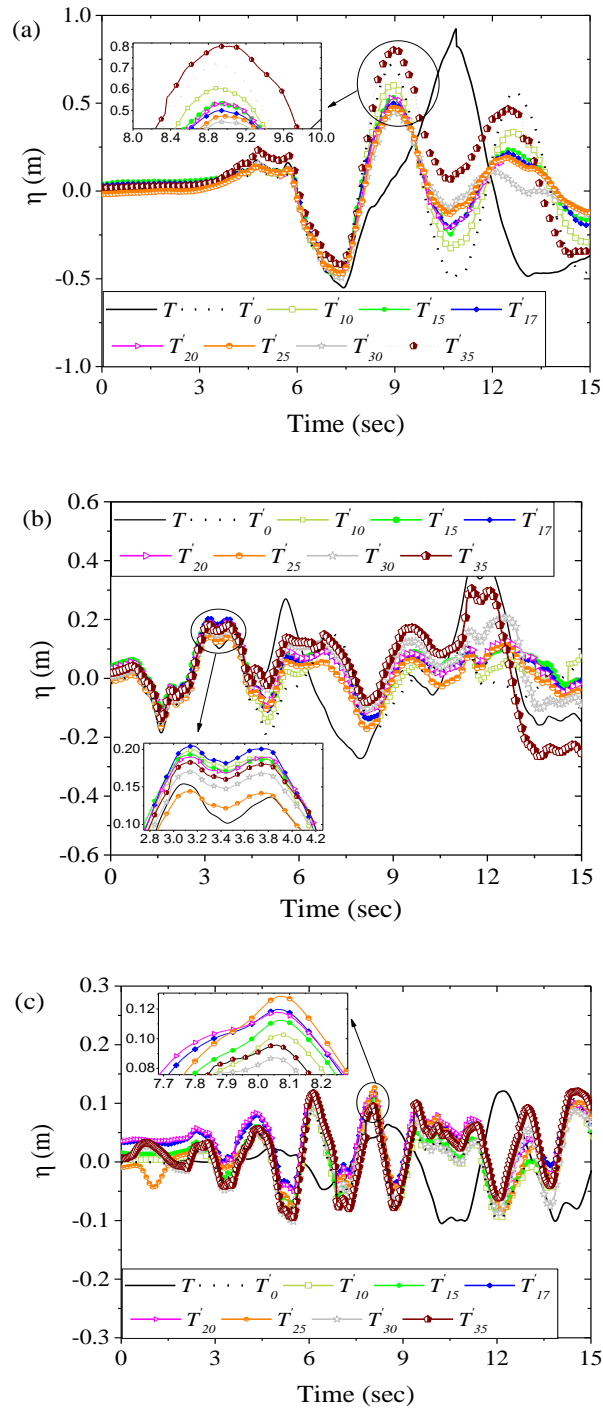


Fig. 6.4 Temporal variation of free surface elevation at a point (-10,0,0) on left wall of the tank under (a) Imperial Valley (b) El Centro (c) Kobe.

Fig. 6.5 depicts the peak values of free surface elevations (η_{max}), obtained from the time history plot, shown in Fig. 6.4, considering the tank models without baffle (T) and with baffle plate of varying percentage of perforations. The peak value of surface elevation of a tank without baffle under the three ground motions is denoted as ' η_T '. Considering the seismic excitation with intermediate frequency, the tank with a solid baffle (0% perforation) causes a reduction of 46% in the peak sloshing elevation compared to the un baffled tank due to the blockage effect and vortex formation. It is a rapid reduction in the free surface elevation compared to the cases under low and high frequency ground motions. However, considering the cases of the tank fitted with perforated baffle plates, the reduction in the peak surface elevation is more in the case of the tank under low frequency excitation. At 17% perforation, both low and intermediate frequency ground motions cause the same reduction of 46% in the peak surface elevation compared to the un baffled case.

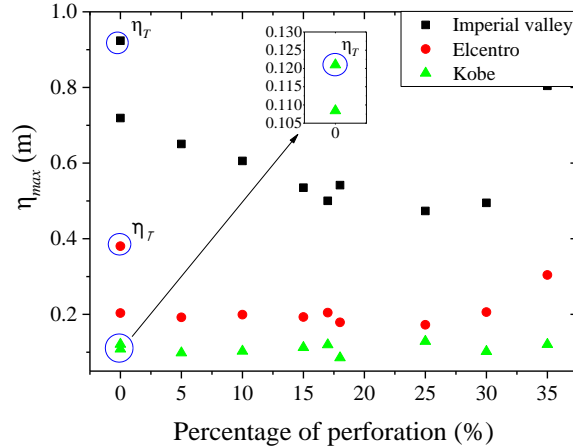
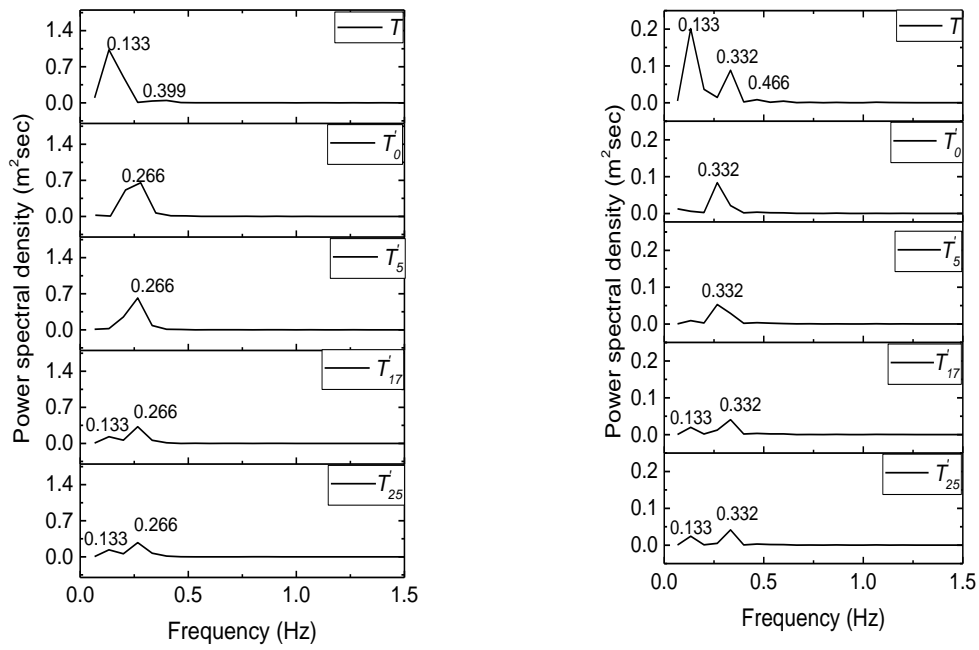


Fig. 6.5 Variation of peak surface elevation at a point (-10,0,0) with respect to the percentage of perforation.

On the other hand, under high frequency ground motion, the peak surface elevation reduces by an average value of 11% at a perforation of 17%. These percentage values of reduction caused due to the additional formation of vortices portray the effectiveness of perforated baffle with low values of perforations under both intermediate and high frequency ground

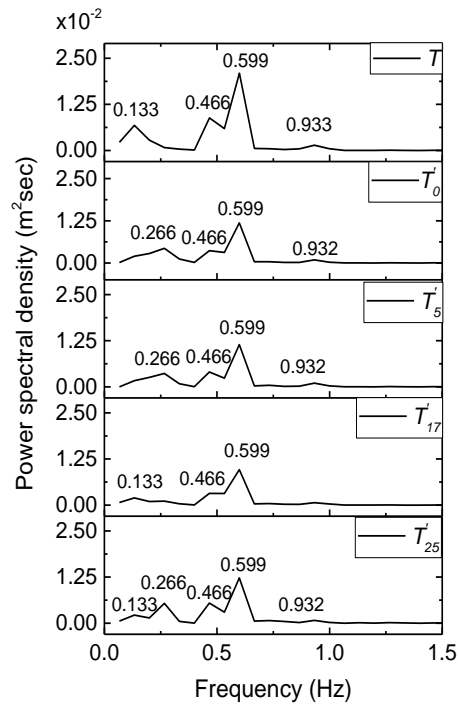
motions. The maximum reductions of 49% and 15% are obtained for the peak value of surface elevation, corresponding to the perforations of 15% and 10% under intermediate and high frequency excitations, respectively.

The damping effect of the perforated baffle plate on the slosh response is noticeable in the power spectral density of temporal variation of sloshing elevation, as shown in Fig. 6.6. In this, the spectral density of the free surface elevation of the tank without baffle (T), and the tank fitted with the baffle of varying perforations of 0%, 5%, 17% and 25% are illustrated. The initial peak value of 0.133 Hz, as shown in the figure for all three cases of ground motions, is the near fundamental sloshing frequency of the unbaffled tank. This frequency is missing in the subsequent sketches of the power spectrum corresponding to the liquid tank models fitted with the perforated baffle plate. This disappearance accounts for the dominance of the excitation frequency compared to the fundamental frequency of the tank. Particularly, the near excitation frequency values of 0.266 Hz, 0.332 Hz and 0.599 Hz dominate the cases with a tank-baffle combination under Imperial Valley, El Centro and Kobe earthquakes, respectively. The slosh damping increases with the increase in the percentage of perforation. It may be due to the presence of a larger number of edges in the perforated plate. The flow through these additional edges causes additional damping of the slosh response, and therefore, it alters the dominant frequency of the slosh response. In the case of 17% perforation, the fundamental frequency value reappears, though the peak value is smaller than that of the preceding cases of perforations. It indicates the tendency of tank structure to behave similarly to that of an unbaffled tank. Beyond 17% of perforations, the reduction in energy dissipation is evident under all three cases of ground motions. Furthermore, under the Kobe earthquake, the energy dissipation is less for all the perforation values compared to the cases under the other two ground motions. It may be due to the effectiveness of the perforated baffle plate to damp the slosh response for the first mode (Faltinsen et al. 2011).



(a)

(b)



(c)

Fig. 6.6 Power spectral density corresponding to the free surface elevation under (a) Imperial Valley (b) El Centro (c) Kobe.

Based on these observations, the optimum percentage of perforation to damp the slosh response under low, intermediate and high frequency ground motions is obtained as 17%, 15% and 10%, respectively. Therefore, it can be noted that corresponding to the far-resonant to the near-resonant frequency content of the ground motions, the optimum range of percentage of perforation varies from 10% to 17%. The perforated baffle plate is more effective under violent sloshing conditions of near-resonant ground motions.

6.2.1.2 Effect of clear spacing of perforations

The dynamic response analysis has been carried out for the tank models with baffle plates of various configurations of perforations. Fig. 6.7 illustrates the effect of clear spacing (*b*) between the perforations on the free surface elevation of the liquid tank models with 10%, 15% and 17% perforated baffle plates. It is apparent from Fig. 6.7 that any changes in the spacing of the perforations change the free surface elevation of the liquid. Moreover, the peak amplitude of the liquid surface elevation depends primarily on the frequency of the input excitation (Xue et al. 2012). An evident reduction in the free surface elevation occurs under low frequency earthquake with a maximum perforation spacing of 0.9 m to 0.91 m constrained to the given geometric conditions. This value of effective clear spacing applies to the considered tank-baffle combination under the intermediate frequency of excitation as well. On the other hand, under the high frequency of excitation, the maximum reduction in the free surface elevation is obtained at an effective spacing of 0.9 m. Beyond this range, the elevation of the free surface increases slightly. Particularly, more number of widely spaced perforations restrain the elevation of the free surface effectively. It may be due to the increased flow separation and vortex shedding (Chandrasekaran and Madhavi 2015a) caused by the particular configuration of the baffle plate.

The energy dissipation ratio can be expressed as follows (Xue et al. 2012):

$$\xi = \frac{(E_S - E_B)}{E_S} \times 100 \quad (6.1)$$

where, ' E_B ' and ' E_S ' are the maximum slosh-induced wave energy for with baffle and without baffle conditions, respectively. The total energy dissipation will be proportional to the square of the wave amplitude. Based on Eq.(6.1), the average energy dissipation ratios are given in Table. 6.1, corresponding to the wide perforation spacing of 0.85 m, 0.9 m and 0.95 m. It reports the efficiency of perforations with 0.9 m spacing in reducing the slosh response of the tank model of the given geometry. A slight reduction in the energy dissipation is observed at the clear spacing of 0.95 m. It may be due to the flow separation and subsequent constructive interference. Under these conditions, the amplitude of resulting sloshing waves will increase due to the interference of the waves passing through different perforations constructively and causing a subsequent reduction in the energy dissipation. A similar observation is noted for perforation spacing of 0.85 m as well. It may be due to the reduction in the solid area of the baffle plate. The perforated baffle plate with reduced solid area tends to behave as an un baffled case, which results in reduced energy dissipation. Additionally, the energy dissipation reduces with the increase in the frequency of the input excitation.

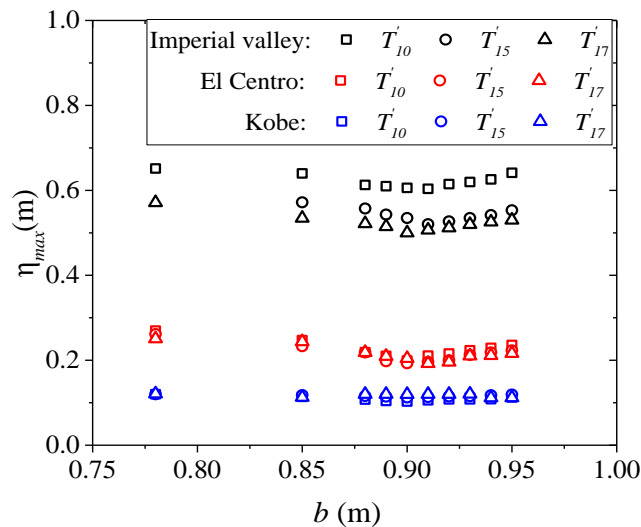


Fig. 6.7 Variation of peak surface elevation with clear spacing ' b '.

Table. 6.1 Maximum energy dissipation ratio corresponding to various clear spacing

Ground motion	Maximum energy dissipation ratio (%)		
	$b=0.85\text{ m}$	$b=0.90\text{ m}$	$b=0.95\text{ m}$
Imperial Valley	66	70	67
El Centro	58	71	67
Kobe	10	14	10

6.2.1.3 Effect of offset of perforated baffle plate from the tank wall

The effect of different horizontal positions of the perforated baffle plate on the slosh response is studied by varying the offset distance (x_w) of the baffle plate from the left tank wall. For this, the baffle plates with perforations of 10%, 15% and 17% are considered. The change in the maximum free surface elevation (η_{\max}) for different offset distances of the perforated plate is shown in Fig. 6.8. Half the length of the tank is represented as ‘ l ’.

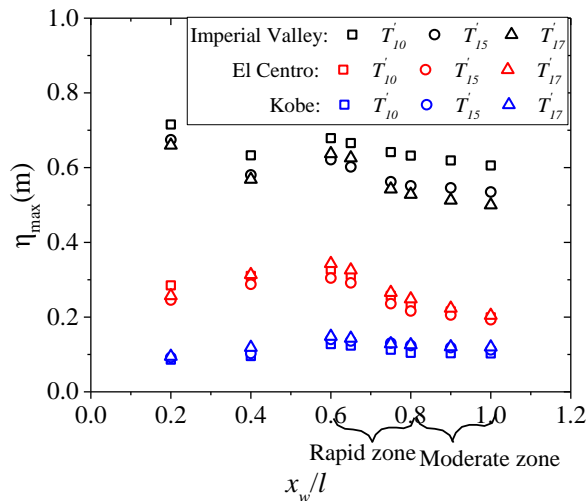


Fig. 6.8 Effect of offset distance of perforated baffle plate on free surface elevation.

The offset distance or the horizontal position of the baffle plate affects the peak surface elevation nonlinearly. A sudden reduction in the maximum free surface elevation is observed in the range of x_w/l ratio of 0.6 to 0.8. In this range, the average reduction in the peak surface elevation is 13%, 28%, and 15% under low, intermediate and high frequency ground motions, respectively. Since this region caused a rapid change in the peak surface elevation, it can be named as ‘Rapid zone’ (R-zone). On the other hand, from $x_w/l=0.8$ to 1, the reduction in the elevation of the free surface is moderate, and hence, this region can be named as ‘Moderate zone’ (M-zone). However, placing the baffle in the M-zone causes a further reduction in the elevation and results in the least value of peak surface elevation as compared to the R-zone. From the observations, it is evident that the installation of the perforated baffle plate at the middle or near-middle region of the liquid tank (which is identified as M-zone) will be more effective in reducing the peak surface elevation of the liquid medium. Velocity streamlines corresponding to different offset distances (x_w) of 2 m, 4 m, 6 m and 8 m of the perforated plate under the three ground motions are shown in Fig. 6.9.

Vortices are formed near the perforated baffle plate due to the flow of liquid through the perforations, which leads to the damped flow. The velocity of streamlines slightly increases near the perforated plate due to the reduction in the flow path of the liquid. Nevertheless, the velocity of the streamlines decreases as the position of the baffle plate is displaced from $x_w=2$ m to $x_w=8$ m. This reduction in the velocity of streamlines accounts for the energy dissipation caused by the viscous damping and flow separation. However, in the case of intermediate and high frequency ground motions, the velocity of streamlines slightly increases at certain locations of the tank, particularly for the offset distance of 4 m to 6 m. It may be due to the constructive interference caused by the perforated baffle. In this region, the energy of the wave passing through the baffle plate increases slightly due to the presence of perforations.

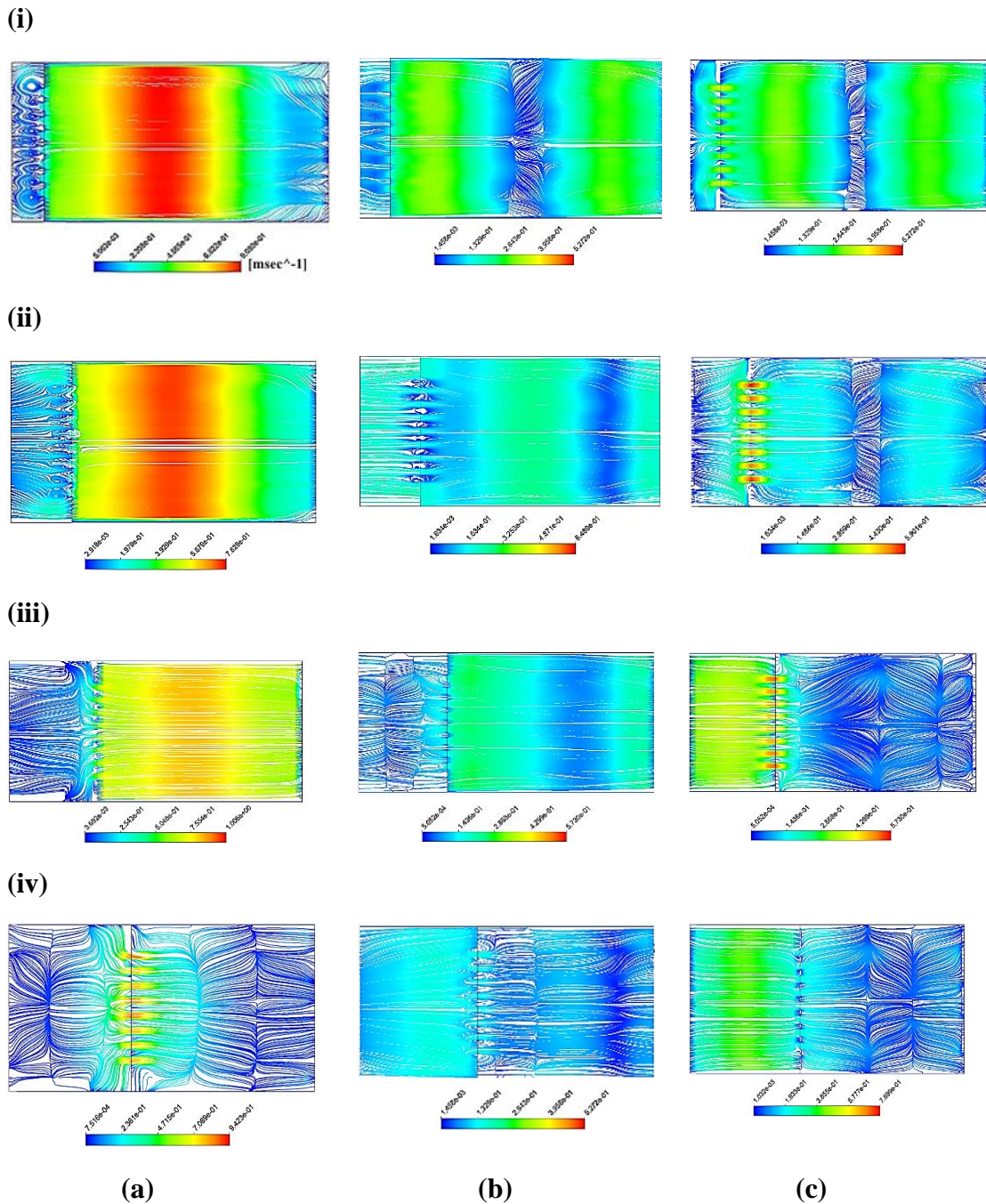


Fig. 6.9 Streamlines of flow corresponding to (i) $x_w=2$ m (ii) $x_w=4$ m (iii) $x_w=6$ m (iv) $x_w=8$ m under (a) Imperial Valley (b) El Centro (c) Kobe.

Additionally, the transformation of streamline from turbulent to uniform flow as the position of the baffle plate shifts towards the middle of the tank ($x_w=8$ m) is noted. It

indicates the tendency of the flow to reach the initial steady-state condition. The velocity of streamlines is higher under the Imperial Valley earthquake, leading to an increased peak value of the free surface elevation compared to that under the other two earthquakes. The energy dissipation is also more under the Imperial Valley earthquake, and it is less under the Kobe earthquake. Therefore, it is noted that the perforated baffle plate located at the ‘M-zone’ of the tank is effective under near-resonant conditions developed due to the ground motions.

Fig. 6.10 shows the fluctuations of the liquid medium under the three ground motions considered. The efficiency of the perforated baffle plate to damp the slosh response under the ground motions of different frequencies are evident from the deformation of the liquid medium without baffle and with baffle cases. The perforated baffle plate reduces the fluctuations of the liquid medium effectively under near-resonant conditions.

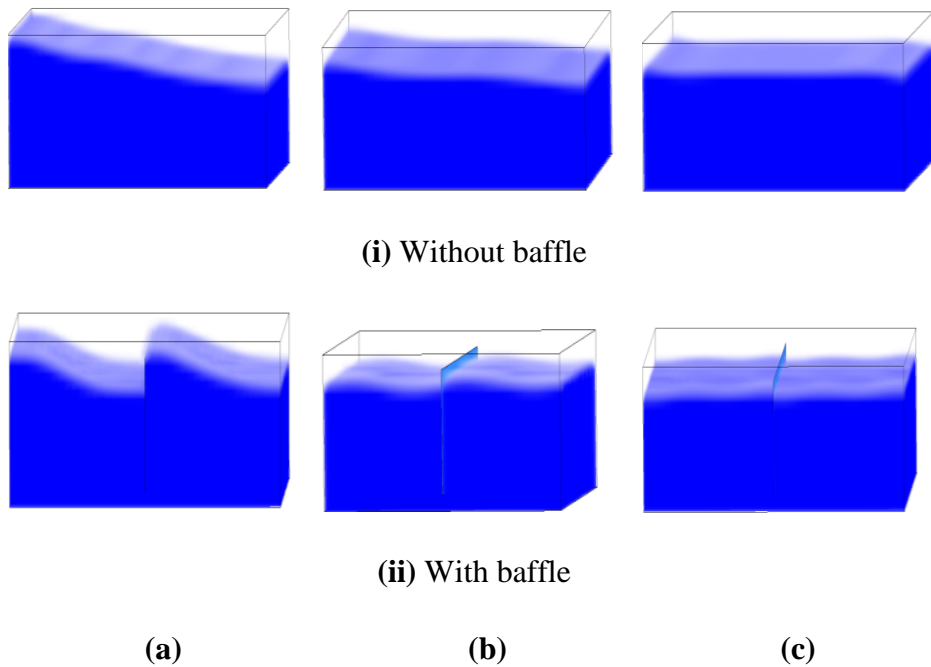


Fig. 6.10 Fluctuations of liquid medium under (a) Imperial Valley (b) El Centro (c) Kobe.

6.2.2 Analysis of slosh response of the tank fitted with multiple baffle plates

In this section, tank models fitted with three baffle plates are analysed under seismic ground motions. A parametric study is carried out by considering the parameters such as the percentage of perforations and the alignment of perforations, which are the major influencing parameters of the slosh suppression mechanism of the perforated baffle plates (Chen et al. 2016; Bellezi et al. 2019).

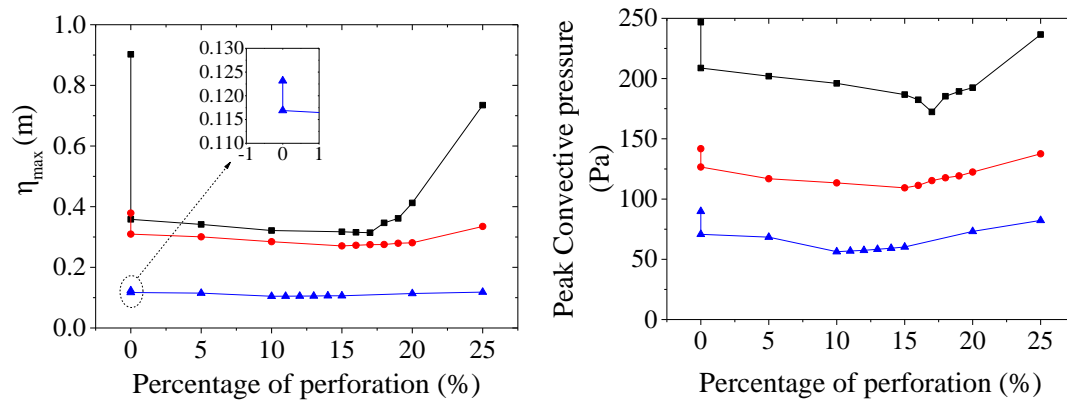
6.2.2.1 Effect of percentage of perforations

Fig. 6.11(a) illustrates the maximum sloshing surface elevation (η_{max}) of the liquid tank models with baffle plates of different percentages of perforations. The elevation of the sloshing surface is measured at point-a (-10,0,0), which is at the extreme left edge of the sloshing surface. Two response points are marked one above the other, corresponding to 0% perforation under all three cases of ground motions. Among these, the point marked on the top represents the response of the unbaffled tank (T), and that on the bottom represents the response of the tank fitted with the solid baffle (T_0'''). The elevation of the sloshing surface reduces with the incorporation of the baffle plate in the tank under all the three ground motions. However, the percentage reduction in the elevation varies under different ground motions. Notably, the percentage reduction in the peak free surface elevation of tank model T_0''' under the Imperial Valley, El Centro and Kobe ground motions are 60%, 18% and 5%, respectively. These significant variations may be due to the different frequency contents of the ground motions considered. Larger slosh damping under Imperial Valley ground motion may be due to the more effectiveness of the perforated baffle to damp the slosh response for the first mode of sloshing (Faltinsen et al. 2011). Maximum reduction in the elevation of the sloshing surface is observed for the tank models with 17% (T_{17}'''), 15% (T_{15}''') and 10% (T_{10}''') perforated baffle plates under the Imperial Valley, El Centro and Kobe ground motions, respectively. This reduction may be due to the combined effect of shear layer (Akyildiz and Ünal 2005) formation and the localized vortex (Bellezi

et al. 2019) near the perforations. Beyond these effective perforations, the elevation of the free surface increases and tends to be that of an un baffled tank.

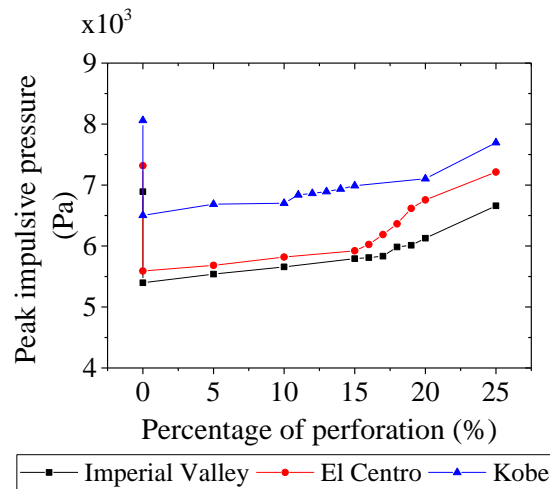
The hydrodynamic pressure generated by the sloshing liquid is also measured on point-a, where the free surface elevation is noted. The pressure response of T and T_0''' are marked, corresponding to the 0% perforation in Fig. 6.11(b), as in the case of free surface elevation. The trend of variation in the convective pressure corresponding to the different percentages of perforation is the same as that of sloshing surface elevation. Additionally, the maximum damping efficiency is noted under the Imperial Valley ground motion.

On the other hand, in the case of impulsive pressure, an increasing trend is observed with the increase in the percentage of perforations, as shown in Fig. 6.11(c). However, the increase in the pressure value is less up to the model with 17% perforation under the Imperial Valley ground motion. Beyond 17% perforation, a sudden increase is observed in the impulsive pressure values, which may be due to the reduction in the effective solid area of the baffle plate. A similar pattern is observed under the El Centro, and Kobe ground motions, with the effective perforations being 15% and 10%, respectively. Comparing Fig. 6.11(b) and Fig. 6.11(c), the maximum pressure response for the convective and impulsive mode is observed under the Imperial Valley and Kobe ground motions, respectively. This is due to the two different natural frequencies, one under the convective and the other under the impulsive modes of vibration. The existence of two natural frequencies under these two modes causes two near-resonant conditions, one under the low frequency convective mode and the other under the high frequency impulsive mode. Therefore, in the case of impulsive mode, the pressure response is minimum under the Imperial Valley ground motion due to the far-resonant condition. The pressure response under the El Centro ground motion is intermediate compared to that under the other two ground motions due to the intermediate frequency content.



(a)

(b)



(c)

Fig. 6.11 Effect of percentage of perforation with reference to (a) free surface elevation (b) peak convective pressure (c) peak impulsive pressure.

The minimum impulsive pressure response is obtained corresponding to the tank model fitted with the solid baffle (T_0'''), which accounts for an average reduction of 22% considering the cases under three ground motions. Therefore, the effective percentage of perforations to obtain a damped response under convective and impulsive conditions are different. An effective baffle configuration should account for the reduction of the total hydrodynamic response, including the impulsive and convective conditions. The

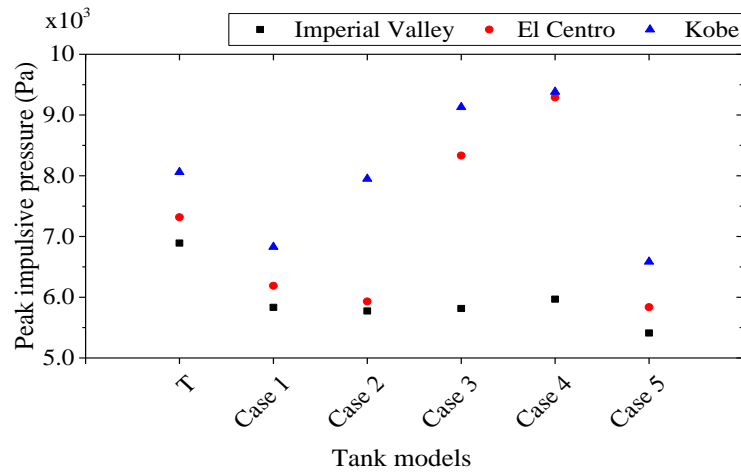
importance of the alignment of perforations in reducing the slosh response is apparent from these observations considering the points of maximum responses under the impulsive and convective conditions.

6.2.2.2 Effect of alignment of perforations

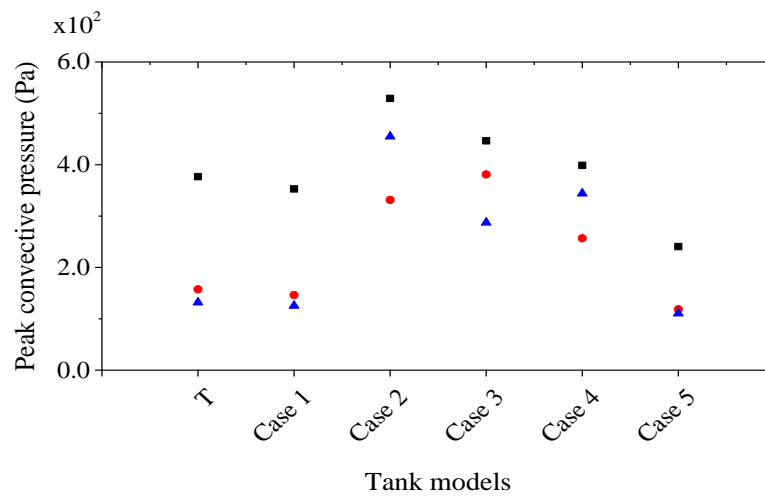
The effect of the alignment of perforations on the slosh response is investigated by considering five different configurations of tank model ' T_{17}''' ' under the seismic ground motions. The maximum values of hydrodynamic pressure for all these five cases, measured along a line a-b, are illustrated in Fig. 6.12.

An average reduction of 15% and 10% is observed in the hydrodynamic pressure with the introduction of the centrally perforated baffle (case 1) under the impulsive and convective conditions, respectively. The reduction in the damping efficiency of the perforated baffle plate, when used in multiple numbers with the same baffle configurations, is evident from the trend of the responses under the case 1 to case 4 configurations.

However, the damping efficiency is increased when the perforated baffle plates with different baffle configurations are used alternately. This fact is proved with the response under case 5 configuration. Among different configurations of baffles, the case 5 configuration resulted in the maximum slosh damping, which accounts for an average reduction of 16% and 47% in the hydrodynamic pressure, compared to the unbaffled tank ' T ' under the impulsive and convective conditions, respectively.



(a)



(b)

Fig. 6.12 Effect of alignment of perforation with reference to

(a) peak impulsive pressure (b) peak convective pressure.

6.2.3 Effective configuration of perforated baffle plates

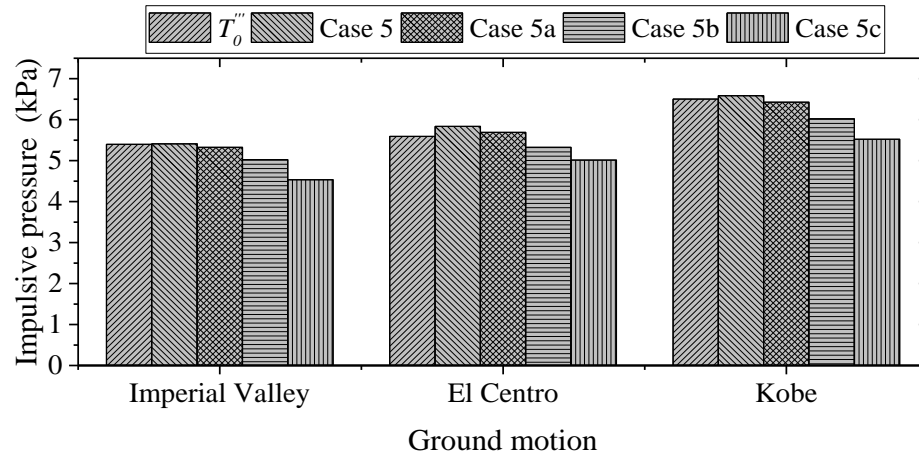
The slosh damping is less under the impulsive condition than that under the convective condition when the case 5 configuration is used. Additionally, it is noted from section 6.2.2.1 that the impulsive response decreases with an increase in the effective solid area of the baffle plate. Therefore, further analysis is carried out for the tank models by varying

the percentage of perforations as 15%, 10% and 5%, provided the alignment of perforations follows the case 5 configuration. These tank models are designated as case 5a, case 5b and case 5c corresponding to 15%, 10% and 5% perforations, respectively. Fig. 6.13 illustrates the maximum hydrodynamic pressure on the left tank wall of these models. Under the impulsive mode, the damping efficiency of the proposed baffle configurations increases with the reduction in the percentage of perforations. The maximum damping efficiency is obtained with the case 5c baffle configuration. Particularly, the impulsive pressure response is reduced by 15% compared with the case 5 configuration and 31% compared with the unbaffled tank when the percentage perforation is reduced to 5% (case 5c). The reduction in the impulsive pressure response may account for the increase in the solid area of the baffle plate towards the bottom of the tank, which causes an additional blockage effect.

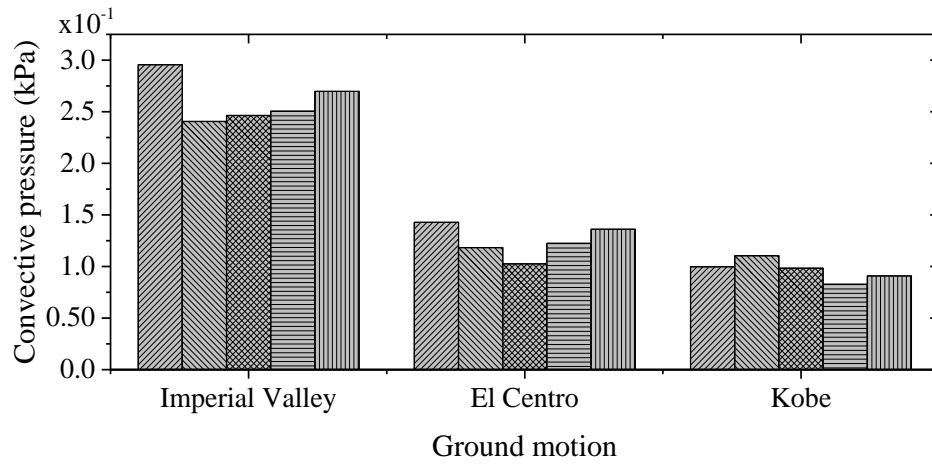
On the other hand, in the case of the convective response, the effective percentage of perforation is noted as the same as discussed in section 6.2.2.1, provided the baffle configuration is case 5. Therefore, under the convective mode of response, the maximum damping efficiency is noted for case 5, case 5a and case 5b configurations under the Imperial Valley, El Centro and Kobe ground motions, respectively. The free surface displacement of these models is compared with that of the unbaffled tank model in Fig. 6.14(a). The maximum damping is observed under the near-resonant condition with the use of the case 5 baffle configuration.

Fig. 6.14(b) emphasizes the increased slosh damping under the near-resonant condition in terms of turbulence eddy dissipation. In the case of the unbaffled tank, the maximum turbulence eddy dissipation is observed near the walls of the tank. The eddy dissipation increases with the installation of the baffle plate with the case 5 configuration due to the increased blockage effect and the flow separation. The proposed configuration increases the turbulence eddy dissipation by an average value of 58% compared with the unbaffled case. The effectiveness of the case 5 configuration for slosh damping is apparent from these observations. The increased slosh damping may be caused due to the additional blockage

effect generated by the zig-zag arrangement of perforations at the top of the successive baffle plates, as shown in Fig. 6.15(a).

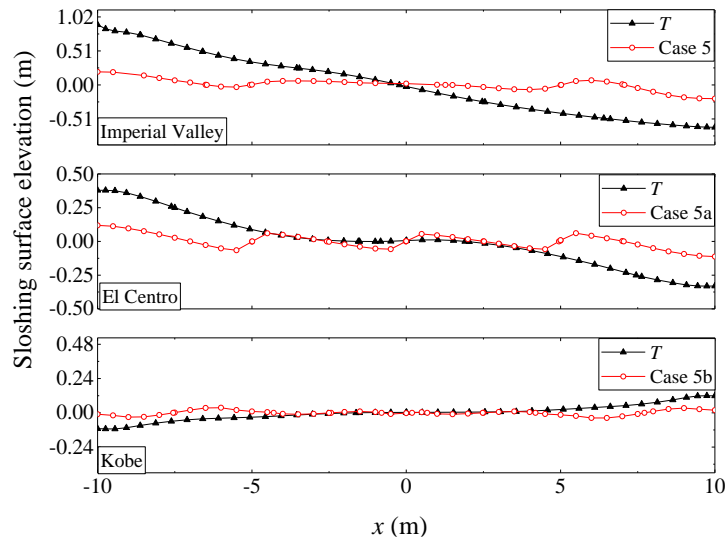


(a)

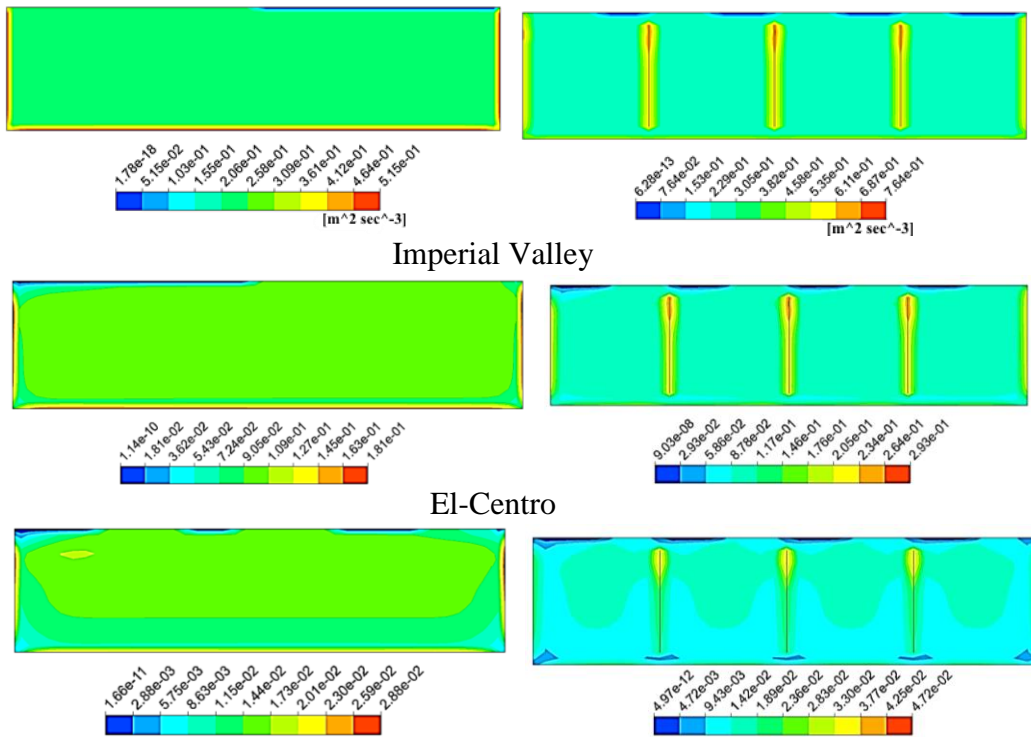


(b)

Fig. 6.13 Peak value of hydrodynamic pressure for various baffle configurations (a) Impulsive pressure (b) convective pressure.



(a)

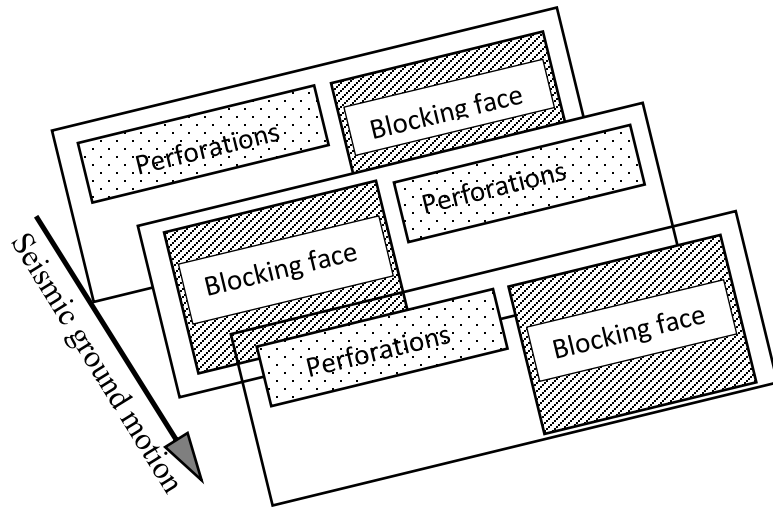


(i) Unbaffled tank 'T'

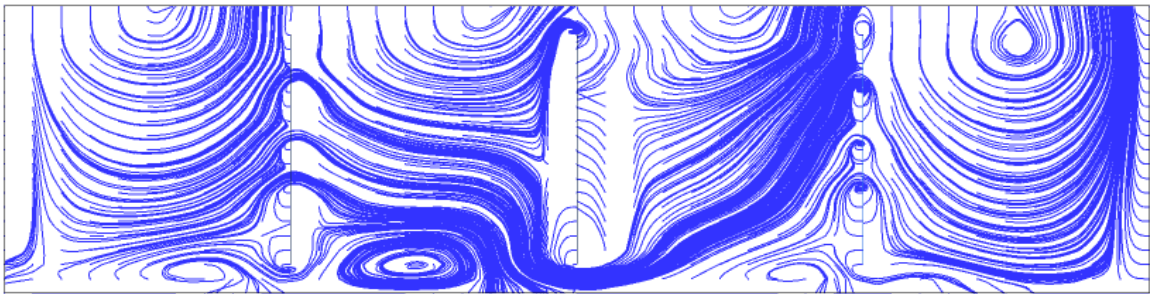
(ii) case 5

(b)

Fig. 6.14 Effectiveness of case 5 configuration with reference to (a) sloshing surface elevation (b) turbulence eddy dissipation.



(a)



(b)

Fig. 6.15 Slosh damping action by case 5 baffle configuration

(a) details of case 5 configuration (b) streamlines of flow in case 5 configuration.

The direct flow through the perforations is blocked by the successive blocking faces and generates more localized vortices, as shown in Fig. 6.15(b). From different configurations of the baffle plates considered in this study, the blockage effect is noted as the primary cause of slosh damping. The localized vortices formed by the combined effect of the blockage and the perforations are the secondary cause. Further, considering the different frequency ranges of the impulsive and convective modes, the effective perforations vary. Therefore, the percentage of perforation has to be selected in the range of 5% to 17% based on the dominating mode of response and considering the need for weight reduction.

The applicability of the proposed baffle configuration is studied using the experimental data of the unbaffled tank obtained from Xue et al. (2013). For this, the numerical model of the tank has been developed with a dimension of 0.57 m x 0.31 m x 0.5 m. The liquid volume is generated with a depth of 0.28 m. The computational domain is discretized to 353400 cells with the smallest mesh size of 0.005m. The numerical model is subjected to a surge excitation $x = -a \cos \omega t$. Here, 'a' and ' ω ' are equal to 0.015 m and $0.85\omega_0$, respectively. The impulsive hydrodynamic pressure measured at a point 0.065 m above the base of the generated numerical model of the tank without baffle is comparable with that obtained from the reference work, as shown in Fig. 6.16(a).

Later, the proposed configuration of the perforated baffle plate (case 5) is incorporated into the tank domain with an equivalent percentage of perforation of the baffle plate as that considered in the reference work. The response of the numerical model is quantified in terms of the hydrodynamic pressure and free surface elevation, as depicted in Fig. 6.16 (a) and Fig. 6.16(b). Incorporation of the baffle plate with the case 5 configuration reduces the impulsive hydrodynamic pressure by 65% compared to the tank model with the solid baffle plate. Further, the convective pressure almost reduces to a negligible value due to the reduction in the free surface elevation by 88% compared to the unbaffled tank. The slosh damping efficiency of the proposed baffle configuration is apparent from these observations.

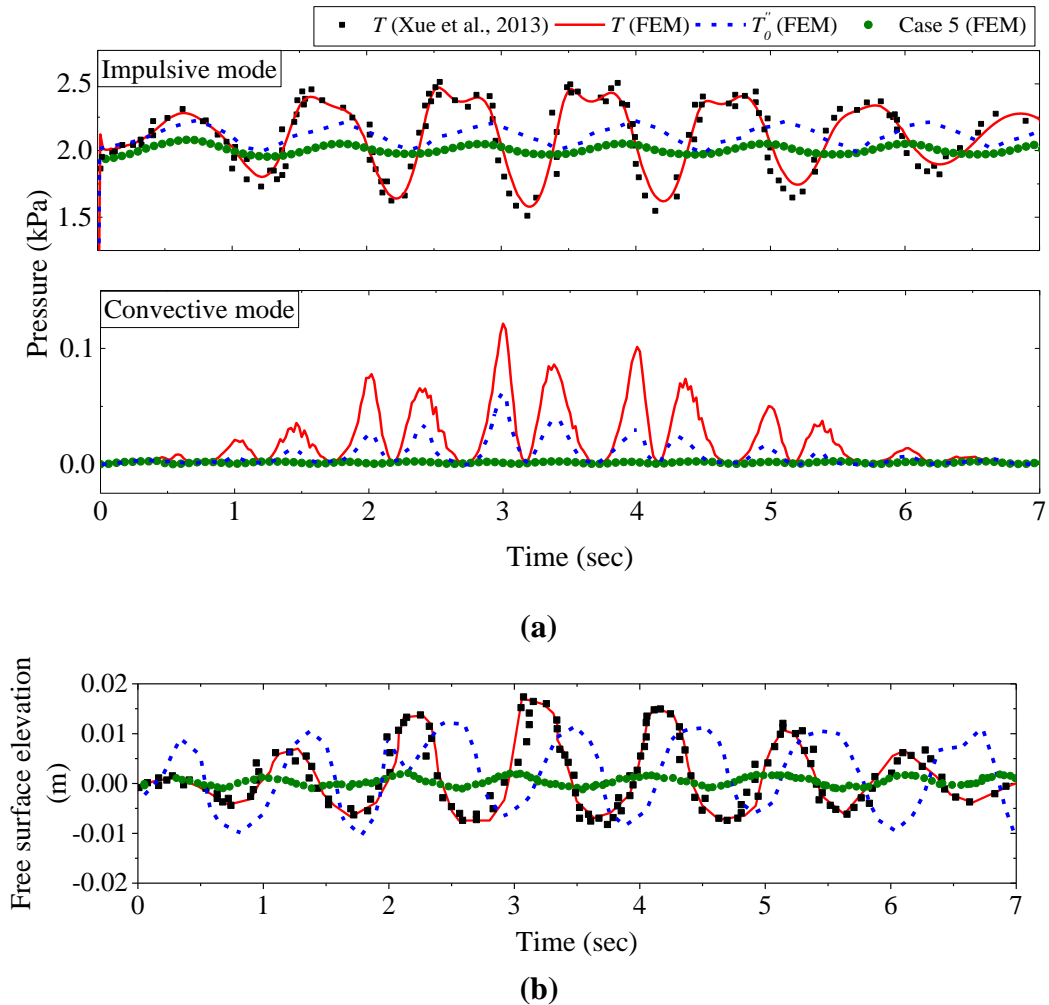


**Fig. 6.16 Applicability of case 5 configuration in terms of
(a) Hydrodynamic pressure (b) Free surface elevation at (-0.275,0,0).**

6.3 ANALYSIS OF GEOMETRIC CONFIGURATION OF PERFORATED BAFFLE PLATES UNDER PITCH EXCITATION

Most of the previous studies on liquid tanks were reported under surge excitations. However, the nature of external excitation, which triggers the sloshing motion of liquid, can be of any kind, including pitch motions. Therefore, a detailed parametric study is carried out under pitch excitation, considering tank models with and without baffle plates. The area of perforations, inter perforation distance, size of the perforations, the distance

between the perforated baffle plates, alignment of perforations, and the vertical position of the perforated baffle plate are considered as the parameters of the study.

6.3.1 Effect of area of perforations

The area of perforations of the baffle plate is the major parameter that influences the slosh damping efficiency of a perforated baffle plate (Bellezi et al. 2019). The area of perforation is represented in terms of the percentage of the total area of a baffle plate. The perforations are assumed to be drilled about the centre of the baffle plate in a rectangular pattern. The effects of the area of perforations are depicted in Fig. 6.17(a) and Fig. 6.17(b) under convective and impulsive modes of response, respectively. The responses of the tank without (T) and with solid baffle (T_0'') are represented, corresponding to 0% perforation. The convective response reduces with an increase in the percentage of perforation, and this trend continues up to 10% perforation with a maximum reduction of 44% compared to the un baffled tank. Beyond 10% perforation, the trend of response reverses. The reduction in the convective response with an increase in the percentage of perforation may be due to the increased number of edges, which damp the liquid sloshing by generating additional vortices. However, beyond 10% perforation, the blockage caused by the baffle plate reduces, causing increased slosh response.

On the other hand, in the case of impulsive response, the introduction of the perforated baffle plates reduces the slosh damping. Maximum slosh damping is observed for the tank model fitted with the solid baffle plate, which is observed to be 22% as compared to the un baffled tank. However, with the introduction of perforations in the baffle plate, the slosh response gradually increases. The impulsive response can be reduced by creating a blockage effect in the liquid medium. The introduction of perforations in the baffle plate reduces the blockage, and thereby the slosh response increases. The dominance of the blockage effect caused by the baffle plate on the slosh damping of impulsive response is evident from these observations. Additionally, it is noted that the perforated baffle plates are effective in damping the convective response of the sloshing liquid.

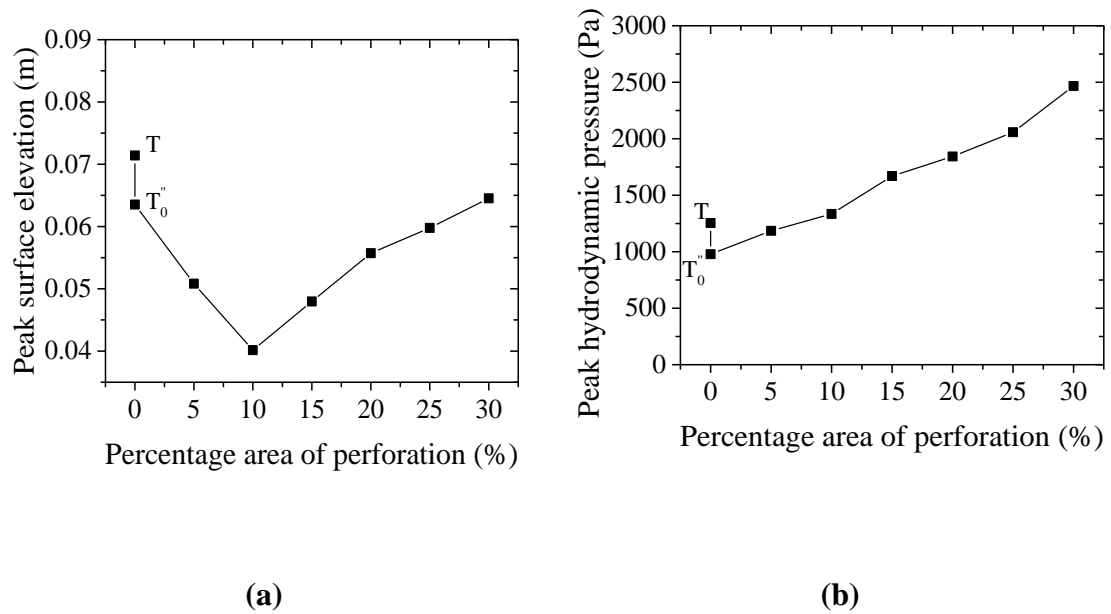
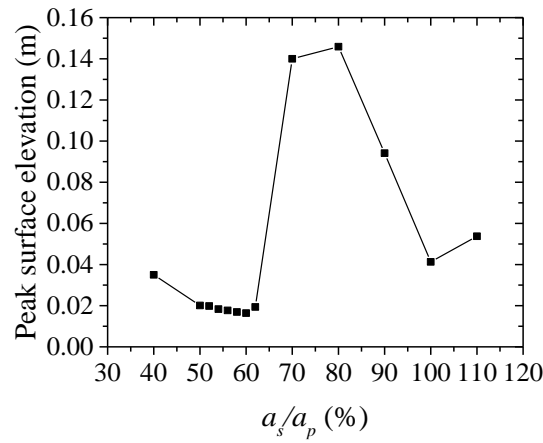


Fig. 6.17 Variation of response with percentage of perforation in terms of

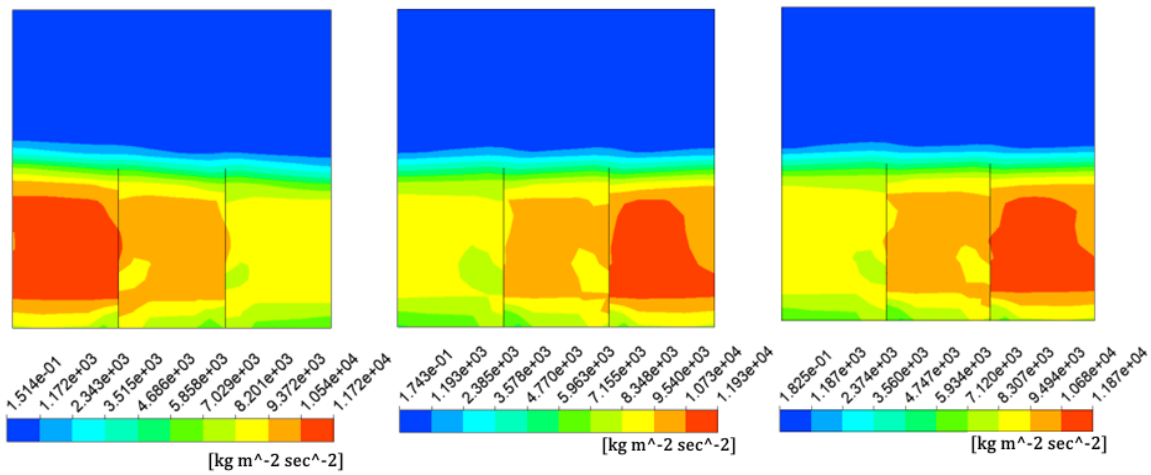
(a) Free surface elevation (b) hydrodynamic pressure.

6.3.2 Effect of inter perforation distance

The variations in the inter perforation distance affect the slosh damping performance of the perforated baffle plate, as shown in Fig. 6.18(a). The inter perforation distance is varied as the ratio of the total area of solid (a_s) in the perforated region to the total area of perforations (a_p). Here, the tank models fitted with the bottom-mounted perforated baffle plates of 10% perforations is considered for the analysis. The slosh responses are observed in terms of peak values of free surface elevation and the corresponding pressure gradient. An increase in the solid area up to 60% of the total area of perforations increases the slosh damping by 53% due to the increase in the blockage effect. A rapid reduction in the slosh damping is noted with a further increase in the solid area in the perforated region. It may be due to the constructive interference of the waves passing through the nearby perforations.



(a)



(i)

(ii)

(iii)

(b)

Fig. 6.18 Variation of response with percentage area of solid in terms of (a) Free surface elevation (b) Contours of pressure gradient corresponding to peak surface elevation for the ratio a_s/a_p of (i) 60% (ii) 80% (iii) 100%.

The slosh damping is slightly improved with a further increase in the area of solid in the perforated region. However, the increase in the slosh damping is less than that obtained

with a solid area of 50% to 60%. This trend of slosh damping with variation in the area of solid between the perforations is explained by the contours of the pressure gradient as depicted in Fig. 6.18(b). The pressure gradient is minimum for the tank model with perforated baffle plates of 60% solid area in the perforated region. The reduced pressure gradient further reduces the slosh response of the tank.

6.3.3 Effect of size of perforations

The effect of the size of perforations is studied by varying the number of perforations (n_p) of the baffle plate, as shown in Fig. 6.19(a). For this, the tank models fitted with baffle plates of 10% perforations with varying diameters are considered. The peak value of surface elevation decreases with an increase in the diameter of perforations up to 2 cm, with a maximum reduction of 12%. It may be due to the gradual reduction in the velocity of the sloshing wave, and it further causes increased vortex formation. The additional vortices dissipate more energy and reduce the slosh response. Beyond a diameter of 2 cm, the slosh response slightly increases, and the liquid tank tends to behave as an unbaffled tank after a diameter of 2.5 cm. This may be due to the increase in the turbulence kinetic energy, as shown in Fig. 6.19(b), which reduces the vortex formation. The horizontal distance measured along the x-direction, with respect to the centre of the tank is represented as 'x'.

The turbulence kinetic energy of the tank-baffle model with 50 numbers of perforations (1 cm diameter) is slightly more than that of the tank-baffle model with 12 numbers of perforations (2 cm diameter). It may be due to the increased velocity of the sloshing wave passing through the perforations of smaller diameter, which reduces the turbulence eddy formation near the baffle plate. Therefore, the diameter of perforations should be minimum, provided the adequate flow passes through the perforations to cause the energy dissipation by forming localized vortices and blockage effect.

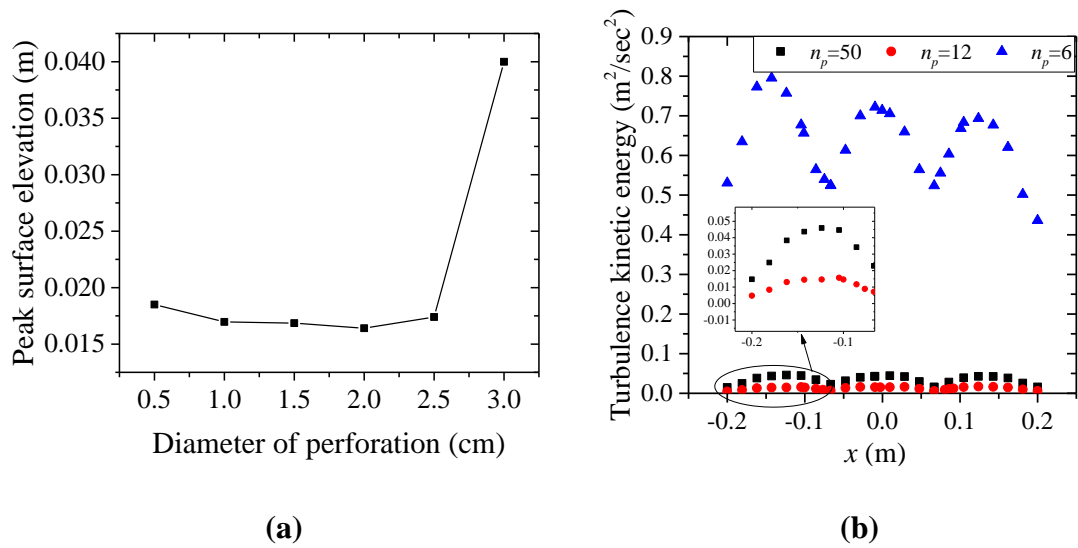


Fig. 6.19 Variation of response with number of perforations in terms of (a) Free surface elevation (b) Turbulence kinetic energy.

6.3.4 Effect of distance between perforated baffle plates

The tank model fitted with 10% perforated baffle plates having 60% solid in the perforated region is considered to study the effect of the distance between the perforated baffles on the slosh responses of the liquid in a rectangular tank. The size of the perforations is assumed to be 2 cm. The distance between the two vertical perforated baffle plates is varied as the ratio ' x_b/x_w '. The response parameters are observed under varying x_b/x_w ratios in terms of the free surface elevation, as shown in Fig. 6.20(a).

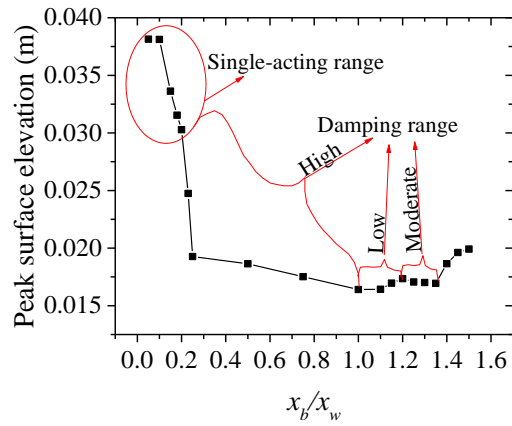
The slosh damping generated by the tank-baffle model with x_b/x_w ratio up to 0.2 is less, which is apparently similar to that generated by the tank-baffle model with a single perforated baffle plate with a peak surface elevation of 0.0416 m. In this range of x_b/x_w ratio, the distance between the two baffle plates is insufficient to generate adequate damping either by the blockage effect or by the vortex formation separately as two baffles. Specifically, the multiple baffles installed in this range of x_b/x_w ratio will act as a single baffle. Therefore, the range of x_b/x_w ratio up to 0.2 is named as 'single-acting range'.

Beyond this range, a rapid increase in the slosh damping due to the combined action of two baffles is noted up to an x_b/x_w ratio of 1. Notably, the slosh response reduced by 46% from $x_b/x_w=0.2$ to $x_b/x_w=1$.

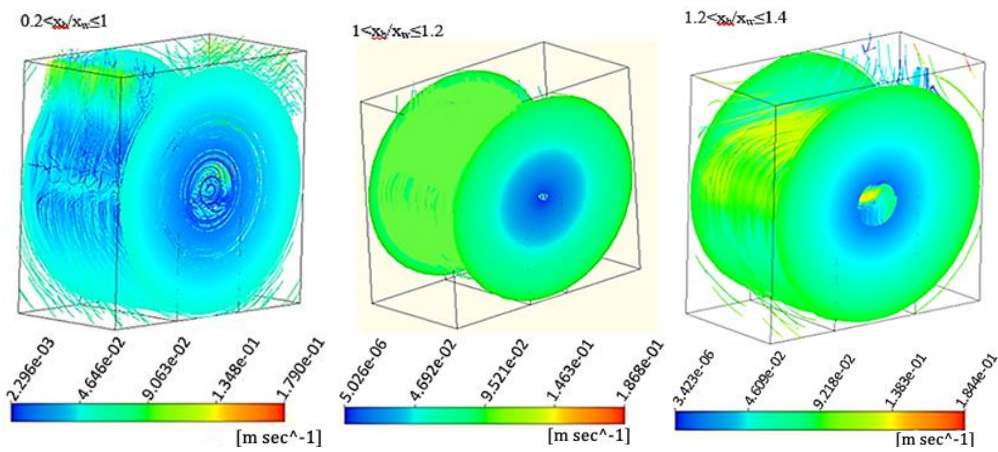
This increased slosh damping is evident from the streamlines of velocity, as shown in Fig. 6.20(b). The velocity of the sloshing wave reduces in the range of $0.2 < x_b/x_w \leq 1$, which causes a reduction in the slosh response. At $x_b/x_w=1$, the slosh response is minimum due to the formation of additional vortices. Therefore, the range of $0.2 < x_b/x_w \leq 1$ is named as 'high damping range'. Beyond this range, the damping is slightly less up to $x_b/x_w=1.2$, which is named as 'low damping range'. In the range of $1.2 < x_b/x_w \leq 1.4$, the damping is slightly improved compared to the low damping range. This may be due to the increase in the travel length of the wave after undergoing initial damping by the baffle plate at either side of the tank. This range is named as 'moderate damping range'. For the range of $x_b/x_w > 1.4$, the damping is reduced as the general trend of the velocity of streamlines is to increase towards the sides of the tank under pitch oscillations.

6.3.5 Effect of alignment of perforations

The peak values of convective and impulsive responses occur at the free surface and the bottom of the tank, respectively. Moreover, the configurations of baffle plates to damp the slosh response under convective and impulsive modes are noted to be different, as discussed in section 6.3.1. Therefore, considering the advantages of the perforated baffle plate in reducing the overall structural weight, the perforations should be drilled on a baffle plate in such an alignment that will reduce the convective and impulsive responses.



(a)



(i)

(ii)

(iii)

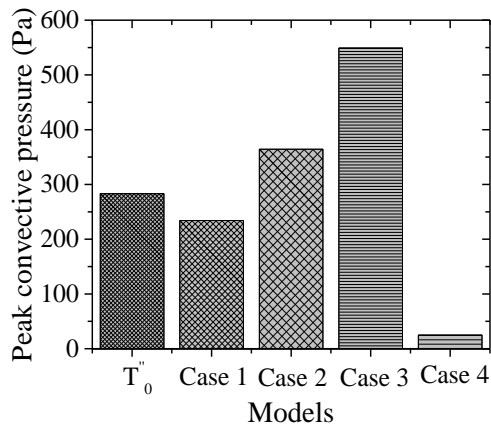
(b)

Fig. 6.20 Variation of response with distance between perforated baffle plates
(a) Free surface elevation (b) Velocity streamlines of flow for the tank models with
 x_b/x_w equal to (i) 0.25 (ii) 1.1 (iii) 1.25.

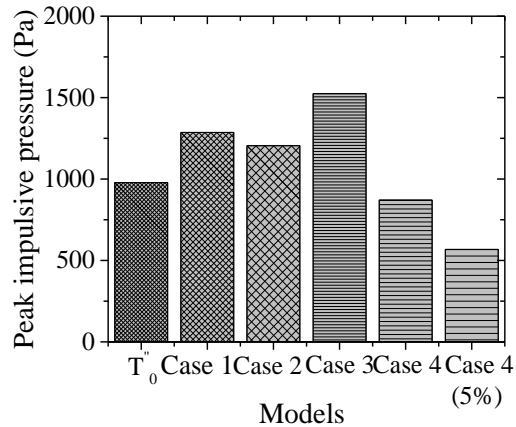
The variations in the slosh damping with the variations in the alignment of perforations are studied by analysing the slosh responses of the tank models fitted with four different cases of perforations under convective and impulsive modes. For this, the baffle plates with 10%

perforations are considered. The peak values of hydrodynamic pressure under convective and impulsive modes of response, measured on points $(-0.2,0,0)$ and $(-0.2,-0.2,0)$, respectively, are illustrated in Fig. 6.21(a) and Fig. 6.21(b). The minimum value of pressure response is obtained under case 4 type alignment of perforations under convective and impulsive modes of response. Compared to the liquid tank model with solid baffle plates, the impulsive pressure response is reduced by 11% for the case 4 type alignment of perforations. The corresponding reduction in the convective pressure response under case 4 type alignment is 91%. The effectiveness of this type of alignment to damp the convective response is evident from the magnitude of reduction in the slosh response. Considering the impulsive response, the slosh damping increases under case 4 type alignment compared to the tank model with the solid baffles due to the additional blockage and the consequent formation of vortices. The blockage effect is found to be the major factor that causes slosh damping under impulsive condition. Therefore, further study is carried out by considering the perforated baffle plates of case 4 type alignment with 5% perforations to provide an increased solid area of the baffle plate. Consequently, the impulsive response is reduced by 42% compared to the tank model with the solid baffle plates, as shown in Fig. 6.21(b).

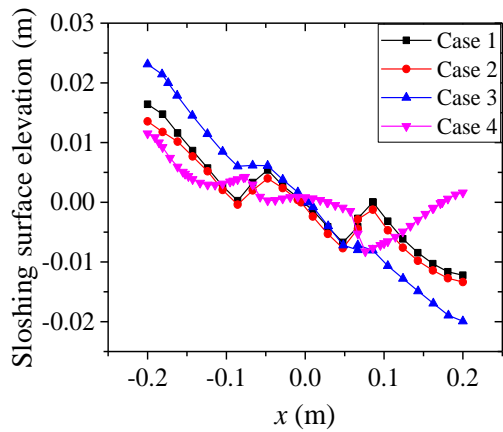
Fig. 6.21(c) depicts the sloshing surface elevation under different cases of alignment considered. The maximum reduction in the free surface elevation is noted under case 4 type alignment. In this type of alignment, the flow passing through the perforations of a baffle plate is blocked by the solid face of the successive baffle plate, causing reduced slosh response. Specifically, an additional blockage effect is developed in the case 4 type alignment by positioning the perforations in a zig-zag manner in the successive baffles. Therefore, this new alignment is named as ‘zig-zag blocking alignment’. The power spectral density corresponding to the temporal variation of the free surface elevation measured at point $(-0.2,0,0)$ is illustrated in Fig. 6.21(d). Here, the peak value is noted for 1.329 Hz, which is the near excitation frequency. The minimum spectral density is noted under case 4 type alignment. The effectiveness of the case 4 type alignment is evident from the trend of power spectral density corresponding to the four different cases considered.



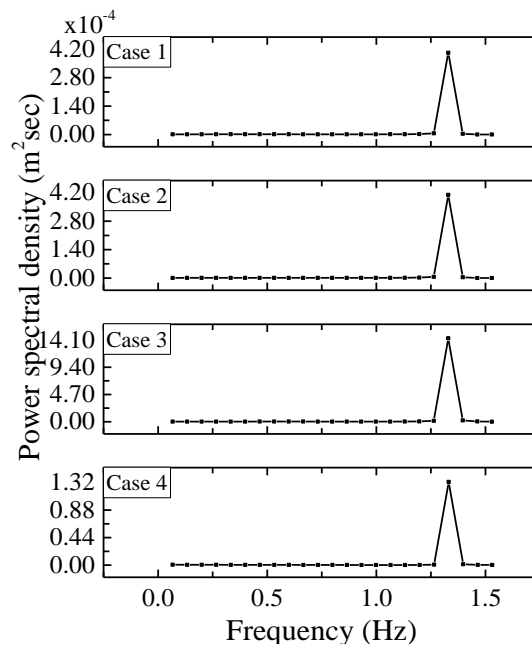
(a)



(b)



(c)

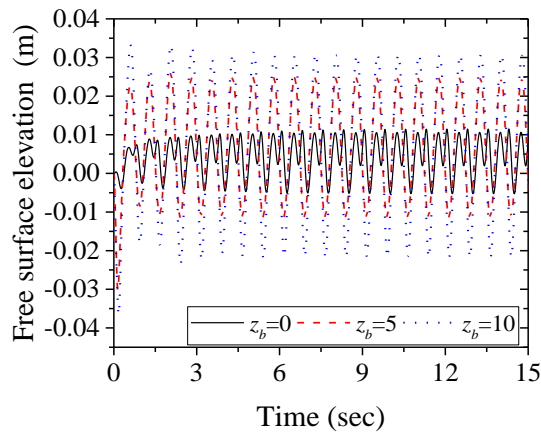


(d)

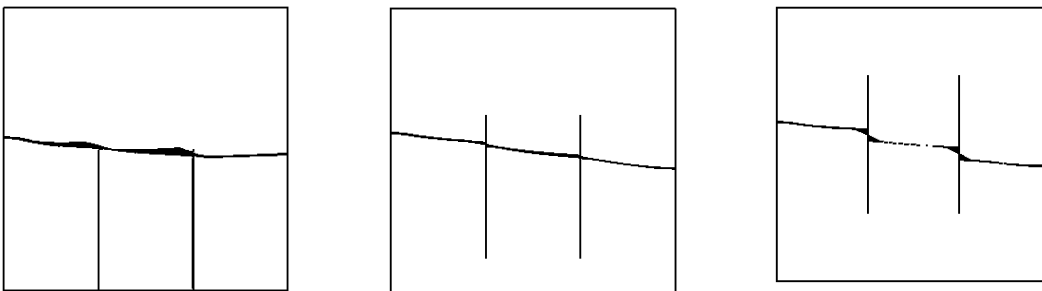
Fig. 6.21 Variation of response with alignment of perforation in terms of
 (a) dynamic pressure (b) Impulsive pressure (c) sloshing surface elevation
 (d) power spectral density.

6.3.6 Effect of vertical position of perforated baffle plate

The effect of the vertical position of the perforated baffle plate on the slosh damping is studied by considering the tank models fitted with 10% perforated baffle plates having zig-zag blocking alignment of perforations. The distance between the base of the baffle plate and that of the tank (z_b) is varied as 0, 5 cm, and 10 cm. Fig. 6.22(a) shows the variations of the free surface elevations in the time domain, measured on point '(-0.2,0,0)' of the liquid medium for the various vertical positions of the perforated baffle plate. The maximum slosh damping is noted for the tank model with baffle plates fixed at the bottom of the tank ($z_b=0$). Specifically, a maximum reduction in the free surface elevation is noted to be 66% for the tank model with baffle plates fixed at $z_b=0$, compared with that of the tank-baffle model with $z_b=10$. The baffle plates extending from the bottom to the top of the liquid surface cause hindrance to the sloshing wave, generating a shear layer. Consequently, the slosh damping is increased due to the viscous action (Akyildiz and Ünal 2005). The free surface elevation is increased as the baffle is shifted towards the top. It may be due to the reduction in the submerged perforations, which further reduces the blockage and the vortex formation. The effect of the vertical position of the baffle plates on the free surface deformation of the liquid is evident from Fig. 6.22(b), which depicts the front view of the isosurface of the liquid corresponding to the peak surface elevation. The liquid deformation is noted to be minimum for the tank model with the baffle plates positioned at $z_b=0$. In the other two cases, the step formation with increased deformations is noted for the liquid free surface. Therefore, the sloshing wave is highly interrupted, and the energy of the sloshing wave is reduced when the baffle plates with the zig-zag blocking alignment of perforations that extend from the bottom of the tank to the free surface of the liquid are installed in the liquid tank.



(a)



(i)

(ii)

(iii)

(b)

Fig. 6.22 Variation of response with vertical position of baffle plate in terms of

(a) Free surface elevation (b) Free surface deformation of tank models with

(i) $z_b=0$ (ii) $z_b=5$ (iii) $z_b=10$.

6.3.7 Effect of fill depth of liquid

The variations in the fill depth of the liquid cause variations in the convective and impulsive mass of the liquid that further affects the slosh response under the corresponding modes. Initially, a tank model without the baffle plates is analysed by varying the fill depth of the liquid from 0.05 m to 0.3 m. The slosh response decreases with an increase in the fill depth

of liquid for both the tank models considered, as illustrated in Fig. 6.23. This may be due to the decrease in the convective mass of the liquid. The effect of the fill depth of the liquid is also investigated by considering the tank model with a 10% perforated baffle plate with a zig-zag blocking alignment of perforations (case 4). The use of the baffle plates with case 4 type alignment reduces the free surface elevation by an average value of 80% compared with that of an unbaffled tank. A maximum reduction of 82% is noted under minimum fill depth, where the free surface elevation will be maximum. Therefore, the perforated baffle plate with zig-zag blocking alignment effectively reduces the slosh response of the liquid tank of given geometry filled up to any depth of liquid under the pitch excitation.

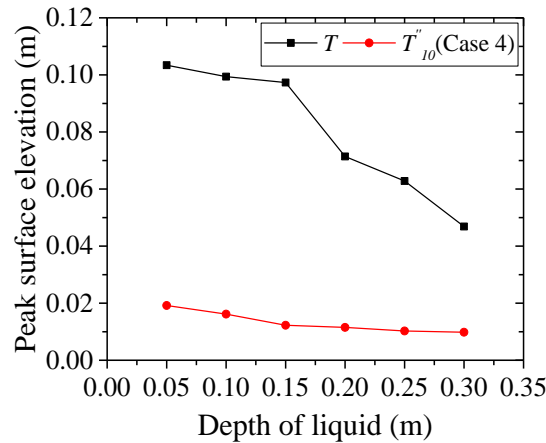


Fig. 6.23 Variations in the peak surface elevations with fill depth of liquid.

6.3.8 Effect of frequency and amplitude of input motion

The slosh responses of the liquid tank for different frequencies of excitation are observed in terms of the sloshing surface elevation, as depicted in Fig. 6.24(a). The unbaffled tank and the tank model fitted with the baffle plates of the case 4 type configuration are considered for the study. The installation of the perforated baffle plate with the zig-zag blocking alignment of perforations shifts the fundamental frequency to a lower value. Therefore, the initial peak occurs at a lower value of frequency. The peak response is more at the higher frequency ranges due to the occurrence of resonance conditions at higher

modes. However, the response is highly damped under near-resonant and far-resonant conditions compared to the un baffled tank.

Fig. 6.24(b) shows the variations in the slosh response with the variations in the amplitude of input motion. The study is conducted by varying the amplitude of input motion from 4° to 20° . An increase in the amplitude of input motion causes a rapid increase in the peak values of the free surface elevation of the un baffled tank in the initial stage. However, in the case of the tank model fitted with the perforated baffle plates of the case 4 type configuration, the increase in the slosh response with the increase in the amplitude of excitation is gradual. It may be due to the damping provided by the perforated baffle plates of the case 4 type configuration. Notably, the perforated baffle plate with the case 4 type configuration causes an average reduction of 80% for the slosh response in terms of the free surface elevation under varying amplitude of excitation considered. The effectiveness of the perforated baffle plates with the zig-zag blocking alignment over a wide range of frequency and amplitude of input motion is evident from these observations.

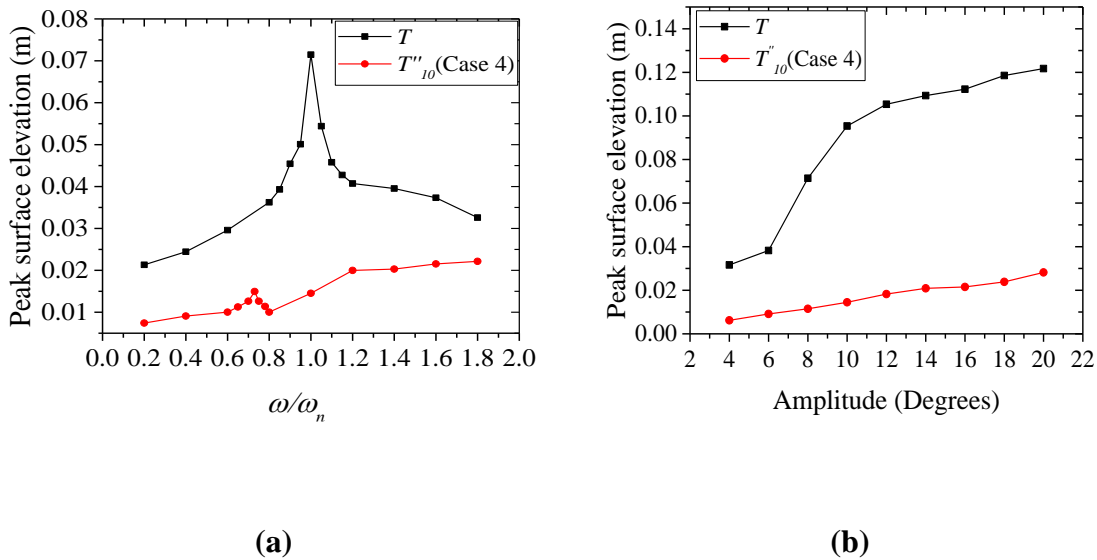


**Fig. 6.24 Variation in free surface elevation with (a) Frequency of input motion
(b) Amplitude of input motion.**

6.4 EXPERIMENTAL EVALUATION OF DEVELOPED CONFIGURATION OF PERFORATED BAFFLE PLATE

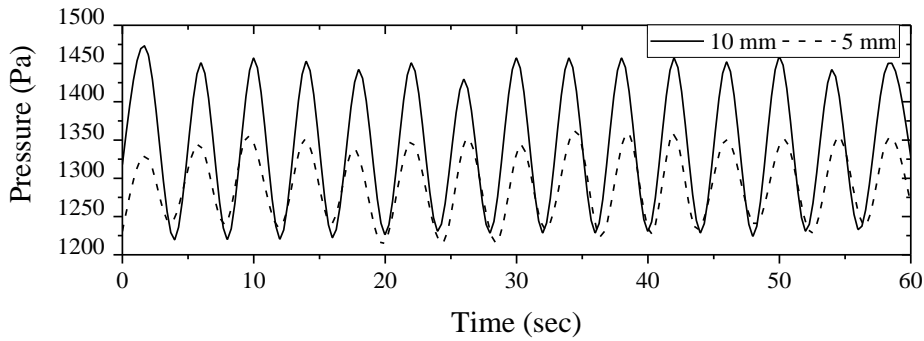
The experimental validation of the effectiveness of developed configuration of the perforated baffle plate is done by conducting a shake table test on the laboratory models. The slosh responses are observed in terms of pressure, free surface elevation and liquid deformation.

6.4.1 Effect on pressure

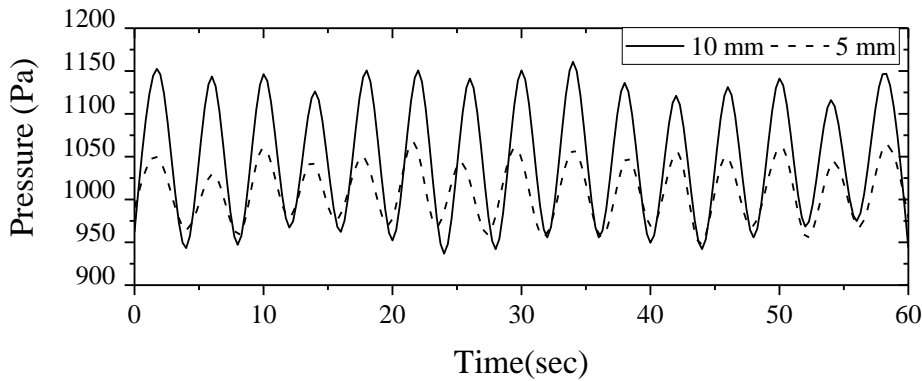
The temporal variation of pressure at probe 1 corresponding to the un baffled tank is shown in Fig. 6.25(a). The fill depth is kept equal to 0.2 m, and the shake table is excited with a frequency of 1.7 Hz. The response is recorded for 60 sec, corresponding to the amplitude of excitations of 5 mm and 10 mm. Rapid variation in the response can be noted with maximum and minimum pressure values equal to 1459 Pa and 1220 Pa under 10 mm amplitude of excitation. The magnitude of response decreases with the decrease in the amplitude of excitation.

The incorporation of solid baffle plates in the tank decreases the pressure response by 21% and 13%, corresponding to the maximum and minimum values, as shown in Fig. 6.25(b). As the shake table moves to and fro, the liquid surface elevates in the opposite direction of movement, exerting maximum and minimum pressure on the tank walls for each cycle of excitation. The movement of liquid is blocked with the insertion of the solid baffle in the tank, which reduces the slosh response on the tank wall.

However, the incorporation of perforated baffle plates slightly increases the pressure response due to the reduction in the blockage caused by the baffle plate. As the percentage of perforation increases, the blockage caused by the baffle plate further decreases. Therefore, the pressure response exerted on the tank walls increases as the percentage of perforations increases, as shown in Fig. 6.26(a) to Fig. 6.26(c). However, under all these cases, the magnitude of response decreases with a decrease in the amplitude of excitation.



(a)



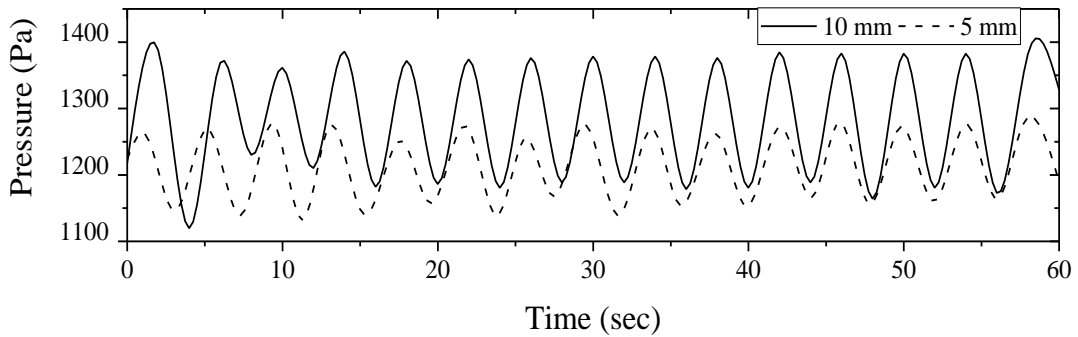
(b)

**Fig. 6.25 Variation in pressure at probe 1 for
(a) un baffled tank (b) tank fitted with solid baffles.**

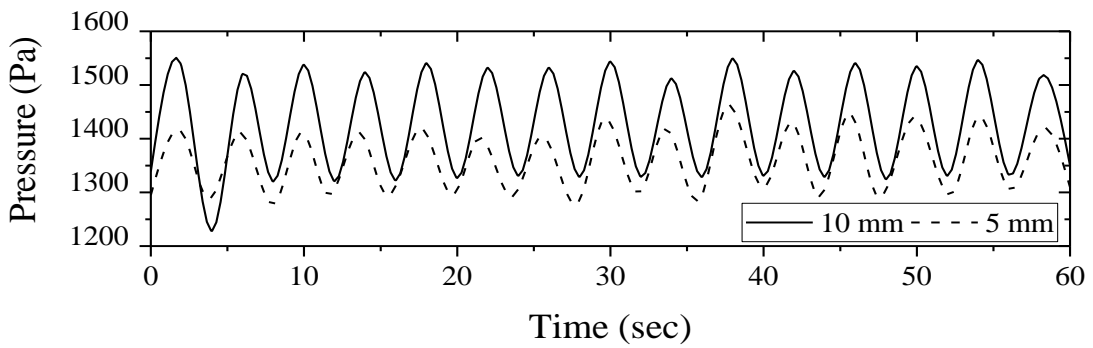
The peak values of pressure for different tank models with and without baffle plates are depicted in Fig. 6.27. The responses corresponding to the amplitude of excitation of 5 mm and 10 mm are marked for all cases. The slosh response decreases with the incorporation of solid baffle plates in the tank. However, the slosh response increases slightly with the use of perforated baffle plates.

In view of the observations based on the numerical analysis and considering the advantages of weight reduction with the use of perforated baffle plates, a new set of perforated baffle plates are incorporated into the tank with the zig-zag blocking alignment of perforations.

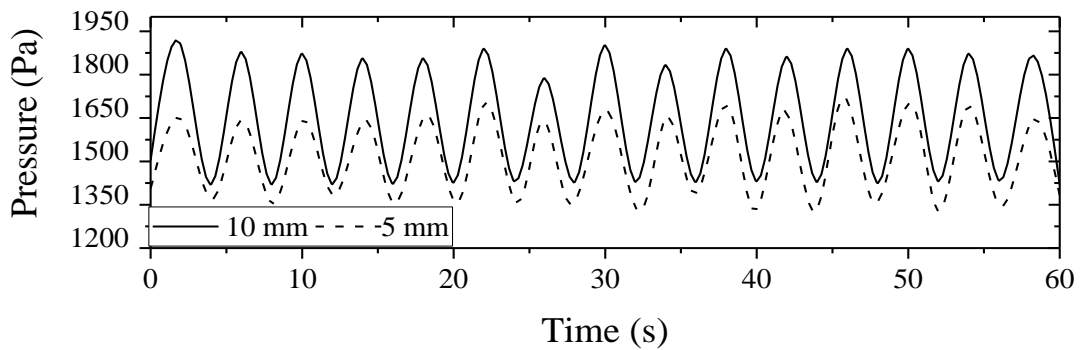
For this, a minimum percentage of perforations of 5% is considered. Notably, an average reduction of 55% is observed in the peak values of pressure under 5 mm and 10 mm amplitudes of excitation compared to the un baffled tank.



(a)



(b)



(c)

Fig. 6.26 Variation in pressure at probe 1 for tank fitted with perforated baffles of percentage of perforations (a) 5% (b) 10% (c) 15%.

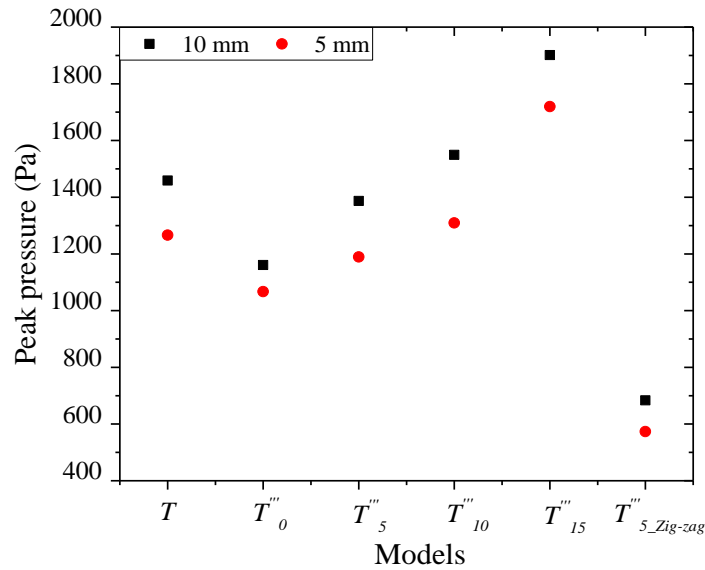


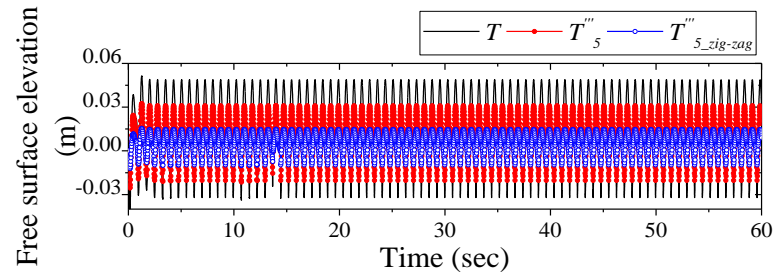
Fig. 6.27 Variation in peak value of pressure for different models with and without baffle plates.

6.4.2 Effect on free surface elevation

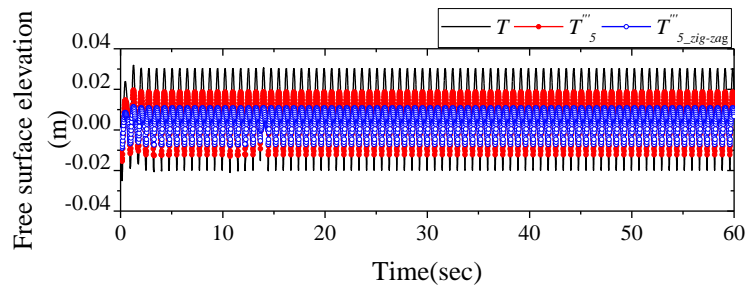
The temporal variation of free surface elevation for the tank models with and without baffle plates is shown in Fig. 6.28(a). The fill depth is kept equal to 0.2 m for all the cases, with the frequency of excitation being 1.7 Hz. The shake table is moved with an amplitude of 10 mm. The free surface elevation is reduced by 70% with the incorporation of perforated baffle plates of zig-zag blocking alignment of perforations in the tank model. A similar observation is noted under the amplitude of excitation of 5 mm as well, as shown in Fig. 6.28(b). However, the magnitude of response is reduced under 5 mm amplitude compared to that under 10mm for all cases.

6.4.3 Liquid deformation

The liquid deformation corresponding to the unbaffled tank and tank fitted with perforated baffle plates of zig-zag blocking alignment of perforations are given in Fig. 6.29. The amplitude of excitation of the shake table is kept equal to 10 mm.

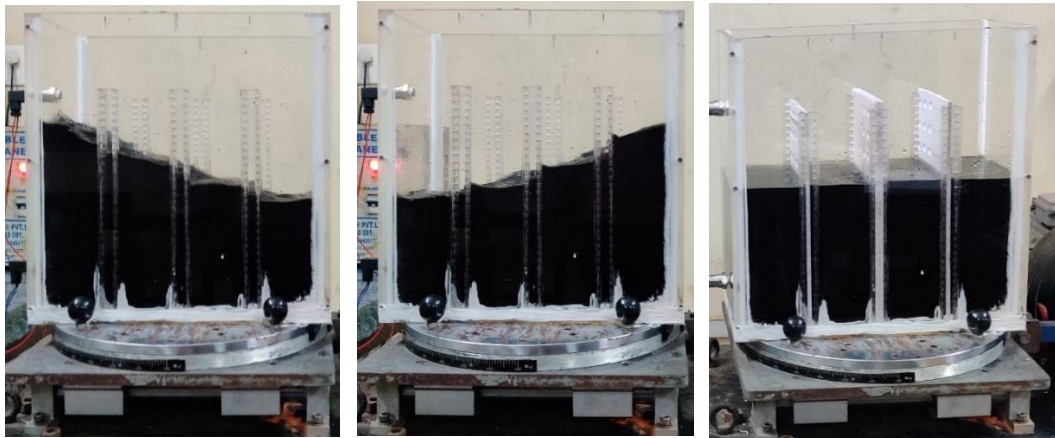


(a)



(b)

Fig. 6.28 Variation in free surface elevation under amplitude of excitation of (a) 10mm (b) 5mm.



(a)

(b)

(c)

Fig. 6.29 Maximum deformation of liquid in (a), (b) unbaffled tank (c) tank fitted with perforated baffle plates of zig-zag blocking alignment of perforations.

The unbaffled tank produced maximum liquid deformation under the excitation exerted by the shake table. The liquid free surface level is reduced to a nearly stable level with the introduction of perforated baffle plates of zig-zag blocking alignment of perforations in the tank. The effectiveness of the zig-zag blocking alignment of perforations is evident from these observations.

6.5 SUMMARY

A detailed parametric study is carried out considering various geometric configurations of solid and perforated baffle plates. The analysis is carried out under seismic ground motions of different frequency ranges and pitch excitation considering impulsive as well as convective conditions. An effective configuration of the perforated baffle plate is developed with the percentage of perforation in the range of 5% to 17%, which should be selected based on the frequency characteristics of the sloshing liquid and the input motion along with the requirement for weight reduction. The developed configuration is validated by conducting a shake table test.

CHAPTER 7

CONCLUSIONS

7.1 GENERAL

The slosh responses of the rectangular tank with baffle plates are investigated, and an anti-slosh mechanism that damp the slosh response effectively has been developed. Initially, the analysis of free vibration characteristics of liquid tanks was carried out. Next, the analysis of the geometric configuration of the perforated baffle plate is performed by carrying out pressure-based transient analysis under seismic ground motions and pitch excitation. A detailed parametric study is conducted, and an effective configuration of the perforated baffle plate is developed to damp the slosh response of the rectangular liquid tanks effectively. Finally, the effectiveness developed configuration of the perforated baffle plate is evaluated experimentally by carrying out a shake table test.

7.2 CONCLUSIONS OF STUDY

Based on the modal analysis on 560 cylindrical tank models and the subsequent ANN and regression analysis, the following conclusions have been drawn:

1. Three International codes considered in this study overestimate the frequency values up to the half-filled conditions of the tank models.
2. For the tanks with more than half-filled conditions, the codes underestimate the frequency values except for tanks with the lowest aspect ratio.
3. The formulae that are given in current codal practices for the estimation of the fundamental impulsive frequency of the cylindrical liquid-tank systems are reliable for the tanks with an aspect ratio of 0.5 and below.

4. The fundamental impulsive frequency of the tanks is directly proportional to the aspect ratio of the tank, thickness of the tank wall and the grade of material.
5. The fundamental impulsive frequency of the tanks decreases with an increase in the density of the filled liquid.
6. The aspect ratio of the tank is a significant factor that affects the fundamental impulsive frequency of cylindrical tanks.
7. The variation in frequency values from that of codes increases with aspect ratio. This variation is more for the tanks with an aspect ratio greater than 1. The general trend of dynamic characteristics of cylindrical liquid tanks follows two cases:
 Case 1: Liquid tank models with an aspect ratio less than or equal to 1
 Case 2: Liquid tank models with an aspect ratio greater than 1
8. Modification coefficients for the standard codal expressions are introduced for the accurate estimation of the fundamental impulsive frequency of the cylindrical liquid tanks. These coefficients are applicable for the liquid tanks with an aspect ratio from 0.7 to 1.9.

Based on the study of free vibration characteristics of rectangular tanks with and without baffle plates, the following conclusions have been obtained:

1. The dynamic interaction of the structural vibration mode and the liquid sloshing mode is negligible due to the large difference in the frequency ranges under convective and impulsive modes.
2. The introduction of baffle plates in the liquid tank reduces the fundamental frequency under both convective and impulsive modes.
3. An increase in the number of perforated baffle plates increases the fundamental frequency under impulsive mode; however, it reduces that under the convective mode.

4. Frequency of tank-baffle models tend to reach that of the unbaffled tank at a higher percentage of perforations.

The seismic analyses of tank-baffle models are carried out under Imperial Valley (1979), El Centro (1940) and Kobe (1995) earthquakes of low to high frequency ranges. The parametric study is carried out to analyse the influence of geometry and location of perforated baffle plates on slosh response of liquid tanks under seismic ground motions. For this, the effects of frequency of ground motion, percentage of perforation of the baffle plate, clear spacing of perforations and offset distance of the perforated plate and alignment of perforations, on the slosh response of the liquid medium are observed. The free surface elevation, hydrodynamic pressure, turbulence eddy dissipation, streamlines of flow and deformed liquid surface are considered as the response parameters. The following conclusions have been drawn from the study:

1. Unlike normal engineering structures, the liquid tank experiences two near-resonant conditions due to the existence of impulsive and convective modes of vibration. The nonlinearity and the consequent turbulence are profound under low frequency ground motions due to the probability of occurrence of the near-resonant condition under convective mode.
2. The magnitude of impulsive response is larger than that of convective mode.
3. Under the impulsive mode, the effective percentage of perforation is 5% of the total area of the baffle plate, which indicates the need for a high percentage of solid area to resist a large magnitude of hydrodynamic pressure generated by the high frequency seismic ground motions.
4. Under the convective mode, the effective percentage of perforation varies from 10% to 17%. An effective percentage of perforation should be selected based on the predominant frequency of the previously recorded seismic ground motions and the need for weight reduction.
5. The energy dissipation increases for moderately spaced perforations.

6. In the case of single baffled tanks, the Rapid zone (R-zone) and the Moderate zone (M-zone) are identified based on the percentage reduction in the peak surface elevation to pilot the positioning of a perforated baffle plate in the liquid tanks.
7. More number of moderately spaced perforations result in a damped free surface elevation due to flow separation and vortex shedding, provided the baffle plate is positioned in the Moderate zone of the tank.
8. Case 5 baffle configuration with a zig-zag arrangement of perforations generates an additional blockage effect on sloshing liquid resulting in the subsequent increase in the slosh damping.
9. The effective baffle configuration is generated by following the case 5 configuration with the percentage of perforation in the range of 5% to 17%, which should be selected based on the frequency characteristics of the sloshing liquid and the seismic ground motion along with the requirement for weight reduction.

The parametric study is extended to study the influence of geometry and location of perforated baffle plates on slosh response of liquid tanks under pitch excitation as well. The area of perforations, inter perforation distance, size of the perforations, the distance between the perforated baffle plates, alignment of perforations, and the vertical position of the perforated baffle plate are considered as the parameters of the study. The slosh responses are observed in terms of free surface elevation, hydrodynamic pressure, turbulence kinetic energy, velocity streamlines, power spectral density corresponding to the free surface elevation and the free surface deformation. Based on the observations of parametric study under seismic ground motion and pitch excitation, an effective baffle configuration is developed. The conclusions of the study are as follows:

1. The blockage effect caused by the baffle plate is the major factor that reduces the impulsive response of the liquid. On the other hand, the convective response is reduced by the combined action of the blockage and the vortices generated by the perforations.

2. The solid baffle plate is effective in reducing the impulsive response, whereas the perforated baffle plate is effective in reducing the convective response.
3. For a particular percentage of the perforation, the diameter of the perforation should be selected such that adequate flow passes through these perforations to cause the energy dissipation by the blockage effect and by forming the localized vortices.
4. The solid area to be provided between the perforations is 50%-60% of the area of perforations, which produces the maximum slosh damping under pitch excitation.
5. The multiple baffle plates installed in the range of $x_b/x_w \leq 0.2$ act as a single baffle plate. Therefore, this range is named as single-acting range.
6. The study identified the $0.2 < x_b/x_w \leq 1.4$ as the damping range. The multiple perforated-baffle plates installed in this range produce maximum slosh damping. Moreover, the damping range is divided into three ranges, namely; low ($1 < x_b/x_w \leq 1.2$), moderate ($1.2 < x_b/x_w \leq 1.4$), and high ($0.2 < x_b/x_w \leq 1$), based on the damping provided by the baffle plates in the corresponding range.
7. The effective baffle configuration is generated by following the zig-zag blocking alignment of perforations with the percentage of perforation in the range of 5% to 17% that should be selected based on the frequency characteristics of the sloshing liquid and the input motion along with the requirement for weight reduction.

The shake table test is carried out to evaluate the effectiveness of the developed configuration of the perforated baffle plate. The slosh response is observed in terms of pressure, free surface elevation and liquid deformation. The conclusions of the experimental study are as follows:

1. The introduction of the solid baffle plate reduces the slosh response. However, an increase in the slosh response is noticed with the introduction of perforated baffle plates.
2. The magnitude of slosh response is directly proportional to the amplitude of input motion.

3. The developed configuration reduced the slosh response by 70% compared to the unbaffled tank.

7.3 SUMMARY

In summary, based on the numerical studies on a large number of models, modification coefficients are introduced for a better representation of the impulsive natural frequency of cylindrical liquid storage tanks. Influence of geometric configuration of perforated baffle plates on the slosh response of liquid tanks are noted. Also, a zig-zag blocking alignment of perforation to damp the slosh response effectively is developed. The recommended percentage of perforation is in the range of 5% to 17%, which should be selected based on the frequency characteristics of the sloshing liquid and the input motion, along with the requirements for weight reduction. The solid area between the perforations should be kept equal to 50%-60% of the area of perforations. Moreover, perforated baffle plates of zig-zag blocking alignment of perforations should be selected in multiple numbers that should be positioned in the damping range along the length of the tank, for effective slosh damping. Finally, the effectiveness of developed configuration of perforated baffle plate is experimentally evaluated by carrying out a shake table test.

7.4 MAJOR CONTRIBUTIONS

1. An extensive parametric study on the geometric configuration of the perforated baffle plates is presented with due consideration to convective as well as impulsive modes of response. Modification coefficients for standard codal expressions are proposed to improve the accuracy of the estimation of the fundamental impulsive frequency of cylindrical liquid tanks.
2. Need for an increased solid area of the baffle plate to resist a large magnitude of impulsive response is identified.
3. The effectiveness of the perforated baffle plate to damp the convective response is identified.

4. The optimum range of perforations for effective slosh damping considering convective as well as impulsive modes of response has been suggested.
5. The study suggests different zones and ranges to effectively position the single and multiple baffle plates in the rectangular tanks.
6. The study developed a zig-zag blocking alignment of perforations to damp the slosh response effectively.

7.5 SCOPE OF FUTURE WORK

1. The study can be extended by coupling the structural part with the fluid medium.
2. Soil-structure interaction can be included.
3. The effectiveness of the developed configuration of the perforated baffle plate for the slosh response damping of the cylindrical tanks can be analysed.
4. The collective Fluid-Structure Interaction of group of baffle plates placed in the fluid medium can be studied.

APPENDIX I

Table. AI-1. Dataset used for modal analysis of cylindrical tank

Sl. No.	D_o (m)	D (m)	H (m)	H/D	h (m)	t (m)	E (N/m ²)	ρ (kg/m ³)
1	4.2	3.9	8.0	1.9	1.17	0.3	2.74E+10	1000
2	4.2	3.9	8.0	1.9	2.4	0.3	2.74E+10	1000
3	4.2	3.9	8.0	1.9	3.5	0.3	2.74E+10	1000
4	4.2	3.9	8.0	1.9	3.57	0.3	2.74E+10	1000
5	4.2	3.9	8.0	1.9	4.7	0.3	2.74E+10	1000
6	4.2	3.9	8.0	1.9	5.87	0.3	2.74E+10	1000
7	4.2	3.9	8.0	1.9	7	0.3	2.74E+10	1000
8	4.7	4.4	8.0	1.7	1.17	0.3	2.74E+10	1000
9	4.7	4.4	8.0	1.7	2.4	0.3	2.74E+10	1000
10	4.7	4.4	8.0	1.7	3.5	0.3	2.74E+10	1000
11	4.7	4.4	8.0	1.7	3.57	0.3	2.74E+10	1000
12	4.7	4.4	8.0	1.7	4.7	0.3	2.74E+10	1000
13	4.7	4.4	8.0	1.7	5.87	0.3	2.74E+10	1000
14	4.7	4.4	8.0	1.7	7	0.3	2.74E+10	1000
15	5.3	5.0	8.0	1.5	1.17	0.3	2.74E+10	1000
16	5.3	5.0	8.0	1.5	2.4	0.3	2.74E+10	1000
17	5.3	5.0	8.0	1.5	3.5	0.3	2.74E+10	1000
18	5.3	5.0	8.0	1.5	3.57	0.3	2.74E+10	1000
19	5.3	5.0	8.0	1.5	4.7	0.3	2.74E+10	1000
20	5.3	5.0	8.0	1.5	5.87	0.3	2.74E+10	1000
21	5.3	5.0	8.0	1.5	7	0.3	2.74E+10	1000
22	6.2	5.9	8.0	1.3	1.17	0.3	2.74E+10	1000
23	6.2	5.9	8.0	1.3	2.4	0.3	2.74E+10	1000
24	6.2	5.9	8.0	1.3	3.5	0.3	2.74E+10	1000
25	6.2	5.9	8.0	1.3	3.57	0.3	2.74E+10	1000
26	6.2	5.9	8.0	1.3	4.7	0.3	2.74E+10	1000
27	6.2	5.9	8.0	1.3	5.87	0.3	2.74E+10	1000
28	6.2	5.9	8.0	1.3	7	0.3	2.74E+10	1000
29	8.0	7.7	8.0	1	1.17	0.3	2.74E+10	1000
30	8.0	7.7	8.0	1	2.4	0.3	2.74E+10	1000

31	8.0	7.7	8.0	1	3.5	0.3	2.74E+10	1000
32	8.0	7.7	8.0	1	3.57	0.3	2.74E+10	1000
33	8.0	7.7	8.0	1	4.7	0.3	2.74E+10	1000
34	8.0	7.7	8.0	1	5.87	0.3	2.74E+10	1000
35	8.0	7.7	8.0	1	7	0.3	2.74E+10	1000
36	8.9	8.6	8.0	0.9	1.17	0.3	2.74E+10	1000
37	8.9	8.6	8.0	0.9	2.4	0.3	2.74E+10	1000
38	8.9	8.6	8.0	0.9	3.5	0.3	2.74E+10	1000
39	8.9	8.6	8.0	0.9	3.57	0.3	2.74E+10	1000
40	8.9	8.6	8.0	0.9	4.7	0.3	2.74E+10	1000
41	8.9	8.6	8.0	0.9	5.87	0.3	2.74E+10	1000
42	8.9	8.6	8.0	0.9	7	0.3	2.74E+10	1000
43	11.4	11.1	8.0	0.7	1.17	0.3	2.74E+10	1000
44	11.4	11.1	8.0	0.7	2.4	0.3	2.74E+10	1000
45	11.4	11.1	8.0	0.7	3.5	0.3	2.74E+10	1000
46	11.4	11.1	8.0	0.7	3.57	0.3	2.74E+10	1000
47	11.4	11.1	8.0	0.7	4.7	0.3	2.74E+10	1000
48	11.4	11.1	8.0	0.7	5.87	0.3	2.74E+10	1000
49	11.4	11.1	8.0	0.7	7	0.3	2.74E+10	1000
50	16.0	15.7	8.0	0.5	1.17	0.3	2.74E+10	1000
51	16.0	15.7	8.0	0.5	2.4	0.3	2.74E+10	1000
52	16.0	15.7	8.0	0.5	3.5	0.3	2.74E+10	1000
53	16.0	15.7	8.0	0.5	3.57	0.3	2.74E+10	1000
54	16.0	15.7	8.0	0.5	4.7	0.3	2.74E+10	1000
55	16.0	15.7	8.0	0.5	5.87	0.3	2.74E+10	1000
56	16.0	15.7	8.0	0.5	7	0.3	2.74E+10	1000
57	26.7	26.4	8.0	0.3	1.17	0.3	2.74E+10	1000
58	26.7	26.4	8.0	0.3	2.4	0.3	2.74E+10	1000
59	26.7	26.4	8.0	0.3	3.5	0.3	2.74E+10	1000
60	26.7	26.4	8.0	0.3	3.57	0.3	2.74E+10	1000
61	26.7	26.4	8.0	0.3	4.7	0.3	2.74E+10	1000
62	26.7	26.4	8.0	0.3	5.87	0.3	2.74E+10	1000
63	26.7	26.4	8.0	0.3	7	0.3	2.74E+10	1000
64	80.0	79.7	8.0	0.1	1.17	0.3	2.74E+10	1000
65	80.0	79.7	8.0	0.1	2.4	0.3	2.74E+10	1000
66	80.0	79.7	8.0	0.1	3.5	0.3	2.74E+10	1000
67	80.0	79.7	8.0	0.1	3.57	0.3	2.74E+10	1000

68	80.0	79.7	8.0	0.1	4.7	0.3	2.74E+10	1000
69	80.0	79.7	8.0	0.1	5.87	0.3	2.74E+10	1000
70	80.0	79.7	8.0	0.1	7	0.3	2.74E+10	1000
71	4.2	3.9	8.0	1.9	1.17	0.4	2.74E+10	1000
72	4.2	3.9	8.0	1.9	2.4	0.4	2.74E+10	1000
73	4.2	3.9	8.0	1.9	3.5	0.4	2.74E+10	1000
74	4.2	3.9	8.0	1.9	3.57	0.4	2.74E+10	1000
75	4.2	3.9	8.0	1.9	4.7	0.4	2.74E+10	1000
76	4.2	3.9	8.0	1.9	5.87	0.4	2.74E+10	1000
77	4.2	3.9	8.0	1.9	7	0.4	2.74E+10	1000
78	4.7	4.4	8.0	1.7	1.17	0.4	2.74E+10	1000
79	4.7	4.4	8.0	1.7	2.4	0.4	2.74E+10	1000
80	4.7	4.4	8.0	1.7	3.5	0.4	2.74E+10	1000
81	4.7	4.4	8.0	1.7	3.57	0.4	2.74E+10	1000
82	4.7	4.4	8.0	1.7	4.7	0.4	2.74E+10	1000
83	4.7	4.4	8.0	1.7	5.87	0.4	2.74E+10	1000
84	4.7	4.4	8.0	1.7	7	0.4	2.74E+10	1000
85	5.3	5.0	8.0	1.5	1.17	0.4	2.74E+10	1000
86	5.3	5.0	8.0	1.5	2.4	0.4	2.74E+10	1000
87	5.3	5.0	8.0	1.5	3.5	0.4	2.74E+10	1000
88	5.3	5.0	8.0	1.5	3.57	0.4	2.74E+10	1000
89	5.3	5.0	8.0	1.5	4.7	0.4	2.74E+10	1000
90	5.3	5.0	8.0	1.5	5.87	0.4	2.74E+10	1000
91	5.3	5.0	8.0	1.5	7	0.4	2.74E+10	1000
92	6.2	5.9	8.0	1.3	1.17	0.4	2.74E+10	1000
93	6.2	5.9	8.0	1.3	2.4	0.4	2.74E+10	1000
94	6.2	5.9	8.0	1.3	3.5	0.4	2.74E+10	1000
95	6.2	5.9	8.0	1.3	3.57	0.4	2.74E+10	1000
96	6.2	5.9	8.0	1.3	4.7	0.4	2.74E+10	1000
97	6.2	5.9	8.0	1.3	5.87	0.4	2.74E+10	1000
98	6.2	5.9	8.0	1.3	7	0.4	2.74E+10	1000
99	8.0	7.7	8.0	1	1.17	0.4	2.74E+10	1000
100	8.0	7.7	8.0	1	2.4	0.4	2.74E+10	1000
101	8.0	7.7	8.0	1	3.5	0.4	2.74E+10	1000
102	8.0	7.7	8.0	1	3.57	0.4	2.74E+10	1000
103	8.0	7.7	8.0	1	4.7	0.4	2.74E+10	1000
104	8.0	7.7	8.0	1	5.87	0.4	2.74E+10	1000

105	8.0	7.7	8.0	1	7	0.4	2.74E+10	1000
106	8.9	8.6	8.0	0.9	1.17	0.4	2.74E+10	1000
107	8.9	8.6	8.0	0.9	2.4	0.4	2.74E+10	1000
108	8.9	8.6	8.0	0.9	3.5	0.4	2.74E+10	1000
109	8.9	8.6	8.0	0.9	3.57	0.4	2.74E+10	1000
110	8.9	8.6	8.0	0.9	4.7	0.4	2.74E+10	1000
111	8.9	8.6	8.0	0.9	5.87	0.4	2.74E+10	1000
112	8.9	8.6	8.0	0.9	7	0.4	2.74E+10	1000
113	11.4	11.1	8.0	0.7	1.17	0.4	2.74E+10	1000
114	11.4	11.1	8.0	0.7	2.4	0.4	2.74E+10	1000
115	11.4	11.1	8.0	0.7	3.5	0.4	2.74E+10	1000
116	11.4	11.1	8.0	0.7	3.57	0.4	2.74E+10	1000
117	11.4	11.1	8.0	0.7	4.7	0.4	2.74E+10	1000
118	11.4	11.1	8.0	0.7	5.87	0.4	2.74E+10	1000
119	11.4	11.1	8.0	0.7	7	0.4	2.74E+10	1000
120	16.0	15.7	8.0	0.5	1.17	0.4	2.74E+10	1000
121	16.0	15.7	8.0	0.5	2.4	0.4	2.74E+10	1000
122	16.0	15.7	8.0	0.5	3.5	0.4	2.74E+10	1000
123	16.0	15.7	8.0	0.5	3.57	0.4	2.74E+10	1000
124	16.0	15.7	8.0	0.5	4.7	0.4	2.74E+10	1000
125	16.0	15.7	8.0	0.5	5.87	0.4	2.74E+10	1000
126	16.0	15.7	8.0	0.5	7	0.4	2.74E+10	1000
127	26.7	26.4	8.0	0.3	1.17	0.4	2.74E+10	1000
128	26.7	26.4	8.0	0.3	2.4	0.4	2.74E+10	1000
129	26.7	26.4	8.0	0.3	3.5	0.4	2.74E+10	1000
130	26.7	26.4	8.0	0.3	3.57	0.4	2.74E+10	1000
131	26.7	26.4	8.0	0.3	4.7	0.4	2.74E+10	1000
132	26.7	26.4	8.0	0.3	5.87	0.4	2.74E+10	1000
133	26.7	26.4	8.0	0.3	7	0.4	2.74E+10	1000
134	80.0	79.7	8.0	0.1	1.17	0.4	2.74E+10	1000
135	80.0	79.7	8.0	0.1	2.4	0.4	2.74E+10	1000
136	80.0	79.7	8.0	0.1	3.5	0.4	2.74E+10	1000
137	80.0	79.7	8.0	0.1	3.57	0.4	2.74E+10	1000
138	80.0	79.7	8.0	0.1	4.7	0.4	2.74E+10	1000
139	80.0	79.7	8.0	0.1	5.87	0.4	2.74E+10	1000
140	80.0	79.7	8.0	0.1	7	0.4	2.74E+10	1000
141	4.2	3.9	8.0	1.9	1.17	0.5	2.74E+10	1000

142	4.2	3.9	8.0	1.9	2.4	0.5	2.74E+10	1000
143	4.2	3.9	8.0	1.9	3.5	0.5	2.74E+10	1000
144	4.2	3.9	8.0	1.9	3.57	0.5	2.74E+10	1000
145	4.2	3.9	8.0	1.9	4.7	0.5	2.74E+10	1000
146	4.2	3.9	8.0	1.9	5.87	0.5	2.74E+10	1000
147	4.2	3.9	8.0	1.9	7	0.5	2.74E+10	1000
148	4.7	4.4	8.0	1.7	1.17	0.5	2.74E+10	1000
149	4.7	4.4	8.0	1.7	2.4	0.5	2.74E+10	1000
150	4.7	4.4	8.0	1.7	3.5	0.5	2.74E+10	1000
151	4.7	4.4	8.0	1.7	3.57	0.5	2.74E+10	1000
152	4.7	4.4	8.0	1.7	4.7	0.5	2.74E+10	1000
153	4.7	4.4	8.0	1.7	5.87	0.5	2.74E+10	1000
154	4.7	4.4	8.0	1.7	7	0.5	2.74E+10	1000
155	5.3	5.0	8.0	1.5	1.17	0.5	2.74E+10	1000
156	5.3	5.0	8.0	1.5	2.4	0.5	2.74E+10	1000
157	5.3	5.0	8.0	1.5	3.5	0.5	2.74E+10	1000
158	5.3	5.0	8.0	1.5	3.57	0.5	2.74E+10	1000
159	5.3	5.0	8.0	1.5	4.7	0.5	2.74E+10	1000
160	5.3	5.0	8.0	1.5	5.87	0.5	2.74E+10	1000
161	5.3	5.0	8.0	1.5	7	0.5	2.74E+10	1000
162	6.2	5.9	8.0	1.3	1.17	0.5	2.74E+10	1000
163	6.2	5.9	8.0	1.3	2.4	0.5	2.74E+10	1000
164	6.2	5.9	8.0	1.3	3.5	0.5	2.74E+10	1000
165	6.2	5.9	8.0	1.3	3.57	0.5	2.74E+10	1000
166	6.2	5.9	8.0	1.3	4.7	0.5	2.74E+10	1000
167	6.2	5.9	8.0	1.3	5.87	0.5	2.74E+10	1000
168	6.2	5.9	8.0	1.3	7	0.5	2.74E+10	1000
169	8.0	7.7	8.0	1	1.17	0.5	2.74E+10	1000
170	8.0	7.7	8.0	1	2.4	0.5	2.74E+10	1000
171	8.0	7.7	8.0	1	3.5	0.5	2.74E+10	1000
172	8.0	7.7	8.0	1	3.57	0.5	2.74E+10	1000
173	8.0	7.7	8.0	1	4.7	0.5	2.74E+10	1000
174	8.0	7.7	8.0	1	5.87	0.5	2.74E+10	1000
175	8.0	7.7	8.0	1	7	0.5	2.74E+10	1000
176	8.9	8.6	8.0	0.9	1.17	0.5	2.74E+10	1000
177	8.9	8.6	8.0	0.9	2.4	0.5	2.74E+10	1000
178	8.9	8.6	8.0	0.9	3.5	0.5	2.74E+10	1000

179	8.9	8.6	8.0	0.9	3.57	0.5	2.74E+10	1000
180	8.9	8.6	8.0	0.9	4.7	0.5	2.74E+10	1000
181	8.9	8.6	8.0	0.9	5.87	0.5	2.74E+10	1000
182	8.9	8.6	8.0	0.9	7	0.5	2.74E+10	1000
183	11.4	11.1	8.0	0.7	1.17	0.5	2.74E+10	1000
184	11.4	11.1	8.0	0.7	2.4	0.5	2.74E+10	1000
185	11.4	11.1	8.0	0.7	3.5	0.5	2.74E+10	1000
186	11.4	11.1	8.0	0.7	3.57	0.5	2.74E+10	1000
187	11.4	11.1	8.0	0.7	4.7	0.5	2.74E+10	1000
188	11.4	11.1	8.0	0.7	5.87	0.5	2.74E+10	1000
189	11.4	11.1	8.0	0.7	7	0.5	2.74E+10	1000
190	16.0	15.7	8.0	0.5	1.17	0.5	2.74E+10	1000
191	16.0	15.7	8.0	0.5	2.4	0.5	2.74E+10	1000
192	16.0	15.7	8.0	0.5	3.5	0.5	2.74E+10	1000
193	16.0	15.7	8.0	0.5	3.57	0.5	2.74E+10	1000
194	16.0	15.7	8.0	0.5	4.7	0.5	2.74E+10	1000
195	16.0	15.7	8.0	0.5	5.87	0.5	2.74E+10	1000
196	16.0	15.7	8.0	0.5	7	0.5	2.74E+10	1000
197	26.7	26.4	8.0	0.3	1.17	0.5	2.74E+10	1000
198	26.7	26.4	8.0	0.3	2.4	0.5	2.74E+10	1000
199	26.7	26.4	8.0	0.3	3.5	0.5	2.74E+10	1000
200	26.7	26.4	8.0	0.3	3.57	0.5	2.74E+10	1000
201	26.7	26.4	8.0	0.3	4.7	0.5	2.74E+10	1000
202	26.7	26.4	8.0	0.3	5.87	0.5	2.74E+10	1000
203	26.7	26.4	8.0	0.3	7	0.5	2.74E+10	1000
204	80.0	79.7	8.0	0.1	1.17	0.5	2.74E+10	1000
205	80.0	79.7	8.0	0.1	2.4	0.5	2.74E+10	1000
206	80.0	79.7	8.0	0.1	3.5	0.5	2.74E+10	1000
207	80.0	79.7	8.0	0.1	3.57	0.5	2.74E+10	1000
208	80.0	79.7	8.0	0.1	4.7	0.5	2.74E+10	1000
209	80.0	79.7	8.0	0.1	5.87	0.5	2.74E+10	1000
210	80.0	79.7	8.0	0.1	7	0.5	2.74E+10	1000
211	4.2	3.9	8.0	1.9	1.17	0.3	3.16E+10	1000
212	4.2	3.9	8.0	1.9	2.4	0.3	3.16E+10	1000
213	4.2	3.9	8.0	1.9	3.5	0.3	3.16E+10	1000
214	4.2	3.9	8.0	1.9	3.57	0.3	3.16E+10	1000
215	4.2	3.9	8.0	1.9	4.7	0.3	3.16E+10	1000

216	4.2	3.9	8.0	1.9	5.87	0.3	3.16E+10	1000
217	4.2	3.9	8.0	1.9	7	0.3	3.16E+10	1000
218	4.7	4.4	8.0	1.7	1.17	0.3	3.16E+10	1000
219	4.7	4.4	8.0	1.7	2.4	0.3	3.16E+10	1000
220	4.7	4.4	8.0	1.7	3.5	0.3	3.16E+10	1000
221	4.7	4.4	8.0	1.7	3.57	0.3	3.16E+10	1000
222	4.7	4.4	8.0	1.7	4.7	0.3	3.16E+10	1000
223	4.7	4.4	8.0	1.7	5.87	0.3	3.16E+10	1000
224	4.7	4.4	8.0	1.7	7	0.3	3.16E+10	1000
225	5.3	5.0	8.0	1.5	1.17	0.3	3.16E+10	1000
226	5.3	5.0	8.0	1.5	2.4	0.3	3.16E+10	1000
227	5.3	5.0	8.0	1.5	3.5	0.3	3.16E+10	1000
228	5.3	5.0	8.0	1.5	3.57	0.3	3.16E+10	1000
229	5.3	5.0	8.0	1.5	4.7	0.3	3.16E+10	1000
230	5.3	5.0	8.0	1.5	5.87	0.3	3.16E+10	1000
231	5.3	5.0	8.0	1.5	7	0.3	3.16E+10	1000
232	6.2	5.9	8.0	1.3	1.17	0.3	3.16E+10	1000
233	6.2	5.9	8.0	1.3	2.4	0.3	3.16E+10	1000
234	6.2	5.9	8.0	1.3	3.5	0.3	3.16E+10	1000
235	6.2	5.9	8.0	1.3	3.57	0.3	3.16E+10	1000
236	6.2	5.9	8.0	1.3	4.7	0.3	3.16E+10	1000
237	6.2	5.9	8.0	1.3	5.87	0.3	3.16E+10	1000
238	6.2	5.9	8.0	1.3	7	0.3	3.16E+10	1000
239	8.0	7.7	8.0	1	1.17	0.3	3.16E+10	1000
240	8.0	7.7	8.0	1	2.4	0.3	3.16E+10	1000
241	8.0	7.7	8.0	1	3.5	0.3	3.16E+10	1000
242	8.0	7.7	8.0	1	3.57	0.3	3.16E+10	1000
243	8.0	7.7	8.0	1	4.7	0.3	3.16E+10	1000
244	8.0	7.7	8.0	1	5.87	0.3	3.16E+10	1000
245	8.0	7.7	8.0	1	7	0.3	3.16E+10	1000
246	8.9	8.6	8.0	0.9	1.17	0.3	3.16E+10	1000
247	8.9	8.6	8.0	0.9	2.4	0.3	3.16E+10	1000
248	8.9	8.6	8.0	0.9	3.5	0.3	3.16E+10	1000
249	8.9	8.6	8.0	0.9	3.57	0.3	3.16E+10	1000
250	8.9	8.6	8.0	0.9	4.7	0.3	3.16E+10	1000
251	8.9	8.6	8.0	0.9	5.87	0.3	3.16E+10	1000
252	8.9	8.6	8.0	0.9	7	0.3	3.16E+10	1000

253	11.4	11.1	8.0	0.7	1.17	0.3	3.16E+10	1000
254	11.4	11.1	8.0	0.7	2.4	0.3	3.16E+10	1000
255	11.4	11.1	8.0	0.7	3.5	0.3	3.16E+10	1000
256	11.4	11.1	8.0	0.7	3.57	0.3	3.16E+10	1000
257	11.4	11.1	8.0	0.7	4.7	0.3	3.16E+10	1000
258	11.4	11.1	8.0	0.7	5.87	0.3	3.16E+10	1000
259	11.4	11.1	8.0	0.7	7	0.3	3.16E+10	1000
260	16.0	15.7	8.0	0.5	1.17	0.3	3.16E+10	1000
261	16.0	15.7	8.0	0.5	2.4	0.3	3.16E+10	1000
262	16.0	15.7	8.0	0.5	3.5	0.3	3.16E+10	1000
263	16.0	15.7	8.0	0.5	3.57	0.3	3.16E+10	1000
264	16.0	15.7	8.0	0.5	4.7	0.3	3.16E+10	1000
265	16.0	15.7	8.0	0.5	5.87	0.3	3.16E+10	1000
266	16.0	15.7	8.0	0.5	7	0.3	3.16E+10	1000
267	26.7	26.4	8.0	0.3	1.17	0.3	3.16E+10	1000
268	26.7	26.4	8.0	0.3	2.4	0.3	3.16E+10	1000
269	26.7	26.4	8.0	0.3	3.5	0.3	3.16E+10	1000
270	26.7	26.4	8.0	0.3	3.57	0.3	3.16E+10	1000
271	26.7	26.4	8.0	0.3	4.7	0.3	3.16E+10	1000
272	26.7	26.4	8.0	0.3	5.87	0.3	3.16E+10	1000
273	26.7	26.4	8.0	0.3	7	0.3	3.16E+10	1000
274	80.0	79.7	8.0	0.1	1.17	0.3	3.16E+10	1000
275	80.0	79.7	8.0	0.1	2.4	0.3	3.16E+10	1000
276	80.0	79.7	8.0	0.1	3.5	0.3	3.16E+10	1000
277	80.0	79.7	8.0	0.1	3.57	0.3	3.16E+10	1000
278	80.0	79.7	8.0	0.1	4.7	0.3	3.16E+10	1000
279	80.0	79.7	8.0	0.1	5.87	0.3	3.16E+10	1000
280	80.0	79.7	8.0	0.1	7	0.3	3.16E+10	1000
281	4.2	3.9	8.0	1.9	1.17	0.4	3.16E+10	1000
282	4.2	3.9	8.0	1.9	2.4	0.4	3.16E+10	1000
283	4.2	3.9	8.0	1.9	3.5	0.4	3.16E+10	1000
284	4.2	3.9	8.0	1.9	3.57	0.4	3.16E+10	1000
285	4.2	3.9	8.0	1.9	4.7	0.4	3.16E+10	1000
286	4.2	3.9	8.0	1.9	5.87	0.4	3.16E+10	1000
287	4.2	3.9	8.0	1.9	7	0.4	3.16E+10	1000
288	4.7	4.4	8.0	1.7	1.17	0.4	3.16E+10	1000
289	4.7	4.4	8.0	1.7	2.4	0.4	3.16E+10	1000

290	4.7	4.4	8.0	1.7	3.5	0.4	3.16E+10	1000
291	4.7	4.4	8.0	1.7	3.57	0.4	3.16E+10	1000
292	4.7	4.4	8.0	1.7	4.7	0.4	3.16E+10	1000
293	4.7	4.4	8.0	1.7	5.87	0.4	3.16E+10	1000
294	4.7	4.4	8.0	1.7	7	0.4	3.16E+10	1000
295	5.3	5.0	8.0	1.5	1.17	0.4	3.16E+10	1000
296	5.3	5.0	8.0	1.5	2.4	0.4	3.16E+10	1000
297	5.3	5.0	8.0	1.5	3.5	0.4	3.16E+10	1000
298	5.3	5.0	8.0	1.5	3.57	0.4	3.16E+10	1000
299	5.3	5.0	8.0	1.5	4.7	0.4	3.16E+10	1000
300	5.3	5.0	8.0	1.5	5.87	0.4	3.16E+10	1000
301	5.3	5.0	8.0	1.5	7	0.4	3.16E+10	1000
302	6.2	5.9	8.0	1.3	1.17	0.4	3.16E+10	1000
303	6.2	5.9	8.0	1.3	2.4	0.4	3.16E+10	1000
304	6.2	5.9	8.0	1.3	3.5	0.4	3.16E+10	1000
305	6.2	5.9	8.0	1.3	3.57	0.4	3.16E+10	1000
306	6.2	5.9	8.0	1.3	4.7	0.4	3.16E+10	1000
307	6.2	5.9	8.0	1.3	5.87	0.4	3.16E+10	1000
308	6.2	5.9	8.0	1.3	7	0.4	3.16E+10	1000
309	8.0	7.7	8.0	1	1.17	0.4	3.16E+10	1000
310	8.0	7.7	8.0	1	2.4	0.4	3.16E+10	1000
311	8.0	7.7	8.0	1	3.5	0.4	3.16E+10	1000
312	8.0	7.7	8.0	1	3.57	0.4	3.16E+10	1000
313	8.0	7.7	8.0	1	4.7	0.4	3.16E+10	1000
314	8.0	7.7	8.0	1	5.87	0.4	3.16E+10	1000
315	8.0	7.7	8.0	1	7	0.4	3.16E+10	1000
316	8.9	8.6	8.0	0.9	1.17	0.4	3.16E+10	1000
317	8.9	8.6	8.0	0.9	2.4	0.4	3.16E+10	1000
318	8.9	8.6	8.0	0.9	3.5	0.4	3.16E+10	1000
319	8.9	8.6	8.0	0.9	3.57	0.4	3.16E+10	1000
320	8.9	8.6	8.0	0.9	4.7	0.4	3.16E+10	1000
321	8.9	8.6	8.0	0.9	5.87	0.4	3.16E+10	1000
322	8.9	8.6	8.0	0.9	7	0.4	3.16E+10	1000
323	11.4	11.1	8.0	0.7	1.17	0.4	3.16E+10	1000
324	11.4	11.1	8.0	0.7	2.4	0.4	3.16E+10	1000
325	11.4	11.1	8.0	0.7	3.5	0.4	3.16E+10	1000
326	11.4	11.1	8.0	0.7	3.57	0.4	3.16E+10	1000

327	11.4	11.1	8.0	0.7	4.7	0.4	3.16E+10	1000
328	11.4	11.1	8.0	0.7	5.87	0.4	3.16E+10	1000
329	11.4	11.1	8.0	0.7	7	0.4	3.16E+10	1000
330	16.0	15.7	8.0	0.5	1.17	0.4	3.16E+10	1000
331	16.0	15.7	8.0	0.5	2.4	0.4	3.16E+10	1000
332	16.0	15.7	8.0	0.5	3.5	0.4	3.16E+10	1000
333	16.0	15.7	8.0	0.5	3.57	0.4	3.16E+10	1000
334	16.0	15.7	8.0	0.5	4.7	0.4	3.16E+10	1000
335	16.0	15.7	8.0	0.5	5.87	0.4	3.16E+10	1000
336	16.0	15.7	8.0	0.5	7	0.4	3.16E+10	1000
337	26.7	26.4	8.0	0.3	1.17	0.4	3.16E+10	1000
338	26.7	26.4	8.0	0.3	2.4	0.4	3.16E+10	1000
339	26.7	26.4	8.0	0.3	3.5	0.4	3.16E+10	1000
340	26.7	26.4	8.0	0.3	3.57	0.4	3.16E+10	1000
341	26.7	26.4	8.0	0.3	4.7	0.4	3.16E+10	1000
342	26.7	26.4	8.0	0.3	5.87	0.4	3.16E+10	1000
343	26.7	26.4	8.0	0.3	7	0.4	3.16E+10	1000
344	80.0	79.7	8.0	0.1	1.17	0.4	3.16E+10	1000
345	80.0	79.7	8.0	0.1	2.4	0.4	3.16E+10	1000
346	80.0	79.7	8.0	0.1	3.5	0.4	3.16E+10	1000
347	80.0	79.7	8.0	0.1	3.57	0.4	3.16E+10	1000
348	80.0	79.7	8.0	0.1	4.7	0.4	3.16E+10	1000
349	80.0	79.7	8.0	0.1	5.87	0.4	3.16E+10	1000
350	80.0	79.7	8.0	0.1	7	0.4	3.16E+10	1000
351	4.2	3.9	8.0	1.9	1.17	0.5	3.16E+10	1000
352	4.2	3.9	8.0	1.9	2.4	0.5	3.16E+10	1000
353	4.2	3.9	8.0	1.9	3.5	0.5	3.16E+10	1000
354	4.2	3.9	8.0	1.9	3.57	0.5	3.16E+10	1000
355	4.2	3.9	8.0	1.9	4.7	0.5	3.16E+10	1000
356	4.2	3.9	8.0	1.9	5.87	0.5	3.16E+10	1000
357	4.2	3.9	8.0	1.9	7	0.5	3.16E+10	1000
358	4.7	4.4	8.0	1.7	1.17	0.5	3.16E+10	1000
359	4.7	4.4	8.0	1.7	2.4	0.5	3.16E+10	1000
360	4.7	4.4	8.0	1.7	3.5	0.5	3.16E+10	1000
361	4.7	4.4	8.0	1.7	3.57	0.5	3.16E+10	1000
362	4.7	4.4	8.0	1.7	4.7	0.5	3.16E+10	1000
363	4.7	4.4	8.0	1.7	5.87	0.5	3.16E+10	1000

364	4.7	4.4	8.0	1.7	7	0.5	3.16E+10	1000
365	5.3	5.0	8.0	1.5	1.17	0.5	3.16E+10	1000
366	5.3	5.0	8.0	1.5	2.4	0.5	3.16E+10	1000
367	5.3	5.0	8.0	1.5	3.5	0.5	3.16E+10	1000
368	5.3	5.0	8.0	1.5	3.57	0.5	3.16E+10	1000
369	5.3	5.0	8.0	1.5	4.7	0.5	3.16E+10	1000
370	5.3	5.0	8.0	1.5	5.87	0.5	3.16E+10	1000
371	5.3	5.0	8.0	1.5	7	0.5	3.16E+10	1000
372	6.2	5.9	8.0	1.3	1.17	0.5	3.16E+10	1000
373	6.2	5.9	8.0	1.3	2.4	0.5	3.16E+10	1000
374	6.2	5.9	8.0	1.3	3.5	0.5	3.16E+10	1000
375	6.2	5.9	8.0	1.3	3.57	0.5	3.16E+10	1000
376	6.2	5.9	8.0	1.3	4.7	0.5	3.16E+10	1000
377	6.2	5.9	8.0	1.3	5.87	0.5	3.16E+10	1000
378	6.2	5.9	8.0	1.3	7	0.5	3.16E+10	1000
379	8.0	7.7	8.0	1	1.17	0.5	3.16E+10	1000
380	8.0	7.7	8.0	1	2.4	0.5	3.16E+10	1000
381	8.0	7.7	8.0	1	3.5	0.5	3.16E+10	1000
382	8.0	7.7	8.0	1	3.57	0.5	3.16E+10	1000
383	8.0	7.7	8.0	1	4.7	0.5	3.16E+10	1000
384	8.0	7.7	8.0	1	5.87	0.5	3.16E+10	1000
385	8.0	7.7	8.0	1	7	0.5	3.16E+10	1000
386	8.9	8.6	8.0	0.9	1.17	0.5	3.16E+10	1000
387	8.9	8.6	8.0	0.9	2.4	0.5	3.16E+10	1000
388	8.9	8.6	8.0	0.9	3.5	0.5	3.16E+10	1000
389	8.9	8.6	8.0	0.9	3.57	0.5	3.16E+10	1000
390	8.9	8.6	8.0	0.9	4.7	0.5	3.16E+10	1000
391	8.9	8.6	8.0	0.9	5.87	0.5	3.16E+10	1000
392	8.9	8.6	8.0	0.9	7	0.5	3.16E+10	1000
393	11.4	11.1	8.0	0.7	1.17	0.5	3.16E+10	1000
394	11.4	11.1	8.0	0.7	2.4	0.5	3.16E+10	1000
395	11.4	11.1	8.0	0.7	3.5	0.5	3.16E+10	1000
396	11.4	11.1	8.0	0.7	3.57	0.5	3.16E+10	1000
397	11.4	11.1	8.0	0.7	4.7	0.5	3.16E+10	1000
398	11.4	11.1	8.0	0.7	5.87	0.5	3.16E+10	1000
399	11.4	11.1	8.0	0.7	7	0.5	3.16E+10	1000
400	16.0	15.7	8.0	0.5	1.17	0.5	3.16E+10	1000

401	16.0	15.7	8.0	0.5	2.4	0.5	3.16E+10	1000
402	16.0	15.7	8.0	0.5	3.5	0.5	3.16E+10	1000
403	16.0	15.7	8.0	0.5	3.57	0.5	3.16E+10	1000
404	16.0	15.7	8.0	0.5	4.7	0.5	3.16E+10	1000
405	16.0	15.7	8.0	0.5	5.87	0.5	3.16E+10	1000
406	16.0	15.7	8.0	0.5	7	0.5	3.16E+10	1000
407	26.7	26.4	8.0	0.3	1.17	0.5	3.16E+10	1000
408	26.7	26.4	8.0	0.3	2.4	0.5	3.16E+10	1000
409	26.7	26.4	8.0	0.3	3.5	0.5	3.16E+10	1000
410	26.7	26.4	8.0	0.3	3.57	0.5	3.16E+10	1000
411	26.7	26.4	8.0	0.3	4.7	0.5	3.16E+10	1000
412	26.7	26.4	8.0	0.3	5.87	0.5	3.16E+10	1000
413	26.7	26.4	8.0	0.3	7	0.5	3.16E+10	1000
414	80.0	79.7	8.0	0.1	1.17	0.5	3.16E+10	1000
415	80.0	79.7	8.0	0.1	2.4	0.5	3.16E+10	1000
416	80.0	79.7	8.0	0.1	3.5	0.5	3.16E+10	1000
417	80.0	79.7	8.0	0.1	3.57	0.5	3.16E+10	1000
418	80.0	79.7	8.0	0.1	4.7	0.5	3.16E+10	1000
419	80.0	79.7	8.0	0.1	5.87	0.5	3.16E+10	1000
420	80.0	79.7	8.0	0.1	7	0.5	3.16E+10	1000
421	4.2	3.9	8.0	1.9	1.17	0.3	2.74E+10	13590
422	4.2	3.9	8.0	1.9	2.4	0.3	2.74E+10	13590
423	4.2	3.9	8.0	1.9	3.5	0.3	2.74E+10	13590
424	4.2	3.9	8.0	1.9	3.57	0.3	2.74E+10	13590
425	4.2	3.9	8.0	1.9	4.7	0.3	2.74E+10	13590
426	4.2	3.9	8.0	1.9	5.87	0.3	2.74E+10	13590
427	4.2	3.9	8.0	1.9	7	0.3	2.74E+10	13590
428	4.7	4.4	8.0	1.7	1.17	0.3	2.74E+10	13590
429	4.7	4.4	8.0	1.7	2.4	0.3	2.74E+10	13590
430	4.7	4.4	8.0	1.7	3.5	0.3	2.74E+10	13590
431	4.7	4.4	8.0	1.7	3.57	0.3	2.74E+10	13590
432	4.7	4.4	8.0	1.7	4.7	0.3	2.74E+10	13590
433	4.7	4.4	8.0	1.7	5.87	0.3	2.74E+10	13590
434	4.7	4.4	8.0	1.7	7	0.3	2.74E+10	13590
435	5.3	5.0	8.0	1.5	1.17	0.3	2.74E+10	13590
436	5.3	5.0	8.0	1.5	2.4	0.3	2.74E+10	13590
437	5.3	5.0	8.0	1.5	3.5	0.3	2.74E+10	13590

438	5.3	5.0	8.0	1.5	3.57	0.3	2.74E+10	13590
439	5.3	5.0	8.0	1.5	4.7	0.3	2.74E+10	13590
440	5.3	5.0	8.0	1.5	5.87	0.3	2.74E+10	13590
441	5.3	5.0	8.0	1.5	7	0.3	2.74E+10	13590
442	6.2	5.9	8.0	1.3	1.17	0.3	2.74E+10	13590
443	6.2	5.9	8.0	1.3	2.4	0.3	2.74E+10	13590
444	6.2	5.9	8.0	1.3	3.5	0.3	2.74E+10	13590
445	6.2	5.9	8.0	1.3	3.57	0.3	2.74E+10	13590
446	6.2	5.9	8.0	1.3	4.7	0.3	2.74E+10	13590
447	6.2	5.9	8.0	1.3	5.87	0.3	2.74E+10	13590
448	6.2	5.9	8.0	1.3	7	0.3	2.74E+10	13590
449	8.0	7.7	8.0	1	1.17	0.3	2.74E+10	13590
450	8.0	7.7	8.0	1	2.4	0.3	2.74E+10	13590
451	8.0	7.7	8.0	1	3.5	0.3	2.74E+10	13590
452	8.0	7.7	8.0	1	3.57	0.3	2.74E+10	13590
453	8.0	7.7	8.0	1	4.7	0.3	2.74E+10	13590
454	8.0	7.7	8.0	1	5.87	0.3	2.74E+10	13590
455	8.0	7.7	8.0	1	7	0.3	2.74E+10	13590
456	8.9	8.6	8.0	0.9	1.17	0.3	2.74E+10	13590
457	8.9	8.6	8.0	0.9	2.4	0.3	2.74E+10	13590
458	8.9	8.6	8.0	0.9	3.5	0.3	2.74E+10	13590
459	8.9	8.6	8.0	0.9	3.57	0.3	2.74E+10	13590
460	8.9	8.6	8.0	0.9	4.7	0.3	2.74E+10	13590
461	8.9	8.6	8.0	0.9	5.87	0.3	2.74E+10	13590
462	8.9	8.6	8.0	0.9	7	0.3	2.74E+10	13590
463	11.4	11.1	8.0	0.7	1.17	0.3	2.74E+10	13590
464	11.4	11.1	8.0	0.7	2.4	0.3	2.74E+10	13590
465	11.4	11.1	8.0	0.7	3.5	0.3	2.74E+10	13590
466	11.4	11.1	8.0	0.7	3.57	0.3	2.74E+10	13590
467	11.4	11.1	8.0	0.7	4.7	0.3	2.74E+10	13590
468	11.4	11.1	8.0	0.7	5.87	0.3	2.74E+10	13590
469	11.4	11.1	8.0	0.7	7	0.3	2.74E+10	13590
470	16.0	15.7	8.0	0.5	1.17	0.3	2.74E+10	13590
471	16.0	15.7	8.0	0.5	2.4	0.3	2.74E+10	13590
472	16.0	15.7	8.0	0.5	3.5	0.3	2.74E+10	13590
473	16.0	15.7	8.0	0.5	3.57	0.3	2.74E+10	13590
474	16.0	15.7	8.0	0.5	4.7	0.3	2.74E+10	13590

475	16.0	15.7	8.0	0.5	5.87	0.3	2.74E+10	13590
476	16.0	15.7	8.0	0.5	7	0.3	2.74E+10	13590
477	26.7	26.4	8.0	0.3	1.17	0.3	2.74E+10	13590
478	26.7	26.4	8.0	0.3	2.4	0.3	2.74E+10	13590
479	26.7	26.4	8.0	0.3	3.5	0.3	2.74E+10	13590
480	26.7	26.4	8.0	0.3	3.57	0.3	2.74E+10	13590
481	26.7	26.4	8.0	0.3	4.7	0.3	2.74E+10	13590
482	26.7	26.4	8.0	0.3	5.87	0.3	2.74E+10	13590
483	26.7	26.4	8.0	0.3	7	0.3	2.74E+10	13590
484	80.0	79.7	8.0	0.1	1.17	0.3	2.74E+10	13590
485	80.0	79.7	8.0	0.1	2.4	0.3	2.74E+10	13590
486	80.0	79.7	8.0	0.1	3.5	0.3	2.74E+10	13590
487	80.0	79.7	8.0	0.1	3.57	0.3	2.74E+10	13590
488	80.0	79.7	8.0	0.1	4.7	0.3	2.74E+10	13590
489	80.0	79.7	8.0	0.1	5.87	0.3	2.74E+10	13590
490	80.0	79.7	8.0	0.1	7	0.3	2.74E+10	13590
491	4.2	3.9	8.0	1.9	1.17	0.3	2.74E+10	748.9
492	4.2	3.9	8.0	1.9	2.4	0.3	2.74E+10	748.9
493	4.2	3.9	8.0	1.9	3.5	0.3	2.74E+10	748.9
494	4.2	3.9	8.0	1.9	3.57	0.3	2.74E+10	748.9
495	4.2	3.9	8.0	1.9	4.7	0.3	2.74E+10	748.9
496	4.2	3.9	8.0	1.9	5.87	0.3	2.74E+10	748.9
497	4.2	3.9	8.0	1.9	7	0.3	2.74E+10	748.9
498	4.7	4.4	8.0	1.7	1.17	0.3	2.74E+10	748.9
499	4.7	4.4	8.0	1.7	2.4	0.3	2.74E+10	748.9
500	4.7	4.4	8.0	1.7	3.5	0.3	2.74E+10	748.9
501	4.7	4.4	8.0	1.7	3.57	0.3	2.74E+10	748.9
502	4.7	4.4	8.0	1.7	4.7	0.3	2.74E+10	748.9
503	4.7	4.4	8.0	1.7	5.87	0.3	2.74E+10	748.9
504	4.7	4.4	8.0	1.7	7	0.3	2.74E+10	748.9
505	5.3	5.0	8.0	1.5	1.17	0.3	2.74E+10	748.9
506	5.3	5.0	8.0	1.5	2.4	0.3	2.74E+10	748.9
507	5.3	5.0	8.0	1.5	3.5	0.3	2.74E+10	748.9
508	5.3	5.0	8.0	1.5	3.57	0.3	2.74E+10	748.9
509	5.3	5.0	8.0	1.5	4.7	0.3	2.74E+10	748.9
510	5.3	5.0	8.0	1.5	5.87	0.3	2.74E+10	748.9
511	5.3	5.0	8.0	1.5	7	0.3	2.74E+10	748.9

512	6.2	5.9	8.0	1.3	1.17	0.3	2.74E+10	748.9
513	6.2	5.9	8.0	1.3	2.4	0.3	2.74E+10	748.9
514	6.2	5.9	8.0	1.3	3.5	0.3	2.74E+10	748.9
515	6.2	5.9	8.0	1.3	3.57	0.3	2.74E+10	748.9
516	6.2	5.9	8.0	1.3	4.7	0.3	2.74E+10	748.9
517	6.2	5.9	8.0	1.3	5.87	0.3	2.74E+10	748.9
518	6.2	5.9	8.0	1.3	7	0.3	2.74E+10	748.9
519	8.0	7.7	8.0	1	1.17	0.3	2.74E+10	748.9
520	8.0	7.7	8.0	1	2.4	0.3	2.74E+10	748.9
521	8.0	7.7	8.0	1	3.5	0.3	2.74E+10	748.9
522	8.0	7.7	8.0	1	3.57	0.3	2.74E+10	748.9
523	8.0	7.7	8.0	1	4.7	0.3	2.74E+10	748.9
524	8.0	7.7	8.0	1	5.87	0.3	2.74E+10	748.9
525	8.0	7.7	8.0	1	7	0.3	2.74E+10	748.9
526	8.9	8.6	8.0	0.9	1.17	0.3	2.74E+10	748.9
527	8.9	8.6	8.0	0.9	2.4	0.3	2.74E+10	748.9
528	8.9	8.6	8.0	0.9	3.5	0.3	2.74E+10	748.9
529	8.9	8.6	8.0	0.9	3.57	0.3	2.74E+10	748.9
530	8.9	8.6	8.0	0.9	4.7	0.3	2.74E+10	748.9
531	8.9	8.6	8.0	0.9	5.87	0.3	2.74E+10	748.9
532	8.9	8.6	8.0	0.9	7	0.3	2.74E+10	748.9
533	11.4	11.1	8.0	0.7	1.17	0.3	2.74E+10	748.9
534	11.4	11.1	8.0	0.7	2.4	0.3	2.74E+10	748.9
535	11.4	11.1	8.0	0.7	3.5	0.3	2.74E+10	748.9
536	11.4	11.1	8.0	0.7	3.57	0.3	2.74E+10	748.9
537	11.4	11.1	8.0	0.7	4.7	0.3	2.74E+10	748.9
538	11.4	11.1	8.0	0.7	5.87	0.3	2.74E+10	748.9
539	11.4	11.1	8.0	0.7	7	0.3	2.74E+10	748.9
540	16.0	15.7	8.0	0.5	1.17	0.3	2.74E+10	748.9
541	16.0	15.7	8.0	0.5	2.4	0.3	2.74E+10	748.9
542	16.0	15.7	8.0	0.5	3.5	0.3	2.74E+10	748.9
543	16.0	15.7	8.0	0.5	3.57	0.3	2.74E+10	748.9
544	16.0	15.7	8.0	0.5	4.7	0.3	2.74E+10	748.9
545	16.0	15.7	8.0	0.5	5.87	0.3	2.74E+10	748.9
546	16.0	15.7	8.0	0.5	7	0.3	2.74E+10	748.9
547	26.7	26.4	8.0	0.3	1.17	0.3	2.74E+10	748.9
548	26.7	26.4	8.0	0.3	2.4	0.3	2.74E+10	748.9

549	26.7	26.4	8.0	0.3	3.5	0.3	2.74E+10	748.9
550	26.7	26.4	8.0	0.3	3.57	0.3	2.74E+10	748.9
551	26.7	26.4	8.0	0.3	4.7	0.3	2.74E+10	748.9
552	26.7	26.4	8.0	0.3	5.87	0.3	2.74E+10	748.9
553	26.7	26.4	8.0	0.3	7	0.3	2.74E+10	748.9
554	80.0	79.7	8.0	0.1	1.17	0.3	2.74E+10	748.9
555	80.0	79.7	8.0	0.1	2.4	0.3	2.74E+10	748.9
556	80.0	79.7	8.0	0.1	3.5	0.3	2.74E+10	748.9
557	80.0	79.7	8.0	0.1	3.57	0.3	2.74E+10	748.9
558	80.0	79.7	8.0	0.1	4.7	0.3	2.74E+10	748.9
559	80.0	79.7	8.0	0.1	5.87	0.3	2.74E+10	748.9
560	80.0	79.7	8.0	0.1	7	0.3	2.74E+10	748.9

REFERENCES

- ACI 350.3-06. (2006). "Seismic design of liquid-containing concrete structures and commentary." ACI Committee 350, American Concrete Institute.
- Akyildiz, H. (2012). "A numerical study of the effects of the vertical baffle on liquid sloshing in two-dimensional rectangular tank." *Journal of Sound and Vibration*, 331(1), 41–52.
- Akyildiz, H. and Ünal, E. (2005). "Experimental investigation of pressure distribution on a rectangular tank due to the liquid sloshing." *Ocean Engineering*, 32(11–12), 1503–1516.
- Akyildiz, H., Erdem Unal, N. and Aksoy, H. (2013). "An experimental investigation of the effects of the ring baffles on liquid sloshing in a rigid cylindrical tank." *Ocean Engineering*, 59, 190–197.
- Amabili, M., Frosali, G. and Kwak, M. K. (1996). "Free vibrations of annular plates coupled with fluids." *Journal of Sound and Vibration*, 191(5), 825–846.
- Amiri, M. and Sabbagh-Yazdi, S. R. (2012). "Influence of roof on dynamic characteristics of dome roof tanks partially filled with liquid." *Thin-Walled Structures*, 50(1), 56–67.
- ANSYS. (2011). "ANSYS Mechanical APDL Element Reference." ANSYS Inc, Vol. Release14, Canonsburg, PA.
- ANSYS Inc. (2013). "ANSYS Mechanical APDL Theory Reference." ANSYS Inc, Vol. Release15, Canonsburg, PA.
- Balendra, T., Ang, K. K., Paramasivam, P. and Lee, S. L. (1982). "Seismic design of flexible cylindrical liquid storage tanks." *Earthquake Engineering and Structural Dynamics*, 10(3), 477–496.
- Bathe, K.-J. (2014). "Finite Element Procedures." Second edi., Prentice Hall, Pearson Education, Inc. United States of America.

- Bauer, H. F. (1981). "Hydroelastic vibrations in a rectangular container." *International Journal of Solids and Structures*, 17(7), 639–652.
- Bellezi, C. A., Cheng, L. Y., Okada, T. and Arai, M. (2019). "Optimized perforated bulkhead for sloshing mitigation and control." *Ocean Engineering*, 187(September 2018), 106171.
- Belostosky, A. M., Akimov, P. A., Kaytukov, T. B., Afanasyeva, I. N., Usmanov, A. R., Scherbina, S. V. and Vershinin, V. V. (2014). "About finite element analysis of fluid-structure interaction problems." *Procedia Engineering*, 91(TFoCE), 37–42.
- Biswal, K. C., Bhattacharyya, S. K. and Sinha, P. K. (2003). "Free-vibration analysis of liquid-filled tank with baffles." *Journal of Sound and Vibration*, 259(1), 177–192.
- Biswal, K. C., Bhattacharyya, S. K. and Sinha, P. K. (2004). "Dynamic response analysis of a liquid-filled cylindrical tank with annular baffle." *Journal of Sound and Vibration*, 274(1–2), 13–37.
- Biswal, K. C., Bhattacharyya, S. K. and Sinha, P. K. (2006). "Non-linear sloshing in partially liquid filled containers with baffles." *International Journal for Numerical Methods in Engineering*, 68(3), 317–337.
- Brar, G. S. and Singh, S. (2014). "An Experimental and CFD Analysis of Sloshing in a Tanker." *Procedia Technology*, 14, 490–496.
- Chaduvula, U., Patel, D. and Gopalakrishnan, N. (2013). "Fluid-Structure-Soil Interaction Effects on Seismic Behaviour of Elevated Water Tanks." *Procedia Engineering*, 51 (NUiCONE 2012), 84–91.
- Chandrasekaran, A. and Krishna, J. (1954). "Water towers in seismic zones." *Proceedings of the Third World Conference on Earthquake Engineering*, New Zealand, 161–171.
- Chandrasekaran, S. and Madhavi, N (2014a). "Hydrodynamic performance of retrofitted offshore structures using perforated cylinders." *International Journal of Forensic Engineering*, 2(2), 100.

Chandrasekaran, S. and Madhavi, N (2014b). “Numerical Study on Geometrical Configurations of Perforated Cylindrical Structures under Regular Waves.” *Journal of Performance of Constructed Facilities*, 30(1), 1–12.

Chandrasekaran, S. and Madhavi, N (2015a). “Retrofitting of offshore cylindrical structures with different geometrical configuration of perforated outer cover.” *International Shipbuilding Progress*, 62, 43–56.

Chandrasekaran, S. and Madhavi, N (2015b). “Variation of flow field around twin cylinders with and without the outer perforated cylinder-numerical study.” *China ocean Engineering*, 30(5), 763–771.

Chandrasekaran, S. and Madhavi, N. (2015c). “Flow field around outer perforated circular cylinder under regular waves: numerical study.” *Marine Systems and Ocean Technology*, 10(2), 91–100.

Chen, W., Haroun, M. A. and Liu, F. (1996). “Large amplitude liquid sloshing in seismically excited tanks.” *Earthquake Engineering and Structural Dynamics*, 25(7), 653–669.

Chen, X., Wan, D. and Huang, W. (2016). “Numerical simulation of effects of two different baffles on liquid sloshing by MPS method.” *In Proceedings of the Twenty-Sixth International Ocean and Polar Engineering Conference - ISOPE*, Rhodes, Greece. ISOPE.

Cherif, S. M. H. and Ouissi, M. N. (2016). “Free vibration analysis of a liquid in a circular cylindrical rigid tank using the hierarchical finite element method.” *Latin American Journal of Solids and Structures*, 13(7), 1265–1280.

Cho, J. R., Kim, K. W., Lee, J. K., Park, T. H. and Lee, W. Y. (2002). “Axisymmetric modal analysis of liquid-storage tanks considering compressibility effects.” *International Journal for Numerical Methods in Engineering*, 55(6), 733–752.

Cho, J. R., Lee, H. W. and Ha, S. Y. (2005). “Finite element analysis of resonant sloshing response in 2-D baffled tank.” *Journal of Sound and Vibration*, 288(4–5), 829–845.

- Cho, J. R. and Song, J. M. (2001). "Assessment of classical numerical models for the separate fluid-structure modal analysis." *Journal of Sound and Vibration*, 239(5), 995–1012.
- Chu, C., Wu, Y., Wu, T. and Wang, C. (2018). "Slosh-induced hydrodynamic force in a water tank with multiple baffles." *Ocean Engineering*, 167(August), 282–292.
- Daniel, W. J. T. (1980). "Modal methods in finite element fluid–structure eigenvalue problems." *International Journal for Numerical Methods in Engineering*, 15(8), 1161–1175.
- Dehghan Manshadi, S. H. and Maheri, M. R. (2010). "The effects of long-term corrosion on the dynamic characteristics of ground based cylindrical liquid storage tanks." *Thin-Walled Structures*, 48(12), 888–896.
- Demirel, E. and Aral, M. M. (2018). "Liquid Sloshing Damping in an Accelerated Tank Using a Novel Slot-Baffle Design." *Water*, 10(1565), 1–12.
- Dogangun, A., Durmus, A. and Ayvaz, Y. (1996). "Static and dynamic analysis of rectangular tanks by using the lagrangian fluid finite element." *Computers and Structures*, 59(3), 547–552.
- Dogangun, Adem. and Livaoglu, R. (2004). "Hydrodynamic pressures acting on the walls of rectangular fluid containers." *Structural Engineering and Mechanics*, 17(2), 203–214.
- Donea, J., Giuliani, S. and Halleux, J. p. (1982). "An arbitrary Lagrangian-Eulerian finite element for transient dynamic fluid-structure interactions." *Computer Methods in Applied Mechanics and Engineering*, 33, 689–723.
- Eswaran, M., Saha, U. K. and Maity, D. (2009). "Effect of baffles on a partially filled cubic tank: Numerical simulation and experimental validation." *Computers and Structures*, 87(3–4), 198–205.
- Eurocode 8. (2006). "Design of structures for earthquake resistance—part 4: silos, tanks and pipelines." European committee for standardization.

Faltinsen, O. M., Firoozkoobi, R. and Timokha, A. N. (2011). “Steady-state liquid sloshing in a rectangular tank with a slat-type screen in the middle : Quasilinear modal analysis and experiments.” *Physics of Fluids*, 042101(23).

Faltinsen, O. M. and Timokha, A. (2009). “Sloshing.” Cambridge University Press, New York.

Franklin T. Dodge. (2000). “The new dynamic behavior of liquids in moving containers.” San Antonio, TX: South West Research Institute.

Goudarzi, M. A., Sabbagh-Yazdi, S. R. and Marx, W. (2010). “Investigation of sloshing damping in baffled rectangular tanks subjected to the dynamic excitation.” *Bull Earthquake Eng*, 8, 1055–1072.

Gupta, R. K. and Hutchinson, G. L. (1988). “Free vibration analysis of liquid storage tanks.” *Journal of Sound and Vibration*, 122(3), 491–506.

Haroun, B. M. A. and Abou-lzzeddine, W. (1992). “Parametric study of seismic soil-tank interaction. I: horizontal excitation.” *Journal of Structural Engineering, ASCE*, 118(3), 783–797.

Haroun, M. A. (1983). “Vibration studies and tests of liquid storage tanks.” *Earthquake Engineering and Structural Dynamics*, 11(June), 179–206.

Haroun, M. A. and A.Tayel, M. (1985). “Axisymmetrical vibrations of tanks—numerical.” *Journal of Engineering Mechanics*, 111(3), 329–345.

Hashemi, S., Saadatpour, M. M. and Kianoush, M. R. (2013). “Dynamic behavior of flexible rectangular fluid containers.” *Thin Walled Structures*, 66, 23–38.

Hasheminejad, S. M. and Aghabeigi, M. (2012). “Sloshing characteristics in half-full horizontal elliptical tanks with vertical baffles.” *Applied Mathematical Modelling*, 36(1), 57–71.

Hasheminejad, S. M. and Mohammadi, M. M. (2011). "Effect of anti-slosh baffles on free liquid oscillations in partially filled horizontal circular tanks." *Ocean Engineering*, 38(1), 49–62.

Hasheminejad, S. M., Mohammadi, M. M. and Jarrahi, M. (2014). "Liquid sloshing in partly-filled laterally-excited circular tanks equipped with baffles." *Journal of Fluids and Structures*, 44, 97–114.

Hatayama, K. (2013). "Sloshing damage to oil storage tanks due to long-period strong ground motions during the 2011 Tohoku, Japan Earthquake." *10th International Workshop on Seismic Microzoning and Risk Reduction*, at Sokairo Hall, GRIPS, Tokyo, Japan.

Hejazi, F. S. A. and Mohammadi, M. K. (2019). "Investigation on sloshing response of water rectangular tanks under horizontal and vertical near fault seismic excitations." *Soil Dynamics and Earthquake Engineering*, 116(October 2018), 637–653.

Hoskins, L. M. and Jacobsen, L. S. (1934). "Water pressure in a tank caused by a simulated earthquake." *Bulletin of the Seismological Society of America*, 24(1), 1–32.

Hosseini, M., Goudarzi, M. A. and Soroor, A. (2017). "Reduction of seismic sloshing in floating roof liquid storage tanks by using a Suspended Annular Baffle (SAB)." *Journal of Fluids and Structures*, 71, 40–55.

Hosseinzadeh, N., Kaypour Sangsari, M. and Tavakolian Ferdosiyeh, H. (2014). "Shake table study of annular baffles in steel storage tanks as sloshing dependent variable dampers." *Journal of Loss Prevention in the Process Industries*, 32, 299–310.

Housner, G.W. (1955). "Dynamic pressures on accelerated fluid containers." *Bulletin of the Seismological Society of America*, 15–35.

Housner, George W. (1963). "The dynamic behavior of water tanks." *Bulletin of the Seismological Society of America*, 53(2), 381–387.

- Iranmanesh, A. and Passandideh-Fard, M. (2017). "A 2D numerical study on suppressing liquid sloshing using a submerged cylinder." *Ocean Engineering*, 138(November 2016), 55–72.
- IS1893(Part2). (2014). "Criteria for earthquake resistant design of structures Part2 Liquid retaining tanks." Bureau of Indian Standards, New Delhi, India.
- Jaiswal, O. R. and Jain, S. K. (2005). "Modified proposed provisions for aseismic design of liquid storage tanks: Part II - Commentary and examples." *Journal of Structural Engineering*, 32(4), 297–310.
- Jaiswal, O. R., Rai, D. C. and Jain, S. K. (2003). "Review of Code Provisions on Seismic Analysis of Liquid Storage Tanks." IITK-GSDMA Project on Building Codes, 1–25.
- James, R. W. and Raba, G. W. (1991). "Behavior of welded steel water-storage tank." *Journal of Structural Engineering*, 117(1), 61–79.
- Je, S. Y., Chang, Y. S. and Kang, S. S. (2017). "Dynamic characteristics assessment of reactor vessel internals with fluid-structure interaction." *Nuclear Engineering and Technology*, 49(7), 1513–1523.
- Jhung, M. J., Kim, W. T., and Ryu, Y. H. (2009). "Dynamic characteristics of cylindrical shells considering fluid-structure interaction." *Nuclear Engineering and Technology*, 41(10), 1333–1346.
- Jhung, M. J., Yu, S. O. and Lim, Y. T. (2011). "Dynamic characteristics of a partially fluid filled cylindrical shell." *Nuclear Engineering and Technology*, 43(2), 167–174.
- Jhung, M. jo., Jo, jong chull. and Jeong, kyeong hoon. (2006). "Modal analysis of conical shell filled with fluid." *Journal of Mechanical Science and Technology*, 20(11), 1848–1862.
- Jin, H., Liu, Y. and Li, H. J. (2014). "Experimental study on sloshing in a tank with an inner horizontal perforated plate." *Ocean Engineering*, 82, 75–84.

Jung, J. H., Yoon, H. S., Lee, C. Y. and Shin, S. C. (2012). “Effect of the vertical baffle height on the liquid sloshing in a three-dimensional rectangular tank.” *Ocean Engineering*, 44, 79–89.

Kalogerakou, M. E., Maniatakis, C. A., Spyrakos, C. C. and Psarropoulos, P. N. (2017). “Seismic response of liquid-containing tanks with emphasis on the hydrodynamic response and near-fault phenomena.” *Engineering Structures*, 153, 383–403.

Kamara, M. E. (2010). “Design of Circular Concrete Tanks.” *Structures Congress, ASCE*, 2439–2449.

Kangda, M. Z., Sawant, S. S. and Jaiswal, O. R. (2019). “Sloshing in liquid storage tanks with internal obstructions.” In *Lecture Notes in Civil Engineering, Recent Advances in Structural Engineering*, Springer Nature Singapore Pte Ltd. 12.

Kianoush, M. R. and Ghaemmaghami, A. R. (2011). “The effect of earthquake frequency content on the seismic behavior of concrete rectangular liquid tanks using the finite element method incorporating soil – structure interaction.” *Engineering Structures*, 33(7), 2186–2200.

Kilic, S. A. (2009). “Simulation of Sloshing Effects in Cylindrical Tanks and Evaluation of Seismic Performance.” *Lifeline Earthquake Engineering in a Multihazard Environment, ASCE*, 650, 1–10.

Kim, S., Choi, H., Park, D., Baek, E. and Kim, J. (2018). “Water level response measurement in a steel cylindrical liquid storage tank using image filter processing under seismic excitation.” *Mechanical Systems and Signal Processing*, 101, 274–291.

Kotrasová, K. (2017). “Study of Hydrodynamic Pressure on Wall of Tank.” *Procedia Engineering*, 190, 2–6.

Kruntcheva, M. R. (2007). “Free Vibrations of Cylindrical Storage Tanks: Finite-Element Analysis and Experiments.” *Journal of Engineering Mechanics*, 133(6), 728–733.

- Kumar, A. and Sinhamahapatra, K. P. (2013). “Effects of porous internal components on liquid slosh dynamics.” *Journal of Porous Media*, 16(8), 725–747.
- Kumar, K. and Maity, D. (2016). “Pressure Based Eulerian Approach for Investigation of Sloshing in Rectangular Water Tank.” *Procedia Engineering*, 144(033), 1187–1194.
- Kumar, P. D., Alok, A. and Maiti, P. R. (2016). “Comparative Study of Dynamic Analysis of Rectangular Liquid Filled Containers Using Codal Provisions.” *Procedia Engineering*, 144, 1180–1186.
- Lauder, B. E. and Spalding, D. B. (1974). “The numerical computation of turbulent flows.” *Computer Methods in Applied Mechanics and Engineering*, 3(2), 269–289.
- Lay, K. S. (1993). “Seismic coupled modeling of axisymmetric tanks containing liquid.” *Journal of Engineering Mechanics*, 119(9), 1747–1761.
- Lepelletier, T. G. and Raichlen, F. (1988). “Nonlinear oscillations in rectangular tanks.” *Journal of Engineering Mechanics*, 114(1), 1–23.
- Liu, D. and Lin, P. (2009). “Three-dimensional liquid sloshing in a tank with baffles.” *Ocean Engineering*, 36(2), 202–212.
- Liu, Z. (John). (2018). “Seismic Design and Analysis of Concrete Liquid-Containing Tanks.” *Structures Congress, ASCE*, 444–454.
- Livaoglu, R. and Dogangun, A. (2006). “Simplified seismic analysis procedures for elevated tanks considering fluid – structure – soil interaction.” *Journal of Fluids and Structures*, 22, 421–439.
- Livaoglu, Ramazan, Turan, A., Naggar, M. H. El. and Dogangun, A. (2012). “The numerical and empirical evaluation of structural performance of elevated tanks considering soil–structure interaction effects.” *Journal of Earthquake and Tsunami*, 6(2), 1–20.
- Maleki, A. and Ziyaeifar, M. (2007). “Damping enhancement of seismic isolated cylindrical liquid storage tanks using baffles.” *Engineering Structures*, 29(12), 3227–3240.

- Malhotra, P. K. and Veletsos, A. S. (1994). "Uplifting response of unanchored liquid-storage tanks." *Journal of Structural Engineering*, 120(12), 3525–3547.
- Mandal, K. K. and Maity, D. (2016). "Nonlinear finite element analysis of water in rectangular tank." *Ocean Engineering*, 121, 592–601.
- Manser, W. S., Touati, M. and Barros, R. C. (2017). "The maximum sloshing wave height evaluation in cylindrical metallic tanks by numerical means." *MATEC Web of Conferences*, 95, 4–8.
- Močilan, M., Žmindák, M. and Pastorek, P. (2016). "Dynamic analysis of fuel tank." *Procedia Engineering*, 136, 45–49.
- Moslemi, M. and Kianoush, M. R. (2012). "Parametric study on dynamic behavior of cylindrical ground-supported tanks." *Engineering Structures*, 42, 214–230.
- Nakayama, T. and Washizu, K. (1980). "Nonlinear analysis of liquid motion in a container subjected to forced pitching oscillation." *International journal for numerical methods in engineering*, 15, 1207–1220.
- Nakayama, T. and Washizu, K. (1981). "The boundary element method applied to the analysis of two-dimensional nonlinear sloshing problems." *International Journal for Numerical Methods in Engineering*, 17(11), 1631–1646.
- Nayak, santosh kumar. (2013). "Seismic response of partially filled rectangular liquid tank with internal objects." Ph.D Thesis, National Institute of Technology Rourkela.
- Nayak, Santosh Kumar. and Biswal, K. C. (2015). "Fluid damping in rectangular tank fitted with various internal objects-An experimental investigation." *Ocean Engineering*, 108, 552–562.
- Nomura, T. and Hughes, T. J. R. (1992). "An arbitrary Lagrangian-Eulerian finite element method for interaction of fluid and a rigid body." *Computer Methods in Applied Mechanics and Engineering*, 95, 95, 115–138.

- Pal, N. C., Bhattacharyya, S. K. and Sinha, P. K. (1999). "Coupled slosh dynamics of liquid-filled, composite cylindrical tanks." *Journal of Engineering Mechanics*, 125(4), 491–495.
- Pal, N. C., Bhattacharyya, S. K. and Sinha, P. K. (2001). "Experimental investigation of slosh dynamics of liquid-filled containers." *Experimental Mechanics*, 41(1), 63–69.
- Panigrahy, P. K., Saha, U. K. and Maity, D. (2009). "Experimental studies on sloshing behavior due to horizontal movement of liquids in baffled tanks." *Ocean Engineering*, 36(3–4), 213–222.
- Radnić, J., Grgić, N., Kusić, M. S. and Harapin, A. (2018). "Shake table testing of an open rectangular water tank with water sloshing." *Journal of Fluids and Structures*, 81, 97–115.
- Rawat, A., Mittal, V., Chakraborty, T. and Matsagar, V. (2019). "Earthquake induced sloshing and hydrodynamic pressures in rigid liquid storage tanks analyzed by coupled acoustic-structural and Euler-Lagrange methods." *Thin-Walled Structures*, 134(September 2018), 333–346.
- Sakai, F., Nishimura, M. and Ogawa, H. (1984). "Sloshing behavior of floating-roof oil storage tanks." *Computers and Structures*, 19(1–2), 183–192.
- Sanapala, V. S., Rajkumar, M., Velusamy, K. and Patnaik, B. S. V. (2018). "Numerical simulation of parametric liquid sloshing in a horizontally baffled rectangular container." *Journal of Fluids and Structures*, 76, 229–250.
- Sanapala, V. S., Velusamy, K. and Patnaik, B. S. V. (2016). "CFD simulations on the dynamics of liquid sloshing and its control in a storage tank for spent fuel applications." *Annals of Nuclear Energy*, 94, 494–509.
- Shakib, H. and Alemzadeh, H. (2017). "The effect of earthquake site-source distance on dynamic response of concrete elevated water tanks." *Procedia Engineering*, 199, 260–265.
- Singal, V., Bajaj, J., Awalgaonkar, N. and Tibdewal, S. (2014). "CFD analysis of a kerosene fuel tank to reduce liquid sloshing." *Procedia Engineering*, 69, 1365–1371.

- Soroushnia, S., Tafreshi, S. T., Omidinasab, F., Beheshtian, N. and Soroushnia, S. (2011). “Seismic performance of RC elevated water tanks with frame staging and exhibition damage pattern.” *Procedia Engineering*, 14, 3076–3087.
- Tang, Y. (1994). “Free-vibration analysis of tank containing two liquids.” *Journal of Engineering Mechanics*, 120(3), 618–636.
- Thiagarajan, K. P., Rakshit, D. and Repalle, N. (2011). “The air-water sloshing problem: Fundamental analysis and parametric studies on excitation and fill levels.” *Ocean Engineering*, 38(2–3), 498–508.
- Tryggesson, H. (2007). “Analytical Vortex Solutions to the Navier-Stokes Equation.” Växjö University press.
- Tso, W. K., Zhu, T. J. and Heidebrecht, A. C. (1992). “Engineering implication of ground motion A/V ratio.” *Soil Dynamics and Earthquake Engineering*, 11(3), 133–144.
- Veletsos, A. S. and Tang, Y. (1986). “Dynamics of Vertically Excited Liquid Storage Tanks.” *Journal of Structural Engineering*, 112(6), 1228–1246.
- Wang, J. D., Lo, S. H. and Zhou, D. (2012). “Liquid sloshing in rigid cylindrical container with multiple rigid annular baffles: Free vibration.” *Journal of Fluids and Structures*, 34, 138–156.
- Wang, J. D., Lo, S. H. and Zhou, D. (2013). “Sloshing of liquid in rigid cylindrical container with multiple rigid annular baffles : Lateral excitations.” *Journal of Fluids and Structures*, 42, 421–436.
- Wang, J., Wang, C. and Liu, J. (2019). “Sloshing reduction in a pitching circular cylindrical container by multiple rigid annular baffles.” *Ocean Engineering*, 171(July 2018), 241–249.
- Wang, W., Guo, Z., Peng, Y. and Zhang, Q. (2016). “A numerical study of the effects of the T-shaped baffles on liquid sloshing in horizontal elliptical tanks.” *Ocean Engineering*, 111, 543–568.

- Westergaard, H. (1931). "Water pressures on dams during earthquakes." *Proceedings of the ASCE*, 1303.
- Xue, M. A. and Lin, P. (2011). "Numerical study of ring baffle effects on reducing violent liquid sloshing." *Computers and Fluids*, 52(1), 116–129.
- Xue, M. A., Zheng, J. and Lin, P. (2012). "Numerical simulation of sloshing phenomena in cubic tank with multiple baffles." *Journal of Applied Mathematics*, 2012, 21.
- Xue, M. A., Zheng, J., Lin, P. and Yuan, X. (2017). "Experimental study on vertical baffles of different configurations in suppressing sloshing pressure." *Ocean Engineering*, 136(March), 178–189.
- Xue, M., Peng-zhi, L., Jin-hai, Z., Yu-xiang, M., Xiao-li, Y. and NGUYEN, V.-T. (2013). "Effects of Perforated Baffle on Reducing Sloshing in Rectangular Tank - Experimental and Numerical Study." *China Ocean Eng*, 27(5), 615–628.
- Y.S. Choun. (2012). "Sloshing Response of Liquid Storage Tanks Subjected to Earthquakes with Different Peak Acceleration to Velocity Ratios." *15 WCEE*, Lisboa.
- Younes, M. F., Younes, Y. K., El-Madah, M., Ibrahim, I. M. and El-Dannanh, E. H. (2007). "An experimental investigation of hydrodynamic damping due to vertical baffle arrangements in a rectangular tank." *Proceedings of the Institution of Mechanical Engineers Part M: Journal of Engineering for the Maritime Environment*, 221(3), 115–123.
- Zhao, D., Hu, Z., Chen, G., Lim, S. and Wang, S. (2018). "Nonlinear sloshing in rectangular tanks under forced excitation." *International Journal of Naval Architecture and Ocean Engineering*, 10(5), 545–565.

LIST OF PUBLICATIONS

JOURNALS

1. **P. Nimisha**, B. R. Jayalekshmi, and K. Venkataramana. (2022). "Effective configuration of perforated baffle plate for efficient slosh damping in liquid retaining tanks under lateral excitation." *Ocean Engineering*, 259(September), p. 111855, doi: 10.1016/j.oceaneng.2022.111855. [SCI indexed]
2. **Nimisha, P.**, Jayalekshmi, B. R., and Venkataramana, K. (2022). "Slosh Damping in Rectangular Liquid Tank with Additional Blockage Effects under Pitch Excitation." *ASME Journal of Fluids Engineering*, 144, 121403-1-11. doi: <https://doi.org/10.1115/1.4054959> [SCI indexed]
3. **P. Nimisha**, B. R. Jayalekshmi, and K. Venkataramana. (2022). "Effect of Frequency Content of Seismic Excitation on Slosh Response of Liquid Tank with Baffle Plate." *Journal of Earthquake and Tsunami*, 17(2), 2350001-1-28, <https://dx.doi.org/10.1142/S179343112350001X> [SCI indexed]
4. **Nimisha, P.**, B. R. Jayalekshmi, and Katta Venkataramana. (2022). "Parametric Study on Frequency Characteristics of Cylindrical Liquid Tanks." *Journal of The Institution of Engineers (India): Series A*, 103(3), 831-839, <https://doi.org/10.1007/s40030-022-00646-0>. [SCOPUS indexed]
5. **Nimisha P.**, Katta Venkataramana, B R Jayalekshmi. (2019). "An overview of acoustic modelling and seismic design guidelines of liquid storage tanks." *International Journal of Applied Engineering Research*, ISSN 0973-4562 14(12), (Special Issue), -171-175.

BOOK CHAPTERS

1. **P. Nimisha**, B. R. Jayalekshmi, and K. Venkataramana. (2023). "Influence of Geometric Parameters in Self-damping Efficiency of Rectangular Liquid Storage Tanks." S. Saha et al. (eds.), *Recent Advances in Materials, Mechanics and Structures*,

Lecture Notes in Civil Engineering, vol. 269, Springer, Singapore.
https://doi.org/10.1007/978-981-19-3371-4_12 [SCOPUS indexed] (Accepted for publication)

2. **Nimisha P.**, Jayalekshmi B.R., Venkataramana K. (2021). “Study of Dynamic Characteristics of Circular Liquid Storage Tanks Using Acoustic Principles.” Das B.B., Nanukuttan S.V., Patnaik A.K., Panandikar N.S. (eds), Recent Trends in Civil Engineering, Lecture Notes in Civil Engineering, vol 105. Springer, Singapore.
https://doi.org/10.1007/978-981-15-8293-6_10 [SCOPUS indexed]

CONFERENCES

1. B V Anagha., **P Nimisha.** and B R Jayalekshmi (2020) “A Study on Effect of Fluid on the Modal Characteristics of Ground Supported Water Tanks.” *International Conference on Materials Mechanics & Structures (ICMMS 2020)*, March 26-28, 2020, NIT Calicut, Kerala, *IOP Conf. Ser.: Mater. Sci. Eng.* 936 012027. doi:10.1088/1757-899X/936/1/01202.
2. **Nimisha P.**, B R Jayalekshmi and Katta Venkataramana (2019) “An Overview of Dynamic Analysis of Water tanks.” *8th International Engineering Symposium - IES*, March 13-15, Kumamoto University, Japan, pp.C6-9-1-8.

CURRICULUM VITAE

NIMISHA P

Ph No: +919400859886

E-mail: nimisha.187cv017@nitk.edu.in ; nimmigouri@gmail.com

ACADEMIC PROFILE

Ph.D/ Structural Engineering *Under the guidance of Dr. B.R. Jayalekshmi and Prof. Katta Venkataramana, Department of Civil engineering, National Institute of Technology Karnakata, Surathkal, 2018-2022. (on-going)*

Thesis: Development of effective baffle configuration for slosh response control in liquid storage tanks

M. Tech/ Structural Engineering and construction management Vimal Jyothi College of Engineering, Chemperi, Kerala, India (2014-2016)
CGPA 8.64, 1st position in Kannur university, Kerala

B. Tech/ Civil Engineering L B S College of Engineering, Kasaragod, India (2009-2013)

75%

HSE KPC HSS, Pattanur, Kerala, India

89%

SSLC K HSS, Koodali, Kerala, India

90%

WORK EXPERIENCE

2016- 2018 Assistant Professor
Civil Engineering Department
Vimal Jyothi College of Engineering Chemperi,
Kerala, India

2013-2014 Lecturer
Civil Engineering Department
Malabar Institute of Technology Anjarakandy,
Kerala, India

SOFTWARE SKILLS

Professional Software AUTOCAD, STAAD Pro, ANSYS, ETABS,
SAP2000, MATLAB

PUBLICATIONS

1. P. Nimisha, B. R. Jayalekshmi, and K. Venkataramana. (2022). "Effective configuration of perforated baffle plate for efficient slosh damping in liquid retaining tanks under lateral excitation." *Ocean Engineering*.
2. Nimisha, P., Jayalekshmi, B. R., and Venkataramana, K. (2022). "Slosh Damping in Rectangular Liquid Tank with Additional Blockage Effects under Pitch Excitation." *ASME Journal of Fluids Engineering*.

3. Nimisha, P, B. R. Jayalekshmi, and Katta Venkataramana. (2022). “Parametric Study on Frequency Characteristics of Cylindrical Liquid Tanks.” *Journal of The Institution of Engineers (India): Series A*.

CONFERENCES AND WORKSHOP

1. Presented paper titled “Influence of Geometric Parameters in Self-damping Efficiency of Rectangular Liquid Storage Tanks.” *2nd International Conference on Materials Mechanics & Structures (ICMMS 2022)*, March 10-12, 2022, NIT Calicut, Kerala (online mode).
2. Presented paper titled “Study of dynamic characteristics of circular liquid storage tanks using acoustic principles,” International conference on Trending moments and steer forces”-Civil Engineering Today, October 31st and November 1st 2019 at Don Bosco College of Engineering, Goa.
3. Presented paper titled “An Overview of Acoustic Modelling and Seismic Design Guidelines of Liquid Storage Tanks,” National conference on Recent Trends in Civil Engineering, May 30, 2019, Vimal Jyothi Engineering College, Kannur, Kerala.
4. Attended two days workshop on “Finite Element Analysis of Structures using ANSYS,” conducted by Mar Baselios College of Engineering and Technology, Thiruvanthapuram, Kerala, India, held on January 10-11, 2019.
5. Presented paper titled “Proposal of a new lateral load resistance system combining principles of diagrid and tubular buildings.” National Conference, Innovations in civil Engineering, ICGE-2016, conducted by Vimal Jyothi Engineering College, Chemperi, Kerala.

PERSONAL INFORMATION

Father’s Name: Ashokan P

Spouse’s Name: Arun B S

Date of Birth: 10 January 1992

Permanent Address: Pittan House,

P. O. Koodali,

Kannur-670592

Contact Phone: +919400859886